IH 36

# SOLUTION OF CERTAIN HALF-SPACE PROBLEMS AND THEIR APPLICATION TO GEOPHYSICS

TH 36 43027

A thesis submitted to
Tezpur University
in fulfillment of the requirements
for the degree of
Doctor of Philosophy
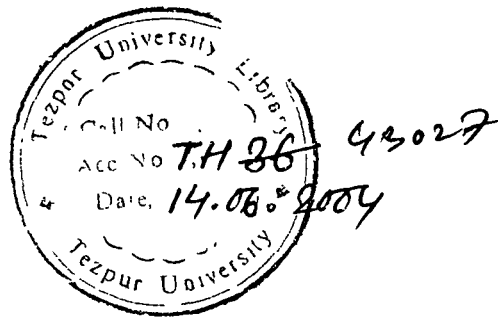
By

## Anjan Kumar Bhattacharyya

Department of Mathematical Sciences
School of Science and Technology
Tezpur University
Napaam – 784 028
India

# CERTIFICATE

This is to certify that **Mr. Anjan Kumar Bhattacharyya** has worked under our supervision for the thesis entitled **"Solution of Certain Half-Space Problems and their Application to Geophysics"** which is being submitted to Tezpur University in fulfillment of the requirements for the degree of Doctor of Philosophy. The thesis is Mr. Bhattacharyya's own work. He has fulfilled all the requirements under the Ph. D. rules and regulations of Tezpur University and to the best of our knowledge, the thesis as a whole or a part thereof has not been submitted to any other university for any degree or diploma.


**(Dr. A. K. Borkakati)**
Professor, Dept. of Mathematical Sciences
Tezpur University
Napaam, Tezpur –784028
Assam, India


Date: 27th December 2002

**(Dr. S. K. Laskar)**
Visiting Professor,
Dept. of Mathematical Sciences
Tezpur University
Napaam, Tezpur –784028
Assam, India


Date: 27th December 2002

# ABSTRACT

For a harmonic function H, anomalous gravity field $\Delta g$ or anomalous component magnetic field $T_z$, with asymptotic behaviour $H = 0(r^{-n}), n \geq 2, r \to \infty$, defined in the upper half-space domain $B_e$ bounded below by a half-space boundary S, the problem of reproduction of H in $B_e$ from the boundary data is formulated as a half-space problem in boundary density in terms of H specified over S. Reproduction of H in $B_e$ is also achieved by Green's formula, formulating the problem in Green's boundary formula. Subsequently, it is shown that a gravity or a component magnetic field can be reproduced in $B_e$ as a potential of simple as well as double layer boundary density from the data specified over the boundary. It is also shown that the fields can be continued upward from the boundary data by Green's formula without finding Green's function for the boundary. When applied to the ground magnetic data of Vishakhapatnam-Srikakulam area of Andhra Pradesh, the up-continued field clearly reveals the basement trend in the coastal area and the basement features in the hilly Lamaput-Araku area. Subsequent analysis of the up-continued data locates the exposed charnokites and identifies the direction of thrust responsible for deformation of the landmass in the area.

# ACKNOWLEDGEMENT

Date : December 27, 2002
Place : Napaam, Tezpur

(Anjan Kumar Bhattacharyya)

# SOLUTION OF CERTAIN HALF-SPACE PROBLEMS AND THEIR APPLICATION TO GEOPHYSICS

## CONTENTS

# Chapter-1

# INTRODUCTION

A subsurface mass declares its existence by producing some fields around it. Contour map of the field at a datum level reveals its structural configuration and also its location below it. Geophysical fields, such as gravity and magnetic responses of a subsurface body, when contoured on a datum level, the contoured data provides a qualitative interpretation of them in terms of size, shape and location of the causative mass. A quantitative analysis of them is supposed to provide complete information about the causative mass.

To understand the subsurface geology of an area, gravity magnetic (GM) data are acquired over the area, which is irregular in general. Reduction of data to a datum level appears as the first geophysical problem in interpretation of them in terms of subsurface geology of the area. The problem of reduction of gravity data to a horizontal level from data acquired in an irregular surface was solved by Hammer (1939) from the knowledge of masses causing the irregularities at the topography. This procedure however, cannot be applied to the magnetic data acquired in an irregular terrain. It requires application of a theoretical approach of reproduction of a harmonic function in the upper half-space domain from the data specified over the boundary.

The problem of reproduction of gravity or component magnetic field in the upper half-space domain, bounded below by a half-space boundary, suggests application of Green's formula for its solution. This requires finding of Green's function for the boundary. Finding of Green's function for a horizontal boundary is straightforward, but finding it for a general boundary is an extremely difficult task. Courtillot et al (1973), Ducruix et al (1974) made the first attempt to find a numerical solution of it. They came out with a numerical approximation of Green's function for the boundary. Their approach deals with non-linear estimation of unknown parameters and for solution, it requires an iterative scheme with a good apriori knowledge of the parameters.

Alternatively, Bhattacharyya and Chan (1977) formulated the problem of upward continuation by boundary integral equations in boundary densities. They used simple layer boundary density for the gravimetric case and double layer boundary density for the magnetostatic case. In their work, they derived the gravity field as a derivative of simple layer potential and reproduced the component magnetic field as potential of double layer boundary density.

Solution of a boundary integral equation analytically is out of question, it is to be solved numerically. This requires approximation of the boundary by sub-elements, subareas in three dimensions, and evaluation of the surface integrals of $r^{-1}$ and $\partial r^{-1} / \partial n_e$ over the subareas and finally solution of a system of linear algebraic equations by numerical means.

To find the numerical solution of the problem, Bhattacharyya and Chan (1977) approximated the boundary by rectangular subareas and used approximate values of the integrals over them. As such, the approximated boundary appeared with gaps between the subareas, interpolation of boundary data at the centroids of the subareas came out with error because of inaccurate representation of the boundary. Further, approximation of the integrals restricted reproduction of the field with reliable accuracy at a point near the boundary.

Again, reproduction of the gravity field involves evaluation of complicated singular integrals. In some cases, depending on the geometry of the boundary, the discretised version of the integral equation in simple layer density becomes non-amenable to solution by Gauss-Seidal iterative method, a method suitable to handle a large system of linear algebraic equations as they appear in solution of a geophysical problem. Further, we know that a component magnetostatic field vanishes at infinity in $O(r^{-3}), r \to \infty$ and the potential due to a double layer density vanishes in $O(r^{-2}), r \to \infty$. As such, reproduction of a component magnetic field, as potential due to a double layer density, remains to be explained in their work.

Laskar (1984) formulated the problem of upward continuation of gravity and magnetic fields from boundary data by formulating the problems in boundary integral equation in double layer boundary density and also derived the component magnetostatic field as derivative of potential due to simple layer boundary density. However, the possibility of reproduction of both gravity and magnetic fields as potential of simple layer boundary density is left to be discussed in his work.

Since approximation of regular integrals suffices finding of reasonable solutions of the boundary equations (Laskar 1971, Bhattacharyya and Chan 1977, Kumar et al 1992), no much efforts were made to evaluate the regular integrals analytically. For a field point lying at a distance $d \leq 2D$ from the boundary; D defining the largest diagonal of the nearest subarea $\Delta S$, approximate values of the integrals appear with more than 5% error (Laskar 1977). This error adversely affects the field value as the field point approaches the boundary. This necessitates analytical evaluation of the integrals at least over the subareas lying within a distance of 2D from the field point.

In this thesis, reproduction of potential fields from the data specified over a half-space boundary is formulated in boundary integral equation. Existence and uniqueness of solution of a half-space problem is discussed as a special case of a closed domain problem. In reproduction of a potential field in the upper half-space domain from boundary data, it is theoretically shown that upward continuation of gravity and magnetic fields can be carried out from a general boundary as potential of simple as well as double layer boundary density. It is also achieved by use of Green's formula without finding Green's function for the boundary. Subsequently, efficacies of the techniques are successfully demonstrated on model data. To carry out numerical work, the boundary is divided into triangular sub-areas to have the best possible approximation of it and the integrals over them are evaluated analytically. Finally, the ground magnetic data of Vishakhapatnam-Srikakulam area are continued upward to a common level grazing the highest topographic point of the area by double layer formulation of the problem and subsequently, these are continued downward for finding the depth to the magnetic causative by use of DEPTHDNC software that determines depth to causative mass from the profile potential field data. The analysis reveals the basement configuration in the relatively flat coastal

3

area of Vishakhapatnam region and mechanism of deformation of the landmass in the undulated hilly region of Lamaput-Araku area that lies at the northwest of the coastal area.

# Chapter-2

# POTENTIAL THEORY

## 2.1 Potential due to Simple Sources

### 2.1.1 Potential due to a Simple Source

For a monopole of mass $\sigma$ placed at a point q the potential $\phi$ due to it at a point P is given by

$$\phi(P) = \frac{\sigma}{r} = \frac{\sigma}{|P-q|} = \sigma|P-q|^{-1} = \sigma(q)g(P,q), \qquad (2.1.1)$$

where **q** and **P** are the position vectors specifying the points q and P respectively with respect to an arbitrary reference point O, r is the distance between P and q (Fig.2.1.1) and $r^{-1}$ is denoted by g(P,q) or g(q,P).



Fig.2.1.1

It is evident from Fiq. 2.1.1 that

$$\overrightarrow{OP} = \overrightarrow{Oq} + \overrightarrow{qP}$$

$$\Rightarrow \overrightarrow{qP} = \overrightarrow{OP} - \overrightarrow{Oq}$$

$$\Rightarrow \vec{r} = \overrightarrow{OP} - \overrightarrow{Oq}.$$
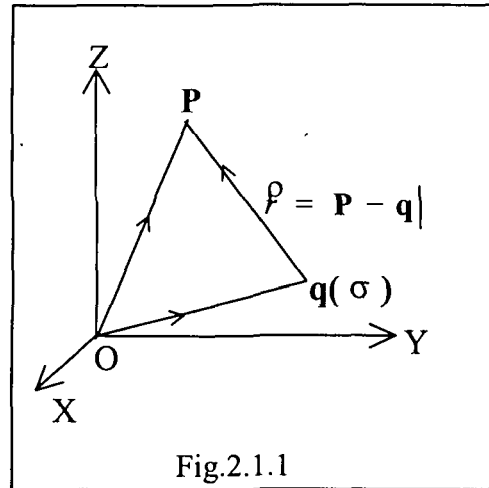
The $\phi$ in (2.1.1) is continuous and differentiable function of P except at the point q, i.e., at P = q. As $|P| \to \infty$, g(P,q) on expansion yields

$$g(P,q) = |P|^{-1} + |P|^{-3}(P.q) + O(|P-q|^{-3}), \quad |P| \to \infty. \qquad (2.1.2)$$

5

Further, this satisfies Laplace's equation

$$\nabla^2\phi(p) = \nabla^2[\sigma(q)g(P,q)] = 0 \qquad\qquad (2.1.3)$$

everywhere except at the point P = q. As such $\phi$ is a harmonic function of P everywhere except at q. Formally $\phi$ satisfies Poisson's equation

$$\nabla^2\phi(P) = -4\pi\sigma(q).\delta(P,q)$$

where $\delta(P,q)$ is the Dirac-Delta function.

## 2.1.2 Potential due to Distribution of Simple Sources

A continuous distribution of simple source of surface density $\sigma$ over a smooth surface S generates simple layer potential

$$\phi(\mathbf{P}) = \int_s \frac{\sigma ds}{r} = \int_s |\mathbf{P} - \mathbf{q}|^{-1}\sigma(q)dq$$

$$= \int_s g(\mathbf{P},\mathbf{q})\sigma(q)dq\,, \mathbf{P}\notin S \qquad (2.1.4)$$

at the field point P, dq (=ds) representing the surface element at the point q. Unlike the potential due to a simple source (monopole), expression



Fig.2.1.2
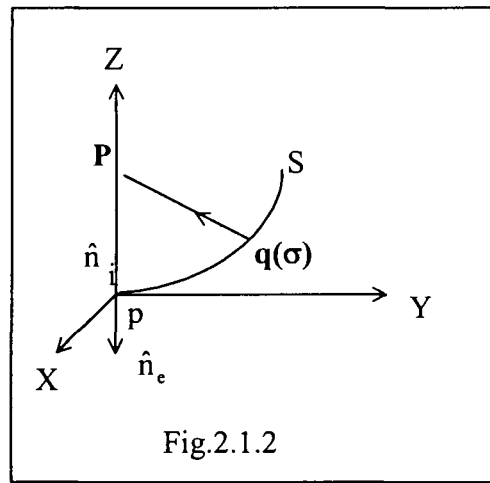
(2.1.4) is continuous everywhere including the surface S. For P→p∈S, following Jaswon and Symm (1977), we obtain

$$\phi(\mathbf{p}) = \int_s g(\mathbf{p},\mathbf{q})\sigma(q)dq\,, \mathbf{p}\in S. \qquad\qquad (2.1.5)$$

Further, the $\phi(\mathbf{P})$ in (2.1.4) has asymptotic behaviour

$$\phi(\mathbf{P}) = |\mathbf{P}|^{-1}\int_s \sigma(q)dq + O\left(|\mathbf{P}|^{-2}\right) \text{ as } \mathbf{P}\to\infty, \qquad (2.1.6)$$

differentiable to 2nd order and satisfies Laplace's equation everywhere except at P∈S , i.e.,

$$\nabla^2\phi(\mathbf{P}) = 0\,, \mathbf{P}\notin S \qquad\qquad (2.1.7)$$

and as such it is a harmonic function in **P** everywhere except P∈S.

For $\sigma$ satisfying Hölder continuity (Kellog 1929, Jaswon and Symm 1977), which is stronger than the continuity and weaker than the differentiability at p∈S, the tangential

6

derivative of $\phi$ exists and continuous at p. But its normal derivatives are discontinuous (Smirnov, 1964). To examine the nature of discontinuity we draw a normal line to one side of S at p and locate points on the normal by a variable $\hat{n}$ which increases as we move away from S (Fig.2.1.2). At any point P on the normal, other than the initial point $p \in S$

$$\frac{\partial \phi}{\partial n} = \int_S \frac{\partial g(\mathbf{P},\mathbf{q})}{\partial n} \sigma(\mathbf{q}) dq$$

$$= \int_S \frac{\partial}{\partial n}\left(\frac{1}{|\mathbf{P}-\mathbf{q}|}\right) \sigma(\mathbf{q}) dq, \mathbf{P} \notin S \qquad (2.1.8)$$

where, $\partial g(\mathbf{P},\mathbf{q})/\partial n$ denotes the derivative of $\phi$ at P. The integrand in (2.1.8) is regular and the integral can be evaluated on S. For p contained in an infinitely small surface element $\delta$ of S, we may rewrite (2.1.8) as

$$\frac{\partial \phi(\mathbf{p})}{\partial n} = \int_\delta \frac{\partial}{\partial n}\left(\frac{1}{|\mathbf{P}-\mathbf{q}|}\right)\sigma(\mathbf{q})dq + \int_{S-\delta} \frac{\partial}{\partial n}\left(\frac{1}{|\mathbf{P}-\mathbf{q}|}\right)\sigma(\mathbf{q})dq.$$

As $P \rightarrow p \in S$, moving along the normal, the second integral is regular, but an apparent indeterminacy occurs in the integral over $\delta$, when $q = P$. Following Kellog (1929), for $P \rightarrow p$ and $\delta \rightarrow 0$, the first integral yields a definite value $-2\pi\sigma(p)$ and the normal derivative of $\phi$ at $p \in S$ becomes

$$\frac{\partial \phi(\mathbf{p})}{\partial n} = -2\pi\sigma(\mathbf{p})dq + \int_S \frac{\partial}{\partial n}\left(\frac{1}{|\mathbf{P}-\mathbf{q}|}\right)\sigma(\mathbf{q})dq, p \in S. \qquad (2.1.9)$$

For the sake of convenience, using the notation of Jaswon and Symm (1977), we rewrite the derivatives (2.1.8) and (2.1.9) as

$$\phi_n'(\mathbf{P}) = \int_S g_n'(\mathbf{P},\mathbf{q})\sigma(\mathbf{q})dq, \mathbf{P} \notin S \qquad (2.1.10)$$

7

and

$$\phi_n'(\mathbf{p}) = \int_S g_n'(\mathbf{p},\mathbf{q})\sigma(\mathbf{q})dq - 2\pi\sigma(\mathbf{p}), \ \mathbf{p}\in S. \qquad (2.1.11)$$

There are two distinct normals at $\mathbf{p}\in S$, one at either side of S. Assuming both sides of S to be positive (Jaswon and Symm 1977), i.e., the relevant variables $n_i$ and $n_e$ both increases on moving away from S, following (2.1.11), putting i for $n_i$ and e for $n_e$, we obtain

$$\phi_i'(\mathbf{p}) = \int_S g_i'(\mathbf{p},\mathbf{q})\sigma(\mathbf{q})dq - 2\pi\sigma(\mathbf{p}) \qquad (2.1.12)$$

and

$$\phi_e'(\mathbf{p}) = \int_S g_e'(\mathbf{p},\mathbf{q})\sigma(\mathbf{q})dq - 2\pi\sigma(\mathbf{p}). \qquad (2.1.13)$$

Since g(p,q) remains continuous as p crosses S, it follows that

$$g_e'(\mathbf{p},\mathbf{q}) + g_i'(\mathbf{p},\mathbf{q}) = 0, \ \mathbf{p}\in S. \qquad (2.1.14)$$

By virtue of this property of $g_i'(\mathbf{p},\mathbf{q})$, on adding (2.1.12) and (2.1.13) we obtain

$$\phi_e'(\mathbf{p}) + \phi_i'(\mathbf{p}) = -4\pi\sigma(\mathbf{p}), \ \mathbf{p}\in S. \qquad (2.1.15)$$

Unlike the normal derivative of the simple layer potential of $\phi$, that has a jump of amount $-2\pi\sigma(\mathbf{q})$ at the boundary point p, the tangential derivative of $\phi$ at $\mathbf{p}\in S$ is continuous as $P\rightarrow\mathbf{p}\in S$ and it can be expressed as

$$\lim_{P_i\rightarrow p}\frac{\partial\phi(\mathbf{P}_i)}{\partial t_i} = \frac{\partial\phi(\mathbf{p})}{\partial t} \qquad (2.1.16)$$

where, $\partial\phi(\mathbf{P}_i)/\partial t_i$ represents the derivative of $\phi$ at the interior point $P_i$ along line $t_i$, which is parallel to the tangent t at $\mathbf{p}\in S$. The limit holds for a smooth S having a second order space derivative at the surface element $S'$ with p in it and $\sigma$ satisfies Hölder continuity at $\mathbf{p}\in S'$ (Kellog 1929). It is now followed from (2.1.11) and (2.1.16) that

8

$$\frac{\partial \phi(\mathbf{p})}{\partial \mathbf{u}} = -2\pi\sigma(\mathbf{p})(\hat{u}.\hat{n}) + \int_S g'_u(\mathbf{p},\mathbf{q})\sigma(\mathbf{q})dq, \quad \mathbf{p} \in S, \tag{2.1.17}$$

as shown by Jaswon and Symm (1977), where $\hat{u}$ is a unit vector in any arbitrary direction at $p \in S$. For $\phi$ considered in the domain indicated by the normal $n_i$, expression (2.1.17) yields

$$\frac{\partial \phi(\mathbf{p})}{\partial \mathbf{u}} = -2\pi\sigma(\mathbf{p})(\hat{u}.\hat{i}) + \int_S g'_u(\mathbf{p},\mathbf{q})\sigma(\mathbf{q})dq \tag{2.1.18}$$

and for $\phi$ considered in the domain indicated by the normal $n_e$, expression (2.1.17) yields

$$\frac{\partial \phi(\mathbf{p})}{\partial \mathbf{u}} = -2\pi\sigma(\mathbf{p})(\hat{u}.\hat{e}) + \int_S g'_u(\mathbf{p},\mathbf{q})\sigma(\mathbf{q})dq \tag{2.1.19}$$

Following old sign convention one side of S is positive and other side negative, Bhattacharyya and Chan (1977) also arrived at (2.1.19).

## 2.2 Potential due to Double Sources

### 2.2.1 Potential due to a double source

A dipole of strength (moment) $\mu$ is placed in a direction $\hat{u}$ at a point q in a cartesian frame with z-axis upward (Fig.2.2.1). Its potential $\phi$ at a field point P is given by



Fig.2.2.1

$$\phi(P) = \mu \frac{\partial}{\partial u}\left(\frac{1}{r}\right)$$

$$= \mu(q)'_u |\mathbf{q} - \mathbf{P}|^{-1}$$

$$= \mu(q)g(\mathbf{P},\mathbf{q})'_u$$

$$= \mu(q)\frac{1}{r^2}(\hat{r}.\hat{u}) = -\mu(q)\frac{1}{r^2}\cos\theta \tag{2.2.1}$$

9
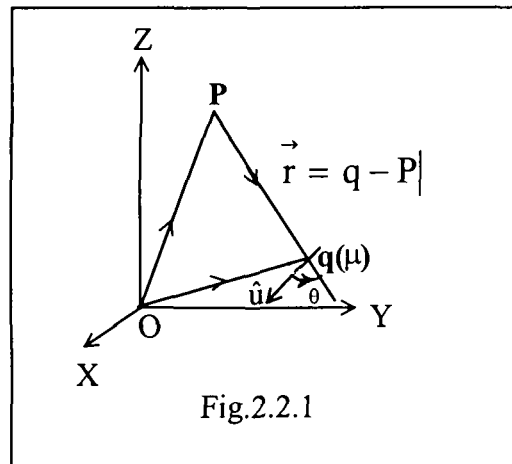
where, $r = |\mathbf{P} - \mathbf{q}| = |\mathbf{q} - \mathbf{P}|$, $g(\mathbf{P}, \mathbf{q})'_u$ is the derivative of $g(\mathbf{P}, \mathbf{q})$ [$= |\mathbf{q} - \mathbf{P}|^{-1}$] at the point q in the direction $\hat{u}$, keeping P fixed. $\hat{r}$ denotes the unit vector in the direction of $\overrightarrow{\mathbf{Pq}}$ and $\theta$ is the angle between the vectors $\overrightarrow{\mathbf{Pq}}$ and $\hat{u}$. The potential is a continuous and differentiable function of P satisfying $\nabla^2\phi = 0$ except at the point q and therefore is a harmonic function everywhere except at q. This $\phi$ vanishes at infinity with asymptotic behaviour

$$\phi(\mathbf{P}) = O\left(|\mathbf{P}|^{-2}\right), \quad |\mathbf{P}| \to \infty. \tag{2.2.2}$$

For P, q defined by (X,Y,Z) and (x,y,z) respectively and $\hat{u}$ by the direction cosine (l,m,n), expression (2.2.1) becomes

$$\phi(\mathbf{P}) = \mu(x,y,z)\frac{\partial}{\partial u}\left(\frac{1}{r}\right)$$

$$= \mu\left[\frac{\partial}{\partial r}\left(\frac{1}{r}\right)\frac{\partial r}{\partial u}\right]_q$$

$$= -\mu\frac{1}{r^2}(\hat{r}.\hat{u})$$

$$= -\mu r^{-2}\left[(x-X)l + (y-Y)m + (z-Z)n\right]/r$$

$$= -\mu r^{-3}\left[(x-X)l + (y-Y)m + (z-Z)n\right], \tag{2.2.3}$$

The upward intensity at P due to the doublet at q,

$$T_z(\mathbf{P}) = -\frac{\partial\phi}{\partial Z}\bigg]_P$$

$$= \mu\left[-nr^{-3} + 3\{l(x-X) + m(y-Y) + n(z-Z)\}(z-Z)r^{-5}\right]. \qquad (2.2.4)$$

For the doublet placed at the origin of the reference frame, in vertically downward direction, and the field point P lying vertically above the doublet by putting x= y= 0, l= m= 0, n= -1 and X =Y =0 in (2.2.4), we obtain the upward intensity $T_Z$ at P as

$$T_z(P) = T(0,0,Z) = \mu\left(r^{-3} - 3Z^2 r^{-5}\right) = -2\mu Z^{-3}.$$

This indicates, the intensity at P(0,0,Z) is vertically downward, as expected.

## 2.2.2 Potential due to Surface Distribution of Double Sources

A double source or a doublet of strength $\mu$ is located at a point q belonging to a smooth surface S (not necessarily closed) with its direction along a unit vector $\hat{i}$ normal to S at q. Its potential at a point outside the surface S (Fig.2.2.2) is given by (2.2.1) as

$$\phi(P) = \mu(q)g(P,q)'_i.$$



Fig.2.2.2
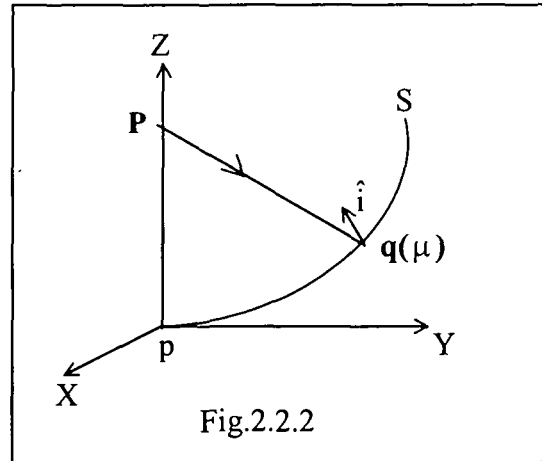
For continuous distribution of double sources of strength $\mu$ per unit area on S, i.e., for surface distribution of doublets of density $\mu$ over S, the potential at P is

$$W(P) = \int_S g(P,q)'_i \mu(q)dq, \quad P \notin S. \qquad (2.2.5)$$

The W(P) in (2.2.5) is continuous and differentiable at P ≠ q. Further, it satisfies Laplace equation at all the points P ≠ q. It is therefore a harmonic function everywhere except at S, where it is discontinuous.

To define the discontinuity properties at S, let us consider two points $P_i$ and $P_e$ on $\hat{i}$ and $\hat{e}$, the internal and external normals respectively at p (Fig.2.2.3) over S.

$$\lim_{P_i \to p} W(P_i) = W(p) + 2\pi\mu(p) \qquad\qquad (2.2.6)$$

and

$$\lim_{P_e \to p} W(P_e) = W(p) - 2\pi\mu(p). \qquad\qquad (2.2.7)$$

The term $-2\,\pi\mu(p)$ appearing in expression (2.2.7) for the doublet at p being directed along the normal $\hat{i}$.

The jumps of an amount $2\pi\mu(p)$ in the integral can be realized on evaluating the integral as sum of the integrals over the surface element $\delta \subset S$ and $S-\delta$ as $\delta \to 0$ containing p, i.e., $p \in \delta$. The value of the integral over $\delta$, when $P_i \to p$ and $\delta \to 0$ is $2\pi\mu(p)$ (Kellogg, 1929), where $\mu(p)$ is the average value of $\mu$ over $\delta$ containing p and $\delta$ is infinitesimally small. It is to be noted here that the direction of the vector



Fig.2.2.3
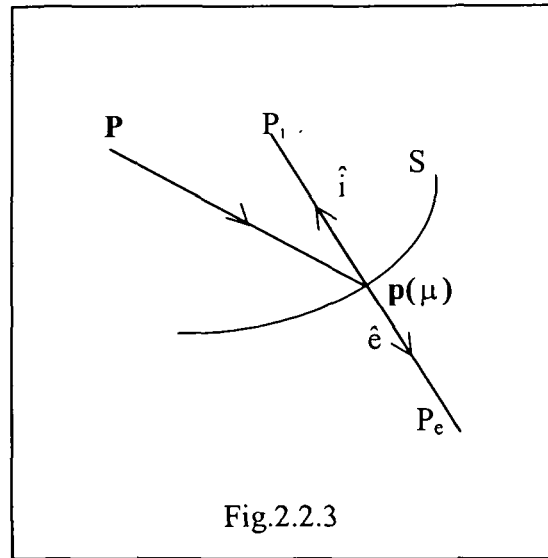
$\vec{r} = (\mathbf{p} - \mathbf{P_i})$ is in the opposite direction of the doublet at p. The integral over $S$-$\delta$ is regular and yield a value W(p) which is less by an amount $2\pi\,\mu(p)$ than the value of the integral (2.2.5), when $P(= P_i)$ is at infinitesimal distance from p. This phenomenon of change of the value of the integral when $P_i$ goes to $p \in S$ moving along $\hat{i}$, is termed as jump in the integral and the limiting value of the integral (2.2.5) at the boundary is therefore $W(p) + 2\pi\,\mu(p)$.

When $P_e \to p \in S$, from the other side of S, the direction of the vector $\vec{r} = (\mathbf{p}\text{-}\mathbf{P_e})$ is in the direction $\hat{i}$, the direction of the doublet at p, which is opposite to the case we see in (2.2.6). Hence as $P_e \to p \in S$, the limiting value of the integral (2.2.5) is given by $W(p) - 2\pi\mu(p)$.

12

## 2.3 Green's Formulae for Half-Space Domain

### 2.3.1 Green's Identities

**(i) Green's Identity-I**

For a harmonic function $\phi$ defined in a domain V bounded by a closed smooth surface S, Green's Identity-I states that

$$\int_s \frac{\partial \phi}{\partial n_i} ds = 0.$$

Using present notation, we express it as

$$\int_{\partial B} \phi_i'(q)dq = 0, \qquad (2.3.1)$$

where $\partial B$ denotes the boundary S, $\phi_i'(q)$ represented the inward normal derivative of $\phi$ at the point $q \in \partial B$, and $dq = ds$. This identity also defines the Gauss condition for $\phi$ to be a harmonic in the interior domain V ($\equiv B_i$, Fig.2.3.1) bounded by $\partial B$.

For a regular harmonic function $\phi$, i.e., $\phi = O(r^{-1})$, $r \to \infty$, defined in the exterior domain $B_e$ (Fig. 2.3.1) bounded at the interior by $\partial B$, the identity becomes

$$\int_{\partial B} \phi_e'(q)dq + \int_{\partial S} \phi_e'(q)dq = 0, \qquad (2.3.2)$$

where $\partial S$ is the outer boundary that encloses the exterior domain $B_e$ within it and $\phi_e'$ stands for the normal derivative of $\phi$ towards the domain $B_e$ at the point $q \in \partial B + S_1 + S_2 + \partial S$ as seen in Fig.2.3.1.
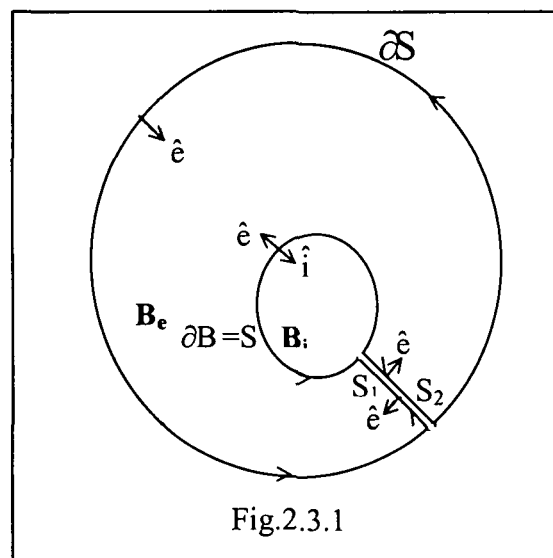


Fig.2.3.1

For $\phi = O(r^{-1})$, $r \to \infty$, the second integral of expression (2.3.2) does not vanish as can be seen from

$$\int_{\partial S} \phi'_e(q)dq = \lim_{r \to \infty} \int_{\partial S} O(r^{-2}).r^2 d\omega = 0(1),$$

where $d\omega$ is the solid angle subtended by $dq \in \partial S$ at the central point of $B_i$ (Fig.2.3.1). In this case, by ( 2.3.2)

$$\int_{\partial B} \phi'_e(q)dq \neq 0 \tag{2.3.3}$$

necessarily.

However, for $\phi = O(r^{-2})$, $r \to \infty$, the second integral on $\partial S$ vanishes for $\phi'_e = O(r^{-3})$. Under this condition, we obtain

$$\int_{\partial B} \phi'_e(q)dq = 0. \tag{2.3.4}$$

**(ii) Green's Identity–II or Green's Reciprocal Formula**

Two functions $\phi$ and $\psi$ are harmonic in a domain V bounded by a closed smooth surface S. Green's Identity–II states that

$$\int_s \phi \frac{\partial \psi}{\partial n_i} ds - \int_s \psi \frac{\partial \phi}{\partial n_i} ds = 0, \tag{2.3.5}$$

where $n_i$ is an inward normal to S .

Following the present notation, the identity (2.3.5) can be written as

$$\int_{\partial B} \phi(q)\psi'_i(q)dq - \int_{\partial B} \psi(q)\phi'_i(q)dq = 0. \tag{2.3.6}$$

For $\phi$ and $\psi$ to be regular and harmonic in the exterior domain $B_e$ (Fig.2.3.1), bounded by $\partial B$ in the interior, the identity (2.3.6), on changing i by e, becomes

14

$$\int_{\partial B}\phi(q)\psi'_e(q)dq - \int_{\partial B}\psi(q)\phi'_e(q)dq + \int_{\partial S}\phi(q)\psi'_e(q)dq - \int_{\partial S}\psi(q)\phi'_e(q)dq = 0,$$

the integrals over $S_1$ canceling those over $S_2$, $S_1$ coinciding with $S_2$ . As $\partial S$ goes to infinity, i.e., as $r \to \infty$, keeping $\partial B$ fixed in position, the integrals over $\partial S$ tends to zero, yielding the identify for $B_e$ as

$$\int_{\partial B}\phi(q)\psi'_e(q)dq - \int_{\partial B}\psi(q)\phi'_e(q)dq = 0.$$ 
(2.3.7)

## 2.3.2 Green's Formulae

Let $\phi$ be a harmonic function in an interior domain $B_1$ bounded by a smooth closed surface S. Given $\phi$ and its interior normal derivative $\phi'_1$ over S Green's formula determined the value of $\phi$ at an interior point P.

Let us enclose the point P by a small spherical surface $\bar{S}$ of radius $a$ and introduce a function $\psi$ defined by $1/r = |p - q|^{-1}$. In the annular region V (= $B_i$, say) bounded by S and $\bar{S}$ (Fig.2.3.2), both $\phi$ and $\psi$ are harmonic functions. As such, by Green's Identity–II, i.e., by (2.3.6), we obtain

Fig.2.3.2
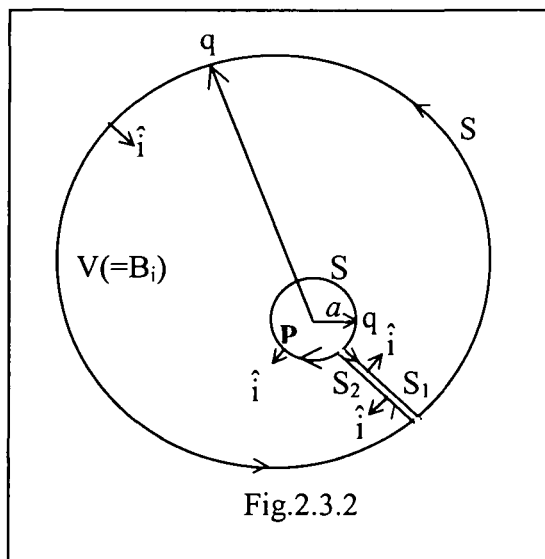
$$\int_{\bar{S}}(\phi\frac{\partial\psi}{\partial n_1} - \psi\frac{\partial\phi}{\partial n_1})d\bar{S} + \int_{S}(\phi\frac{\partial\psi}{\partial n_i} - \psi\frac{\partial\phi}{\partial n_1})ds = 0,$$ 
(2.3.8)

the integrals over $S_1$ and $S_2$ canceling each other.

As the radius $a \to 0$, the first integral over $\bar{S}$ yields

15

$$\lim_{a \to 0}[\int_{\bar{s}} \{\phi \frac{\partial}{\partial r}(\frac{1}{r})\frac{\partial r}{\partial n_i} - \frac{1}{r}\frac{\partial \phi}{\partial n_i}\}d\bar{S}]$$

$$= \lim_{a \to 0}[\int_{\bar{s}} \{\phi(-\frac{1}{r^2})(\hat{r}.\hat{n}_i)d\bar{S} - \int_{\bar{s}}\frac{1}{r}\frac{\partial \phi}{\partial n_i}d\bar{S}]$$

$$= \lim_{a \to 0}[\phi_{av}\int_{\bar{s}}(-\frac{1}{a^2})d\bar{S} - \frac{1}{a}\int_{\bar{s}}\frac{\partial \phi}{\partial n_i}d\bar{S}]$$

$$= -\phi(p)\lim_{a \to 0}\int_w d\omega - \lim_{a \to 0}\frac{1}{a}\int_s \frac{\partial \phi}{\partial n_i}d\bar{S}$$

$$= -4\pi\phi(p), \tag{2.3.9}$$

$\hat{r}$ and $\hat{n}_i$ being both outward, $d\omega$ the solid angle subtended at P by $d\bar{S}$, $\phi_{av}$ being the average value of $\phi$ over the sphere of radius $a$ and the second integral being zero by Green's Identity–I.

On substituting the value of the first integral in (2.3.8), we obtain

$$4\pi\phi(P) = \int_s \phi \frac{\partial}{\partial n_i}\left(\frac{1}{r}\right)ds - \int_s \frac{1}{r}\frac{\partial \phi}{\partial n_i}ds \tag{2.3.10}$$

which is known as Green's formula for the interior function $\phi$. In this case, $\phi$ at an interior point P is expressed in terms of $\phi$ and $\partial \phi / \partial n_i$ given over the boundary S.

Using the current notation, we rewrite (2.3.10) as

$$4\pi\phi(P) = \int_{\partial B} |q - P|^{-1}\phi(q)dq - \int_{\partial B}|q - P|^{-1}\phi_i(q)dq, \quad P \in B, \tag{2.3.11}$$

16

where $\partial B$ is the smooth closed surface S that encloses the domain $B_1$ ( = V ).

For P lying outside $B_1$, we find $\nabla^2 \psi = 0$ in $B_1$ Consequently, by Green's Identity–II, we obtain

$$\int_S (\phi \frac{\partial \psi}{\partial n_1} - \psi \frac{\partial \phi}{\partial n_1}) dS = 0$$

$$\text{or, } \int_S (\frac{\partial}{\partial n_1}\left(\frac{1}{r}\right)\phi - \frac{1}{r}\frac{\partial \phi}{\partial n_1}) dS = 0$$

$$\text{or, } \int_{\partial B}' |q - p|^{-1} \phi(q) dq - \int_{\partial B} |q - p|^{-1} \phi_1'(q) dq = 0, P \in B_e , \qquad (2.3.12)$$

$B_e$ defining the infinite domain exterior to $B_1$.

For a regular $\phi$ defined in the exterior domain $B_e$, bounded at the interior by a closed smooth surface $\partial B$ and at the exterior by a spherical surface $\partial S$ lying at infinity (Fig.2.3.1), using the formula ( 2.3.11), we obtain

$$4\pi\phi(P) = \int_{\partial B}' |q - P|^{-1} \phi(q) dq - \int_{\partial B} |q - P|^{-1} \phi_e'(q) dq$$

$$+ \int_{\partial S}' |q - P|^{-1} \phi(q) dq - \int_{\partial S} |q - P|^{-1} \phi_e'(q) dq, \quad P \in B_e \qquad (2.3.13)$$

omitting the integral over $S_1$ and $S_2$ (Fig.2.3.1) as they cancel each other. As $\partial S$ moves to infinity, the contributions of the last two integrals of (2.3.13) at P, lying in the finite region, are each of $O( r^{-1})$, $r \rightarrow \infty$, where $r = |P - q|$ and $\phi$ being regular . This leads to Green's formula for the exterior domain $B_e$ bounded at the interior by $\partial B$ as

$$4\pi\phi(P) = \int_{\partial B}' |q - P|^{-1} \phi(q) dq - \int_{\partial B} |q - P|^{-1} \phi_e'(q) dq, \quad P \in B_e . \qquad (2.3.14)$$

17

### 2.3.3 Green's Boundary Formula

Green's formula generates $\phi$ throughout the interior domain $B_I$ assuming that $\phi$ and $\phi_I'$ are both available and compatible over $\partial B$. According to fundamental existence theorems, either $\phi$ alone or $\phi'$ alone over $\partial B$ essentially suffices determination of $\phi$ throughout $B_I$ (Jaswon and Symm 1977). Thus application of Green's formula requires more boundary information and as such it cannot be used immediately for solving problems. One well-known approach is elimination of the redundancy in Green's formula by constructing Green's function for the boundary, which is, in general, an extremely difficult task (Courtillot et. al., 1973). An alternative approach is provided by Green's formula taken to the boundary.

For a harmonic function $\phi$ defined in an interior domain $B_I$ bounded by a smooth closed boundary $\partial B$, given $\phi$ and $\phi_I'$ over $\partial B$, Green's formula (2.3.11) provides $\phi$ at an interior point P. Using the notation $|\mathbf{q} - \mathbf{P}|^{-1} \equiv g(\mathbf{P}, \mathbf{q})$ and $_I|\mathbf{q} - \mathbf{P}|^{-1} \equiv g(\mathbf{P}, \mathbf{q})_I$ we rewrite (2.3.11) as

$$4\pi\phi(P) = \int_{\partial B} g(P,q)_I' \phi(q)dq - \int_{\partial B} g(P,q)\phi_I'(q)dq, \quad P \in B_I \ . \tag{2.3.15}$$

Comparing the above integrals with those expressing double and simple layer potentials of surface densities shown in (2.2.5) and (2.1.4) respectively, it can be stated that Green's formula yields the $\phi$ at P as a combination of double and simple layer potentials of boundary densities $\phi$ and $\phi_I'$ respectively. This provides a vital link between the theory of harmonic function and potential theory.

When $P \to p \in \partial B$ the simple layer potential with boundary density $\phi_I'$ remains continuous in $B_I + \partial B$ as seen in (2.1.5), but the double layer potential with boundary density $\phi$ suffers a loss of amount $2\pi\phi(p)$ due to the jump $-2\pi\phi(p)$ in the integral at $p \in \partial B$, as explained in (2.2.6). By virtue of continuity of the simple layer potential and loss in the double layer potential when $P = p \in \partial B$, formula (2.3.15) yields

$$2\pi\phi(p) = \int_{\partial B} g(p,q)'_i \phi(q)dq - \int_{\partial B} g(p,q)\phi'_i(q)dq, \quad p \in \partial B. \tag{2.3.16}$$

This formula is known as Green's boundary formula for the interior domain $B_i$

When p crosses the boundary $\partial B$ moving from $\partial B$ to $B_e$, the double layer potential again jumps by - $2\pi\phi(p)$ yielding the identity

$$0 = \int_{\partial B} g(p,q)'_i \phi(q)dq - \int_{\partial B} g(p,q)\phi'_i(q)dq, \quad P \in B_e. \tag{2.3.17}$$

This identity is deduced earlier in (2.3.12). The formula (2.3.17) can also be realised from formula (2.3.16) considering $p = P_e \in B_e$ and $P_e$ approached $\partial B$ moving form $B_e$ to $\partial B$.

As $P_e \to p \in \partial B$, the double layer integral gains an amount $2\pi\phi(p)$ by a jump at $p \in \partial B$, as seen in (2.2.7). Since the same value appears as the value of the integral in boundary formula (2.3.16), the formula must yield a zero value when $P \in B_e$

The analogous results hold for a regular exterior harmonic function $\phi$, viz.,

$$\int_{\partial B} g(P,q)'_e \phi(q)dq - \int_{\partial B} g(p,q)\phi'_e(q)dq = 4\pi\phi(P), \quad P \in B_e, \tag{2.3.18}$$

$$\int_{\partial B} g(p,q)'_e \phi(q)dq - \int_{\partial B} g(p,q)\phi'_e(q)dq = 2\pi\phi(p), \quad p \in \partial B \tag{2.3.19}$$

and

$$\int_{\partial B} g(P,q)'_e \phi(q)dq - \int_{\partial B} g(P,q)\phi'_e(q)dq = 0, \quad P \in B_i. \tag{2.3.20}$$

## 2.3.4 Formulation of Dirichlet and Neumann Problems

It is now left to show how Green's boundary formula can be directly applied to solve problems when either $\phi$ or $\phi'$ alone is given over $\partial B$.

**(i) Interior Problems**

(a) Given $\phi$ over $\partial B$, the relation (2.3.16) leads to the equation

$$\int_{\partial B} g(p,q)\phi_i'(q)dq = \int_{\partial B} g(p,q)_i'\phi(q)dq - 2\pi\phi(p), \quad p \in \partial B, \tag{2.3.21}$$

a Fredholm integral equation of the first kind in $\phi_i'(q)$ expressed in terms of $\phi$ specified over $\partial B$. This describes an interior Dirichlet problem specified over the boundary. It has been shown in Jaswon and Symm (1977) and similarly in Kress (1989) that there exist a unique solution for $\phi_i'(q)$.

(b) Given $\phi_i'$ over $\partial B$, relation (2.3.16) yields the equation

$$\int_{\partial B} g(p,q)_i'\phi(q)dq - 2\pi\phi(p) = \int_{\partial B} g(p,q)\phi_i'(q)dq, \quad p \in \partial B \tag{2.3.22}$$

which is a Fredholm integral equation of the second kind in $\phi$ in terms of $\phi_i'$ given over $\partial B$. This describes an interior Neumann problem in $\phi$ for $\phi_i'$ given on $\partial B$. General solution of (2.3.22) appears as $\phi = \phi_0 + k$ (Jaswon and Symm 1977) and this can be made unique on proper choice of k.

**(ii) Exterior Problems**

(a) Given $\phi$ on $\partial B$, the boundary formula (2.3.19) yields the equation

$$\int_{\partial B} g(p,q)\phi_e'(q)dq = \int_{\partial B} g(p,q)_e'\phi(q)dq - 2\pi\phi(p), \quad p \in \partial B. \tag{2.3.23}$$

This is an exterior Dirichlet problem expressed in a Fredholm integral equation of the first kind for $\phi_e'$ in terms of $\phi$ given over $\partial B$ and as the exterior Dirichlet problem exists a unique solution (Kress 1989). So solution to (2.3.23) also uniquely defines over $\partial B$.

(b) Given $\phi_e'$ over $\partial B$, relation (2.3.19) yields the boundary equation

$$\int_{\partial B} g(p,q)_e' \phi(q)dq - 2\pi\phi(p) = \int_{\partial B} g(p,q)\phi_e'(q)dq, \quad p \in \partial B \tag{2.3.24}$$

which expresses an exterior Neumann problem in $\phi$, by an integral equation of the second kind for $\phi$, in terms of $\phi_e'$ given over $\partial B$. Solution $\phi$ of (2.3.24) exists and it is unique over $\partial B$ (Jaswon and Symm 1977).

## 2.3.5 Green's Formulae for Half-Space Domain

(i) For a harmonic function $\phi$ defined in an interior domain $B_1$ bounded by a smooth closed boundary $\partial B = S + S_U$, such that $S_U$ is a hemispherical surface of a large radius R (Fig.2.3.3). Given $\phi$ and its interior normal derivative $\phi_1'$ on $\partial B$, the $\phi$ at an interior point P is given by (2.3.15) as
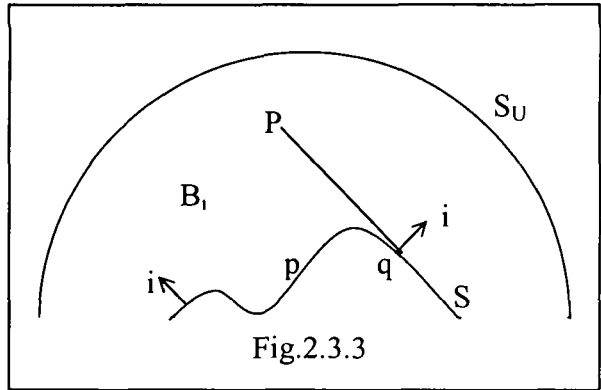
Fig.2.3.3

$$4\pi\phi(P) = \int_{\partial B} g(P,q)_1' \phi(q)dq - \int_{\partial B} g(P,q)\phi_1'(q)dq$$

$$= \int_{S} g(P,q)_1' \phi(q)dq - \int_{S} g(P,q)\phi_1'(q)dq$$

$$+ \int_{S_U} g(P,q)_1' \phi(q)dq - \int_{S_U} g(P,q)\phi_1'(q)dq, \quad P \in B_1, \tag{2.3.25}$$

where $g(P,q) = |P-q|^{-1}$ as usual. For a regular $\phi$ in $B_1$ as $S_U$ moves to infinity the contribution of each the integrals described over $S_U$ to the field point P becomes zero of the same O( 1/r ), $r \to \infty$. This follows from the fact that

$$\int_{S_U} g(P,q)_1' \phi(q)dq = \int_{S_U} |q - P|^{-1}_1 \phi(q)dq$$

21

$$= \lim_{r \to \infty} \int_{S_U} O(r^{-2}).O(r^{-1}).r^2 d\omega$$

$$= O(r^{-1}), \ r \to \infty. \tag{2.3.26}$$

For $dq = r^2 d\omega$, where $d\omega$ is the solid angle subtended by $dq$ at the point P. Hence, as $S_U$ moves to infinity, the formula (2.3.25) yields the Green's formula for the upper half-space domain as

$$4\pi\phi(P) = \int_S g(P,q)_{,i}\phi(q)dq - \int_S g(P,q)\phi_{,i}(q)dq. \tag{2.3.27}$$

It is to be noted here that the formula (2.3.27) is deduced assuming $\phi$ is regular, i.e. $\phi = O(r^{-1})$, $r \to \infty$, in the upper half-space domain. It is evident from (2.3.26) that the formula (2.3.25) holds for a $\phi$ with asymptotic behaviour $\phi = O(r^{-n})$, $n \geq 1$, $r \to \infty$.

(ii) Considering the upper half-space domain as an exterior domain $B_e$ bounded at the interior by a closed boundary $\partial B (= S + S_w$, Fig. 2.3.4), we find

$$4\pi\phi(P) = \int_S g(P,q)_{,e}\phi(q) - \int_S g(P,q)\phi_{,e}(q)dq + \int_{S_w} g(P,q)_{,e}\phi(q)dq - \int_{S_w} g(P,q)\phi_{,e}(q)dq,$$

by (2.3.18). Following the same analysis as carried out in (2.3.26) for $P \in B_e$ the above formula yields

$$4\pi\phi(P) = \int_S g(P,q)_{,e}\phi(q)dq - \int_S g(P,q)\phi_{,e}(q)dq.$$

$$\tag{2.3.28}$$

Formulae (2.3.27) and (2.3.28) are identical in all respects, both representing Green's



Fig.2.3.4

formula for the same upper half–space domain with interchange of unit normals i and e both pointing towards upper half-space domain over S. Hence, for mathematical convenience, the upper half–space domain can be treated either interior or exterior as one wishes.
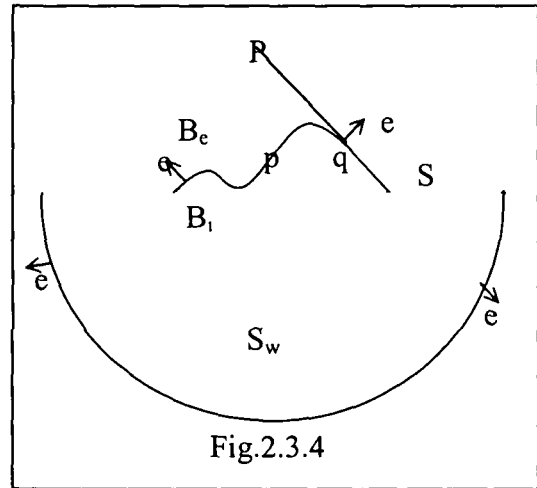
(iii) Green's boundary formula for interior domain $B_i$ is given by expression (2.3.16) as

$$2\pi\phi(p) = \int_{\partial B} g(p,q)_i'\phi(q)dq - \int_{\partial B} g(p,q)\phi_i'(q)dq, \quad p \in \partial B.$$

Considering $\partial B = S + S_U$ (Fig.2.3.3) and following the same procedure as carried out in the case of (2.3.25), we arrive at

$$2\pi\phi(p) = \int_{S} g(p,q)_i'\phi(q)dq - \int_{S} g(p,q)\phi_i'(q)dq, \quad p \in S. \tag{2.3.29}$$

Depending on boundary data two cases arise in (2.3.29):

   a) Given $\phi$ over S, formula (2.3.29) yields a boundary integral equation of the 1st

      kind in $\phi_i'$. This expresses a Dirichlet problem for $\phi_i'$ in terms of $\phi$ over S,

   b) Given $\phi_i'$ over S, formula (2.3.29) yields a boundary integral equation of the 2nd

      kind in $\phi$. This expresses a Nuemann problem for $\phi$ in terms of $\phi_i'$ over S.


(iv) Green's boundary formula for exterior domain $B_e$ is given by expression (2.3.19) as

$$2\pi\phi(p) = \int_{\partial B} g(p,q)_e'\phi(q)dq - \int_{\partial B} g(p,q)\phi_e'(q)dq, \quad p \in \partial B.$$

Considering $\partial B = S + S_w$ (Fig.2.3.4) and following the same procedure carried out in the case of (3.2.28), we arrive at

$$2\pi\phi(p) = \int_{S} g(p,q)_e'\phi(q)dq - \int_{S} g(p,q)\phi_e'(q)dq, \quad p \in S. \tag{2.3.30}$$


Depending on boundary data two cases arise in (2.3.30):

   a) Given $\phi$ over S, formula (2.3.30) yields a boundary integral equation of the 1st

      kind in $\phi_e'$. This expresses a Dirichlet problem for $\phi_e'$ in terms of $\phi$ over S,

b) Given $\phi_e'$ over S, formula (2.3.30) yields a boundary integral equation of the 2nd kind in $\phi$. This expresses a Nuemann problem for $\phi$ in terms of $\phi_e'$ over S.

The formula (2.3.29) and (2.3.30) are also identical in all respects, both representing Green's formula for the same boundary S with interchange of unit normals i and e both pointing towards the half-space domain over S.

# Chapter-3

# HALF-SPACE PROBLEMS IN POTENTIAL THEORY

## 3.1 Representation of Harmonic Function as a Simple and Double Layer Potentials

A harmonic function $\phi$ may be represented throughout the interior domain $B_i$ by Green's formula. On the other hand this may also be represented by a simple layer potential or by a double layer potential. To bring out the connection between these different representations, following Jaswon and Symm (1977), we introduce an arbitrary regular exterior harmonic function f into the exterior domain $B_e$, such that it satisfies the expression (2.3.20) i.e.,

$$\int_{\partial B} g(P,q)'_e f(q)dq - \int_{\partial B} g(P,q)f'_e(q)dq = 0, \quad P \in B_i. \tag{3.1.1}$$

Superposition of this on Greeen's formula (2.3.15) for interior domain, i.e., on

$$\int_{\partial B} g(P,q)'_i \phi(q)dq - \int_{\partial B} g(P,q)\phi'_i(q)dq = 4\pi\phi(P), \quad P \in B_i, \tag{3.1.2}$$

yields the more general continuation formula

$$\int_{\partial B} g(P,q)'_i(\phi(q) - f(q))dq - \int_{\partial B} g(P,q)\left(\phi'_i(q) + f'_e(q)\right)dq = 4\pi\phi(P), P \in B_i. \tag{3.1.3}$$

Now, we consider two distinct possibilities for f.

The first is $f = \phi$ over $\partial B$, providing the representation

$$4\pi\phi(P) = - \int_{\partial B} g(P,q)\left[\phi'_i(q) + f'_e(q)\right]dq, \quad P \in B_i \tag{3.1.4}$$

which is similar to the simple layer potential generated by the source density

$$\sigma = -\frac{1}{4\pi}\left(\phi_i' + f_e'\right).$$

(3.1.5)

This possibility hinges upon the existence of a unique regular f in $B_e$ satisfying $f = \phi$ over $\partial B$, as it is in fact ensured by the exterior Dirichlet existence theorem. The second possibility is $f_e' = -\phi_i'$ over $\partial B$, providing the representation

$$4\pi\phi(P) = \int_{\partial B} g(P,q)_i'[\phi(q) - f(q)]dq, \quad P \in B_i$$

(3.1.6)

which may be identified as the double layer potential generated by source density

$$\mu = \frac{1}{4\pi}(\phi - f).$$

(3.1.7)

This possibility hinges upon the existence of a unique regular f in $B_e$ satisfying $f_e' = -\phi_i'$ over $\partial B$, as it is in fact ensured by the exterior Nuemann existence theorem.

In the case of a harmonic function $\phi$ vanishing at infinity at least in $O(r^{-n})$, $n \geq 1$, the above statements remain valid as these can be derived as a special case of close domain exterior as well as interior problem following article (2.3.5). So, analogous to statements (3.1.4) and (3.1.6), considering $f = \phi$ and $f_i' = -\phi_e'$ respectively, the expression for exterior half-space problem will be

$$4\pi\phi(P) = -\int_{\partial B} g(P,q)[\phi_e'(q) + f_i'(q)]dq, \quad P \in B_e$$

(3.1.8)

which is similar to the simple layer potential generated by the source density

$$\sigma = -\frac{1}{4\pi}\left(f_i' + \phi_e'\right)$$

(3.1.9)

and

$$4\pi\phi(P) = \int_{\partial B} g(P,q)'_e [f(q) - \phi(q)]dq, \quad P \in B_e \qquad (3.1.10)$$

which may be identified as the double layer potential generated by source density

$$\mu = \frac{1}{4\pi}(f - \phi). \qquad (3.1.11)$$

The representation (3.1.8) remains valid at $\partial B$, so yielding the boundary relation

$$\int_{\partial B} g(p,q)\sigma(q)dq = \phi(p), \quad p \in \partial B \qquad (3.1.12)$$

where, $\sigma$ is given by (3.1.9). This may be regarded as an integral equation in $\sigma$ in terms of $\phi$, to which a unique solution exists since $\phi'_e$ and $f'_i$ uniquely exist. Similarly the representation (3.1.10) jumps by $-2\pi\mu(p)$ at $\partial B$, so yielding the boundary relation

$$\int_{\partial B} g(p,q)'_e \mu(q)dq + 2\pi\mu(p) = \phi(p), \quad p \in \partial B. \qquad (3.1.13)$$

where $\mu$ is given by (3.1.11). This may be regarded as integral equation for $\mu$ in terms of $\phi$, to which a unique solution exists since $f$ uniquely exists.

## 3.2 Half-space Problems in Simple and Double Layer Potentials

For a regular harmonic function $\phi$ defined in an exterior domain $B_e$ bounded at the interior by a closed boundary $\partial B (= S + S_w,$ Fig. 2.3.4), we may write $\phi$ following (3.1.8) and (3.1.10) as

$$\phi(P) = \int_S g(P,q)\sigma dq + \int_{S_w} g(P,q)\sigma dq, \quad P \in B_e \qquad (3.2.1)$$

where,

$$\sigma = -\frac{1}{4\pi}\left(f_i^{'} + \phi_e^{'}\right) = O(\phi_e^{'})$$

and

$$\phi(P) = \int_S g(P,q)_e^{'} \mu dq + \int_{S_w} g(P,q)_e^{'} \mu dq, \quad P \in B_e \tag{3.2.2}$$

where,

$$\mu = \frac{1}{4\pi}\left(f - \phi\right) = O(\phi).$$

Following the same analysis as carried out in (2.3.26) for $P \in B_e$ the above formula yields

$$\phi(P) = \int_S g(P,q)\sigma dq, \quad P \in B_e \tag{3.2.3}$$

and

$$\phi(P) = \int_S g(P,q)_e^{'} \mu dq, \quad P \in B_e. \tag{3.2.4}$$

The relation (3.2.3) is valid for the boundary S, so yielding the boundary relation as

$$\phi(p) = \int_S g(p,q)\sigma dq, \quad p \in S. \tag{3.2.5}$$

For $\phi$ given on S the expression (3.2.5) may be regarded as integral equation in $\sigma$. This has unique $\sigma$ as shown in (3.1.6). Similarly the representation (3.2.4) jumps by $-2\pi\mu(p)$ at S, so yielding the boundary relation

$$\phi(p) = \int_S g(p,q)_e^{'} \mu dq + 2\pi\mu(p), \quad p \in S. \tag{3.2.6}$$

For given $\phi$, this may also be regarded as integral equation in $\mu$ to which unique solution exists as shown in (3.1.7) since f exists uniquely.

# Chapter-4

# APPLICATON TO GEOPHYSICS

## 4.1 Representation of Gravity-Magnetic Fields by Simple Layer Boundary Density

For $\phi$ denoting either a gravity field or a component magnetostatic field in $B_e+S$ (Fig. 4.1.1), $\phi$ in $B_e$ is a harmonic function with asymptotic behaviour $\phi = O(r^{-n})$, $n \geq 2$, as $r \to \infty$. As such following (3.2.3), reproduction of $\phi$ in $B_e$ can be obtained as potential due to simple layer density as



Fig.4.1.1
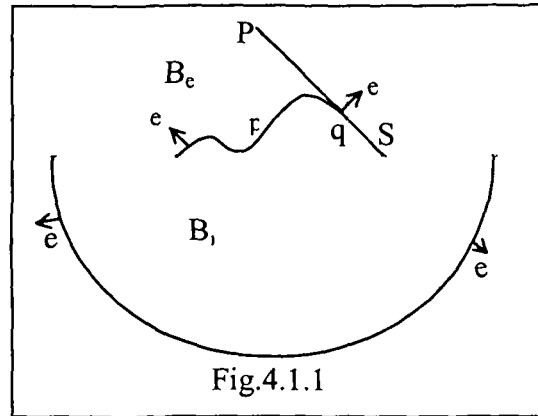
$$\phi(P) = \int_S |q - P|^{-1} \sigma(q) \, dq, \qquad P \in B_e, \qquad (4.1.1)$$

where $\sigma(q)$ is the simple layer boundary density over S at the point q. The gravity and the magnetic field are continuous in $B_e+S$. For the field point P coinciding with the boundary point p, following (3.2.5), we obtain the boundary formula

$$\phi(p) = \int_S |q - p|^{-1} \sigma(q) \, dq, \qquad p \in S. \qquad (4.1.2)$$

Given $\phi$ over S, equation (4.1.2) expresses a Fredholm integral equation of first kind in $\sigma$ in terms of $\phi$ specified over S. It has been shown in (3.2.5) and (3.1.6) that the equation has a unique $\sigma$ over S. Once the $\sigma$ is known as solution of equation (4.1.2), $\phi$ in $B_e$ can be computed by (4.1.1).

29

Now, as **P** moves to infinity, the formula (4.1.1) yields

$$\phi(P) = O\left(\left|P\right|^{-1}\right)\int_S \sigma(q)dq, \quad P \to \infty.$$

For $\phi$ representing the gravity field, $\phi = O(r^{-2})$, $r \to \infty$. As such,

$$\int_S \sigma(q)\, dq = 0$$

For $\phi$ representing a component magnetostatic field, $\phi = O(r^{-3})$, $r \to \infty$. As such for this case also

$$\int_S \sigma(q)\, dq = 0 \qquad\qquad (4.1.3)$$

for $\phi$ representing gravity and component magnetostatic field.

## 4.2 Gravity-Magnetic Fields by Double Layer Boundary Density

For $\phi$ denoting either a gravity field or a component magnetostatic field in $B_e+S$, $\phi$ in $B_e$ is a harmonic function with asymptotic behaviour $\phi = O(r^{-n})$, $n \geq 2$, as $r \to \infty$. As such upward continuation of $\phi$ in $B_e$ can be obtained as a potential due to double layer boundary density by (3.2.4) as

$$\phi(P) = \int_S {}'_e \left|q - P\right|^{-1} \mu(q)\, dq, \qquad P \in B_e \qquad\qquad (4.2.1)$$

where $\mu(q)$ is the double layer boundary density over S at the point q. For the field point P coinciding with boundary point p, we obtain the boundary formula (3.2.6) as

$$\phi(p) = 2\pi\mu(p) + \int_S {}'_e \left|q - p\right|^{-1} \mu(q)\, dq, \qquad p \in S. \qquad\qquad (4.2.2)$$

because the double layer potential jumps by an amount $-2\pi\mu(p)$ at the boundary,

Given $\phi$ over S, equation (4.2.2) presents a boundary integral equation of 2nd kind in $\mu$, which expresses a Dirichlet problem in $\mu$ in terms of $\phi$ over S. It has been shown in (3.2.6) and (3.1.7) that this equation has a unique solution over S. Once $\mu$ is known over S, $\phi$ at $P \in B_e$ can be computed by (4.2.1).

As $|\mathbf{P}| \to \infty$, formula (4.2.1) yields

$$\phi(P) = O\left(|\mathbf{P}|^{-2}\right) \int_S \mu(q)\, dq, \quad |\mathbf{P}| \to \infty. \tag{4.2.3}$$

For $\phi$ representing a gravity field with asymptotic behaviour $\phi = O\left(|\mathbf{P}|^{-2}\right)$, $|\mathbf{P}| \to \infty$, it is evident from (4.2.3) that

$$\int_S \mu(q)\, dq \neq 0 \tag{4.2.4}$$

necessarily.

For $\phi$ representing a magneto-static component field with asymptotic behaviour $\phi = O\left(|\mathbf{P}|^{-3}\right)$, $|\mathbf{P}| \to \infty$, it is evident from (4.23) that

$$\int_S \mu(q)\, dq = 0. \tag{4.2.5}$$

## 4.3 Gravity-Magnetic Fields by Green's Formula

For $\phi$ representing a gravity or a magneto-static component field in the upper half-space domain $B_e$ bounded below by S, $\phi$ is a harmonic function in $B_e$ with asymptotic behaviour $\phi = O(r^{-n})$, $n \geq 2, r \to \infty$. As such given $\phi$ over S, following (2.3.28), $\phi$ in $B_e$ can be obtained by Green's formula

$$4\pi\phi(P) = \int_S |q - p|^{-1}\phi(q)dq - \int_S |q - p|^{-1}\phi_e'(q)dq, \quad P \in B_e \qquad (4.3.1)$$

on obtaining $\phi_e'$ over S as a solution of the boundary integral equation

$$2\pi\phi(p) = \int_S |q - p|^{-1}\phi(q)dq - \int_S |q - p|^{-1}\phi_e'(q)dq, \quad p \in S. \qquad (4.3.2)$$

Given $\phi$ over S, equation (4.3.2) represents a boundary integral equation of the first kind in $\phi_e$ in terms of $\phi$ specified over S. It has been shown in (2.3.24) that this equation has a unique $\phi_e'$ over S. With this $\phi_e'$ over S, $\phi$ at a point $P \in B_e$ can be obtained by (4.3.1).

As $|\mathbf{P}| \to \infty$, the formula (4.3.1) yields

$$4\pi\phi(P) = O(|P|^{-2})\int_S \phi(q)dq - O(|P|^{-1})\int_S \phi_e'(q)dq, \quad P \to \infty. \qquad (4.3.3)$$

Since both gravity and component magnetic fields vanish at infinity in $O(|P|^{-n}), n \geq 2,$ and $\int_S \phi(q)dq$ being bounded, it is evident from (4.3.3) that

$$\int_S \phi_e'(q)dq = 0 \qquad (4.3.4)$$

for both gravity and magnetic cases.

# Chapter-5

# NUMERICAL PROCEDURE

To carry out computational work involving a harmonic function $\phi$, with asymptotic behaviour $\phi = O(r^{-n})$, $n \geq 1$, $r \to \infty$, defined in the upper half-space domain $B_e$, we are to make certain compromises. To solve the problem we choose a large finite boundary surface S and assume that the contribution from the rest part of the half-space boundary is negligibly small at its periphery. Subsequently we delete the solution over the peripheral part and accept it over the central part of S for any practical purpose.

## 5.1 Discretisation of Equations

### 5.1.1 Simple Layer Formulae

A regular harmonic function $\phi$ can be reproduced in the upper half-space domain as a potential of simple layer boundary density. For $\phi$ denoting gravity or a component magnetic field due to a subsurface causative mass m, in the upper half-space domain $B_e$ bounded bel.ow by a ground surface S, given $\phi$ over S, $\phi$ in $B_e$ can be reproduced by simple layer boundary density $\sigma$ by (4.1.1)

$$\phi(P) = \int_S |q - P|^{-1} \sigma(q) \, dq, \qquad P \in B_e, \qquad (5.1.1)$$

To find the numerical value of $\phi$ at $P \in B_e$, we divide the boundary S into n subareas $\Delta S_j$, j=1, 2, ... ...., n and make the fundamental assumption that the function $\sigma$ is constant over a subarea. Under this assumption the formula (5.1.1) becomes

$$\tilde{\phi}(P) = \sum_{j=1}^{n} \sigma_j \int_{\Delta S_j} |q - P|^{-1} dq, \qquad (5.1.2)$$

33

where $\tilde{\phi}$ is the approximation to $\phi$ at P and $\sigma_j$ is constant value of $\sigma$ over the j-th subarea $\Delta S_j$. On finding the $\sigma_j$ over S, an approximation to $\phi$ at P can be obtained by (5.1.1). To find $\sigma_j$ over S, we are to solve the boundary integral equation (4.1.2) in $\sigma$.

To solve it numerically we divide the boundary S into n subareas $\Delta S_j$, $j=1, 2, \ldots \ldots$, n as done earlier and find the nodal point (centroid) of each subarea. For $q_k$ defining the nodal point of k-th subaraea $\Delta S_k$ and p of (4.1.2) coinciding with $q_k$ we obtain '

$$\phi_k = \sum_{j=1}^{n} \sigma_j \int_{\Delta S_j} |q - q_k|^{-1} dq$$

$$= \sum_{j=1}^{n} a_{kj} \sigma_j. \qquad (5.1.3)$$

where $\phi_k$ is the value of $\phi$ at the nodal point $q_k$, $\sigma_j$ is the constant value of $\sigma$ over j-th subarea $\Delta S_j$ and

$$a_{k,j} = \int_{\Delta S_j} |q - q_k|^{-1} dq. \qquad (5.1.4)$$

For successively assuming the values 1, 2, 3,........., n for k, we obtain

$$\sum_{j=1}^{n} a_{kj} \sigma_j = \phi_k, \quad k= 1, 2, 3 \ldots \ldots, n. \qquad (5.1.5)$$

For $\phi_k$ specified over $\Delta S_k$, k=1, 2, 3, ........, n, the equation (5.1.5) provides a system of n simultaneous linear algebraic equations in n unknowns $\sigma_j$, j = 1, 2, 3, ......., n. On finding the $\sigma_j$ as solution of (5.1.5), the field $\phi$ at a point $P \in B_e$ can be computed by (5.1.2), the discretised version of (5.1.1).

## 5.1.2 Double Layer Formulae

It is also possible to reproduce a regular harmonic function $\phi$ in the upper half-space domain as potential of double layer density $\mu$ over the boundary surface S. On dividing the boundary S into n subareas and assuming that the $\mu$ is constant over a subarea, the formula (4.2.1) yields

$$\widetilde{\phi}(P) = \sum_{j=1}^{n} \mu_j \int_{\Delta S_j} |q - P|^{-1} dq, \tag{5.1.6}$$

where $\widetilde{\phi}(P)$ is the approximate value of $\phi$ at P, $\mu_j$ is constant value of $\mu$ over the j-th subarea $\Delta S_j$. The $\widetilde{\phi}$ at $P \in B_e$, can be obtained from (5.1.6) on finding the $\mu_j$ as a solution of the boundary equation (4.2.2).

For the field point $q_j$ defining the nodal point of j-th subarea $\Delta S_j$ and the field point p of (4.2.2) coinciding with the nodal point of k-th subarea $\Delta S_k$, the equation (4.2.2) yields

$$\phi_k = 2\pi \mu_k + \sum_{j=1}^{n} \mu_j \int_{\Delta S_j} |q - q_k|^{-1} dq, \tag{5.1.7}$$

$$b_{kj} = \int_{\Delta S_j} |q - q_k|^{-1} dq \tag{5.1.8}$$

For k assuming successively the values 1, 2, 3, ......., n as $q_k$ moves over S, the equation (5.1.7) yields a system of n simultaneous algebraic equations in n unknowns $\mu_j$, j=1, 2, ......, n for $\phi_k$ specified over S. These equations (5.1.7) can be rewritten as

$$\phi_k = 2\pi \mu_k + \sum_{j=1}^{n} \mu_j b_{kj},$$

35

where $\phi_k$ is the value of $\phi$ at the nodal point $q_k$ of $\Delta S_k$ and $b_{kj} = \int_{\Delta S_j} {}_e |q - q_k|^{-1} dq$

This can be rewritten as

$$\sum_{j=1}^{n} (2\pi\delta_{kj} + b_{kj})\mu_j = \phi_k, \ k=1, 2, 3, \ldots\ldots, n,$$  (5.1.9)

where $\delta_{kj}$ is the Kronecker delta.

On finding the $\mu_j$ as solution of (4.2.2), the field $\phi$ at a point $P \in B_e$ can be computed by discretised version of (4.2.1).

## 5.1.3 Green's Formulae

For a harmonic function $\phi$ with asymptotic behaviour $\phi = O(r^{-n})$, $n \geq 1, r \to \infty$, defined in the upper half-space domain $B_e$ bounded below by S, given $\phi$ over S, $\phi$ in $B_e$ can be obtained by Green's formulae (4.3.1) on obtaining $\phi_e'$ over S as a unique solution of (4.3.2). For a numerical approach to solve the equations (4.3.2) and subsequently to reproduce $\phi$ in $B_e$, as before let us divide a large finite boundary S into n subareas $\Delta S_j$, j=1, 2, 3,......., n and assume that $\phi$ is constant over a subarea, its value being associated with the nodal point of the subarea. Under this condition the discretised version of the formula (4.3.1) becomes

$$4\pi\tilde{\phi}(P) = \sum_{j=1}^{n} \left[ \phi_j \int_{\Delta S_j} {}_e |q - P|^{-1} dq - \phi_{e_j}' \int_{\Delta S_j} |q - P|^{-1} dq \right],$$  (5.1.10)

where $\tilde{\phi}(P)$ is the approximate value of $\phi(P)$, $\phi_j$ is the constant value of $\phi$ over j-th subarea $\Delta S_j$ and $\phi_{e_j}'$ is constant value of $\phi_e'$ over $\Delta S_j$ and that of (4.3.2) becomes

$$2\pi\phi_k = \sum_{j=1}^{n}\left[\phi_j \int_{\Delta S_j}\mathbf{|q - q_k|^{-1}}dq - \phi_{e_j}^{'}\int_{\Delta S_j}\mathbf{|q - q_k|^{-1}}dq\right], \qquad (5.1.11)$$

where $\phi_k$ is the value of $\phi$ at the nodal point $q_k$ of $\Delta S_k$.

For k assuming successively the values 1, 2, 3, ......., n as $q_k$ moves over S, the above equation on reorganization yields

$$\sum_{j=1}^{n}\phi_{e_j}^{'}\int_{\Delta S_j}\mathbf{|q - q_k|^{-1}}dq = \sum_{j=1}^{n}\phi_j\int_{\Delta S_j}\mathbf{|q - q_k|^{-1}}dq - 2\pi\phi_j\delta_{kj}, \quad k = 1,2,...,n. \quad (5.1.12)$$

Denoting as before $\int_{\Delta S_j}\mathbf{|q - q_k|^{-1}}dq$ and $\int_{\Delta S_j}\mathbf{|q - q_k|^{-1}}dq$ by $a_{kj}$ and $b_{kj}$ respectively the above equation (5.1.12) takes the form

$$\sum_{j=1}^{n}\phi_{e_j}^{'}a_{kj} = \sum_{j=1}^{n}\phi_j b_{kj} - 2\pi\phi_j\delta_{kj}, \text{k=1, 2, 3, ........, n}$$

$$\sum_{j=1}^{n}\phi_{e_j}^{'}a_{kj} = D_k, \text{k=1, 2, 3, ......., n,} \qquad (5.1.13)$$

where $D_k = \sum_{j=1}^{n}\phi_j b_{kj} - 2\pi\phi_j\delta_{kj}$

The equation (5.1.13) represents a system of n simultaneous linear algebraic equations in n unknowns $\phi_{e_j}^{'}$. On finding $\phi_{e_j}^{'}$ as a solution of equation (5.1.13), $\phi$ at a point $q_k \in B_e$ can be computed by (5.1.10), the discretised version of (4.3.1).

## 5.2 Evaluation of Coefficients

To solve the equations (5.1.5), (5.1.9) and (5.1.13), we are to evaluate the coefficients $a_{kj}$ and $b_{kj}$. Depending on the values of j and k two distinct cases arise:

i)      For j = k, the integral is singular and it is to be evaluated analytically.

ii)      For j ≠ k, the integral is regular and it can be evaluated analytically or an approximation to them by a numerical means may suffice our purpose.

## 5.2.1 Evaluation of Coefficients for Singular Integrals

To evaluate the singular integral $a_{kk}$ and $b_{kk}$, we consider that the subareas are piecewise flat. Under this assumption to evaluate the singular integral $a_{kk}$, we divide k-th subarea into 3 (4 in case of a rectangular sub-area) triangular sub-areas with their vertices at $q_k$ and evaluate the integral over each of them by the formula (Jaswon and Symm 1977)

$$I = \frac{2\Delta}{a} \log\left(\frac{b + c + a}{b + c - a}\right),$$ 
(5.2.1)

where $\Delta$ is the area of the triangle ABC, $q_k$ coinciding with the vertex A and a, b, c are as usual defining the sides BC, CA, AB respectively of ABC.

To evaluate the singular integral $b_{kk}$, we consider that the subareas are piecewise flat. Under this assumption

$$b_{kk} = \int_k' |\mathbf{q}_k - \mathbf{q}|^{-1} dq = 0, \quad q_k, q \in \Delta S_k$$ 
(5.2.2)

since $_c'|\mathbf{q}_k - \mathbf{q}| = 0$, for $q_k \neq q$ and both lying on the flat k-th subarea and for $q = q_k$, the integral is having a singularity at the isolated point $q_k$, a set of measure zero.

## 5.2.2 Evaluation of Coefficients for Regular Integrals

**i) Approximation of Regular Integrals**

Approximations to $a_{kj}$ and $b_{kj}$, $j \neq k$ can be computed by the centroid rule (Hess and Smith 1967, Laskar 1977). In this method the kernel is considered to be constant; its value being associated with the centroid (nodal point) of the subarea.

Let $I_c$ be the centroid method of approximation to a regular integral of $f(P,q)$ over a subarea $\Delta S$ for $q \in \Delta S$ and P lying outside it. Following the definition,

$$I_c \cong \int_{\Delta S} f(P,q) dq$$

$$\cong f(P,q_0) \int_{\Delta S} dq ,$$

$q_0$ defining the centroid of $\Delta S$. It has been shown by Laskar (1977) that if D be the largest diagonal of $\Delta S$, then the percentage of error in $I_c$ becomes less than 1% if $|P - q_0| \geq 2D$. The error increases when P approaches to $q_0$. The formula is applicable to all kinds of acceptable subareas.

In the case of simple layer representation of the problem

$$I_c = \int_{\Delta S_j} f(P,q) dq = \int_{\Delta S_j} |q - q_k|^{-1} dq \cong |q_0 - q|^{-1} \int_{\Delta S_j} dq \qquad (5.2.3)$$

and for the double layer case,

$$I_c = \int_{\Delta S_j} {}_e|q - q_k|^{-1} dq \cong {}_e|q_0 - q|^{-1} \int_{\Delta S_j} dq \qquad (5.2.4)$$

$q_0$ defining the centroid of the j-th subarea $\Delta S_j$

## ii) Analytical Evaluation of Regular Integrals

We know that for a triangular area ABC and a field point P defined in a cartesian reference frame, the coordinates of the vertices of ABC and those of P can be described in a new

frame with its origin at the foot of the perpendicular dropped from P to the plane of ABC and the (x,y)-plane of the new frame coinciding with the plane of the triangle. This set up can be achieved by necessary transformations.

For analytical evaluation of regular integrals involved in $a_{kj}$ and $b_{kj}$, we consider a flat and triangular subarea and define it by ABC (Fig.5.2.1). To evaluate an integral over the subarea ABC, we consider it as a combination of integrals over the triangular subareas FAB, FBC and FCA with a common vertex at F, the foot of the perpendicular dropped from $q_k$ at the plane of the subarea ABC (Fig.5.2.1).



Fig.5.2.1
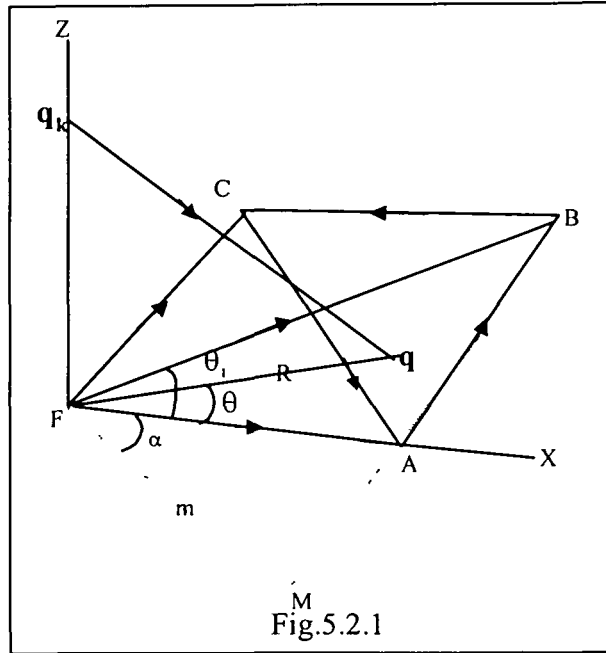
For $f(q_k,q)$ defining the integrand of a regular integral, the integral A over the area ABC is given by

$$A = \int_{\Delta S} f(q_k,q)dq = \eta_1 \int_{FAB} f(q_k,q)dq + \eta_2 \int_{FBC} f(q_k,q)dq + \eta_3 \int_{FCA} f(q_k,q)dq, \qquad (5.2.5)$$

where $\hat{e}\eta_1 = \dfrac{\overrightarrow{FA} \times \overrightarrow{FB}}{\left|\overrightarrow{FA} \times \overrightarrow{FB}\right|}$, $\hat{e}\eta_2 = \dfrac{\overrightarrow{FB} \times \overrightarrow{FC}}{\left|\overrightarrow{FB} \times \overrightarrow{FC}\right|}$, $\hat{e}\eta_3 = \dfrac{\overrightarrow{FC} \times \overrightarrow{FA}}{\left|\overrightarrow{FC} \times \overrightarrow{FA}\right|}$.

It is evident from the above formula that $\eta_1 = 1$, $\eta_2 = 1$, $\eta_3 = -1$ and as such the expression (5.2.5) defines the integral of $f(q_k,q)$ over the triangular subarea ABC. Evaluation of the integral of $r^{-1}$ and $\partial r^{-1}/\partial n$ for r defined by $|q_k - q|$ and $\hat{n}$ defining the vector $(\overrightarrow{FA} \times \overrightarrow{FB})/|\overrightarrow{FA} \times \overrightarrow{FB}|$ in the outward direction of $\Delta S$ (=ABC) are discussed for the various position of $q_k$, which is valid for any orientation of the triangular subarea.

## a. Evaluation of the Integral of $|q - q_k|^{-1}$

For $f(q_k, q) = |q - q_k|^{-1}$, the integral over the triangular sector FAB ( Fig.5.2.1) is regular and it can be expressed as

$$I_{FAB} = \int_{FAB} f(q_k, q) dq = \int_{FAB} |q - q_k|^{-1} dq$$

$$= \int_{\theta=0}^{\theta_1} \int_{R=0}^{R(\theta)} \frac{RdRd\theta}{\sqrt{R^2 + h^2}} = \int_{\theta=0}^{\theta_1} \left[\sqrt{R^2 + h^2}\right]_{R=0}^{mSec(\theta-\alpha)} d\theta$$

$$= \left[h\left(\tan^{-1}\frac{h\tan(\theta-\alpha)}{D} - \theta\right) + m\ln\left\{\tan(\theta-\alpha) + \frac{D}{m}\right\}\right]_{\theta=0}^{\theta_1}, \quad h \neq 0,$$

$$(5.2.6)$$

where m is the perpendicular drawn from F to the line of AB, $\theta_1$ is the angle between FA and FB, $\alpha$ is the angle made by the perpendicular m with FA, the arm coinciding with x-axis, $h = |z|$, z defining the z co-ordinate of $q_k$ in the local cartesian co-ordinate system with origin at F, $\vec{R}(=\vec{Fq})$ makes an angle $\theta$ with x-axis (Fig.4.2.1) and $D = \sqrt{m^2 \sec^2(\theta - \alpha) + h^2}$.

For z = 0, i.e., for $q_k$ coinciding with F, the integral is singular. The value of integral however can be obtained by putting h=0 in (5.2.6) as

$$I_{FAB} = \left[m\ln\left(\tan(\theta-\alpha) + \frac{D}{m}\right)\right]_{\theta=0}^{\theta_1} = \frac{2\Delta}{AB}\ln\frac{FA + FB + AB}{FA + FB - AB}, \quad (5.2.7)$$

as shown in Jaswon and Symm (1977). This holds good for all positions of $q_k$ over the plane of the triangle ABC. Following the same procedure, the singular integrals over the other triangular sectors FBC and FCA can be computed for all positions of $q_k$ as $q_k$ moves along FZ, the z-axis of local frame.

41

## b. Evaluation of Integral of $_c|q - q_k|^{-1}$

### (i) Evaluation of Regular Integral

Considering $f(q_k,q) = {}_c|q - q_k|^{-1}$, the integral over the triangular sector FAB is

regular for $q_k$ does not coinciding with F. On evaluation of the integral, we find

$$J_{FAB} = \int_{FAB} f(q_k,q)dq = \int_{FAB} {}_c|q - q_k|^{-1}dq = z \int_{FAB} |q - q_k|^{-3}dq$$

$$= z \int_{\theta=0}^{\theta_1} \int_{R=0}^{R(\theta)} \frac{R\,dR\,d\theta}{(h^2 + R^2)^{\frac{3}{2}}} = z \int_{\theta=0}^{\theta_1} \left[ -\frac{1}{\sqrt{R^2 + h^2}} \right]_{R=0}^{m\sec(\theta-\alpha)} d\theta$$

$$= \frac{z}{h} \left[ \theta - \tan^{-1} \frac{h\tan(\theta - \alpha)}{D^2} \right]_{\theta=0}^{\theta_1}, \; h=|z| \neq 0. \tag{5.2.8}$$

To compute the integral for $z = 0$ i.e., for $q_k$ coinciding with F, we observe that

the multiplying factor $z/|z| = z/h$ in (5.2.8) is undefined for $z= 0$. Considering

$z/h = 1$, we find $J_{FAB} = \theta_1$.

### (ii) Evaluation of Singular Integral

Two cases arise depending the position of $P(=q_k)$ over $\overline{S}$, the plane of ABC

#### (1) The field point $q_k$ does not belong to triangle ABC

For $q_k$ lying outside ABC, the integral over triangle ABC is regular but it is

singular when described over the sector FAB for the field point

$q_k$ coinciding with F. The integral over ABC then can be obtained by (5.2.5)

on evaluation of the integrals over the triangular sectors FAB, FBC and

FCA. It is evident from the Fig.5.2.1 that when $J_{FAB} = \theta_1 = \angle AFB$, $J_{FAB}$

42

and $J_{FAC}$ will be $\angle BFC$ and $\angle CFA$ respectively. Now putting the values in (5.2.5) we find,

$$J(q_k) = J_{ABC} = 0,$$

for $\angle CFA = \angle AFC + \angle BFC$ and $\eta_1 = 1$, $\eta_2 = 1$ and $\eta_3 = -1$.

Alternatively, for $q_k$ lying in the plane of ABC,

$$J(q_k) = \int\limits_{ABC} {}_e'|q - q_k|^{-1} dq = -\int\limits_{\Delta S} |q - q_k|^{-3}(q - q_k).\hat{e}\,dq = 0, \quad (5.2.9)$$

since $(q - q_k).\hat{e} = 0$, as $q_k, q$ lying in the plane of ABC, $q_k \neq q$ and $\hat{e}$ defining the normal to the plane of ABC.

**(2) The field point $q_k$ belong to triangle ABC**

For $q_k$ to be an interior point of ABC, the integral $J(q_k)$ is singular. On expansion of the integrand as before, we find

$$J(q_k) = -\int\limits_{\Delta S} |q - q_k|^{-3}(q - q_k).\hat{e}\,dq = 0, \quad (5.2.10)$$

for $(q - q_k).\hat{e} = 0$, $q \neq q_k$ and $\hat{e}$ defining the direction of the normal to ABC and for $q = q_k$, the integral has a singularity at an isolated point $q_k$, a set of measure zero.

To carry out the integrals $I_{FBC}$ and $J_{FBC}$ over the triangular sector FBC, the (x,y)-plane is rotated about the new z-axis coinciding with $Fq_k$ such that the x-axis coincides with FB. Now, defining a new set of $\theta_1$, $\alpha$ and m for the sector FBC, the integrals are evaluated by (5.2.6) and (5.2.8) respectively. The same procedure is followed to evaluate the integrals over the sector FCA. Finally the integrals over ABC are evaluated by (5.2.5) on finding the values of $\eta_1$, $\eta_2$ and $\eta_3$.

## 5.3 Solutions of the Equations

The equations (5.1.3), (5.1.7) and (5.1.13) represents a system of n simultaneous linear algebraic equations in n unknowns $x_j, j = 1,2,....,n$. $x_j$ is $\sigma_j$ in case of (5.1.3), $\mu_j$ and $\phi'_j$ in case of (5.1.7) and (5.1.13) respectively. On evaluation of the corresponding coefficient matrices, the equations are solved by Gauss-Seidal iterative method.

In this method, the zeroth order approximation to the solution $x_j, j = 1,2,....,n$ is taken to be zero. The m-th order approximation to $x_j$ is given by

$$x_j^m = (\sum_{j=1}^{k-1} a_{kj} x_j^{m-1} + \sum_{j=k+1}^{n} a_{kj} x_j^{m-1}) / a_{kk}, \quad k = 1, 2, 3, \ldots\ldots, n, \qquad . \qquad (5.3.1)$$

where $a_{kj}$ are the elements of the coefficient matrix. Termination of the iterative process on improvement of the solution, as m increases is given by the condition

$$| x_k^m - x_k^{m-1} | \leq \varepsilon , \quad k=1, 2, 3, \ldots\ldots, n, \qquad\qquad (5.3.2)$$

for a preassigned small value of $\varepsilon$.

It is evident from (5.3.1) that the method works for $a_{kk} \neq 0$, k=1, 2, 3, ......., n and the convergence of the solution is faster for a diagonal dominant system. In the present study, the diagonal elements of (5.1.3), (5.1.7) and (5.1.13) are $\int_{\Delta S_k} |q - q_k|^{-1} dq$, $2\pi + \int_{\Delta S_k} |q - q_k|^{-1} dq$ and $\int_{\Delta S_k} |q - q_k|^{-1} dq$ respectively. It can be easily deduced from (5.2.7) that $\int_{\Delta S_k} |q - q_k|^{-1} dq \neq 0$ and the diagonal element of (5.1.5) contains an additional term $2\pi$ through the integral over $\Delta S_k$. This additional term not only makes the diagonal term nonzero, it makes the system a diagonal dominant one and makes the system highly suitable for application of Gauss-Seidal method for its solution.

# Chapter-6

# ANALYSIS OF MODEL DATA
# UPWARD CONTINUATION OF POTENTIAL FIELD

## 6.1 Boundary and Field Symmetrical about z-Axis

### 6.1.1 Approximation to Boundary and Causative Mass

Let a large horizontal plane with a partial hemispherical relief at its central part be defined in a cartesian reference frame with (x,y)-plane coinciding with the horizontal plane and the z-axis pointing upward through the pole of the spherical part of the surface. Let this surface be denoted by S. Let us now assume that a gravitating mass m and a vertically downward dipole of strength $\mu$ be placed at (0,0,-3), 3 units below the horizontal plane $\overline{S}$ defined by z = 0 and the partial hemispherical part of S with its pole at (0,0,1) meets $\overline{S}$ in a circle of radius $\sqrt{2R-1}$, R(= 7.464 units) defining the radius of curvature of the part S. The sharp edge of the relief over $\overline{S}$ is replaced by a smooth parabolic strip that
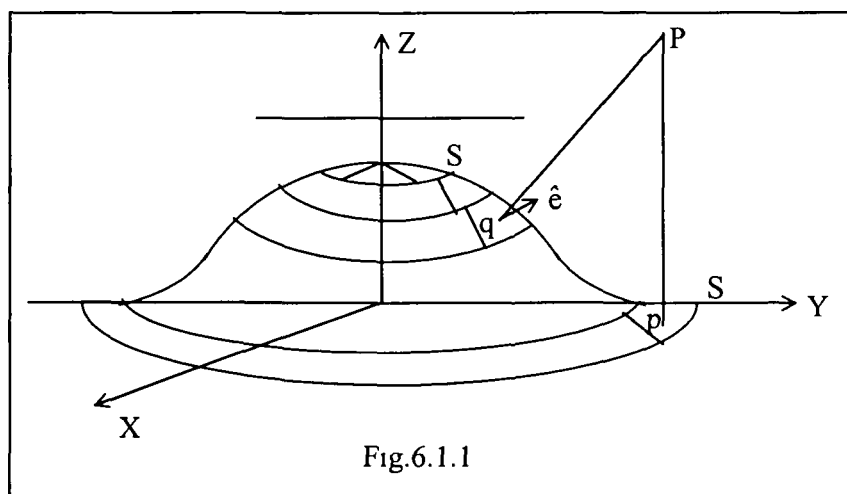


Fig.6.1.1

maintains a smooth continuity as we move from the relief to the plane. Under this setup, the boundary S and the fields due to m and $\mu$, all are symmetrical about the z-axis. The boundary so constructed is shown in Fig.6.1.1.

The boundary is now divided into $n_0$(=130) rings. The top ring is divided into six equilateral triangular subareas and the rest of the rings are divided into $n_k$ (k=2,3,....,130) congruent trapezoidal subareas. The subareas are made such that the arms

of the subareas are nearly equal in length and the ratio of the area of subarea of two consecutive rows having a value lying between 0.79 and 1.126. Outside the partial hemispherical relief, the area of a subarea increases gradually as we move away from the axis of S. The surface S is divided into 30516 subareas. Some of the representative subareas along with number of subareas in a ring are shown in Table-6.1.1.

Table-6.1.1 Side length and area of sub-areas at some representative nodes over S

| Ring No. | Nodal points of sub-area | | | Area $\Delta S$ | No. of sub-area | Arms of sub-area | | |
|---|---|---|---|---|---|---|---|---|
| | x | y | z | | | Top | Bottom | Lateral |
| 1 | 0.0800 | 0.0462 | 0.9989 | 0.0111 | 6 | 0.0000 | 0.1600 | 0.1600 |
| 2 | 0.2080 | 0.0557 | 0.9965 | 0.0123 | 12 | 0.0828 | 0.1415 | 0.1133 |
| 3 | 0.3272 | 0.0577 | 0.9921 | 0.0131 | 18 | 0.0949 | 0.1350 | 0.1156 |
| 17 | 2.1181 | 0.0679 | 0.6922 | 0.0184 | 98 | 0.1313 | 0.1396 | 0.1362 |
| 18 | 2.2489 | 0.0686 | 0.6522 | 0.0188 | 103 | 0.1329 | 0.1408 | 0.1371 |
| 19 | 2.3797 | 0.0692 | 0.6095 | 0.0190 | 108 | 0.1343 | 0.1419 | 0.1379 |
| 29 | 3.3804 | 0.0425 | 0.1057 | 0.0082 | 250 | 0.0838 | 0.0859 | 0.0966 |
| 30 | 3.4655 | 0.0436 | 0.0633 | 0.0082 | 250 | 0.0859 | 0.0881 | 0.0940 |
| 31 | 3.5525 | 0.0445 | 0.0313 | 0.0082 | 250 | 0.0877 | 0.0899 | 0.0919 |
| 62 | 7.2310 | 0.0832 | 0.0000 | 0.0274 | 273 | 0.1643 | 0.1681 | 0.1646 |
| 63 | 7.3976 | 0.0832 | 0.0000 | 0.0286 | 273 | 0.1681 | 0.1720 | 0.1684 |
| 64 | 7.5681 | 0.0871 | 0.0000 | 0.0300 | 273 | 0.1720 | 0.1760 | 0.1722 |
| 123 | 29.0285 | 0.3341 | 0.0000 | 0.4408 | 273 | 0.6597 | 0.6749 | 0.6606 |
| 124 | 29.6976 | 0.3418 | 0.0000 | 0.4614 | 273 | 0.6749 | 0.6905 | 0.6759 |
| 125 | 30.3820 | 0.3496 | 0.0000 | 0.4829 | 273 | 0.6905 | 0.7064 | 0.6915 |

(Total area of S is 3719.91 sq.units divided into 30516 sub areas arranged in 130 rings )

## 6.1.2 Input Data over Boundary

Gravity data due to a unit mass placed at (0,0,-3) and the vertical component magnetic data due to a unit downward doublet placed at the same point are specified at the nodal (centroid) points of the subareas over S. The gravity response at the nodal points are computed by the formula

$$\Delta g(x,y,z) = (z+d)\left[x^2 + y^2 + (z+d)^2\right]^{-3/2},$$

(6.1.1)

46

where d (=3) is the depth of m (=1) below $\overline{S}$ and (x,y,z) defining the nodal point of a subarea. The vertical component magnetic field $T_z$ is computed by the formula

$$T_z(x,y,z) = 3(z+d)^2 r^{-5} - r^{-3},$$  (6.1.2)

where d(=3) is the depth below $\overline{S}$ and r is the distance between the boundary point $q(x,y,z)$ and the doublet $\mu$ placed at Q(0,0,-d).

### 6.1.3 Upward Continuation of Gravity-Magnetic Field

**i) Up-continuation as Simple Layer Potential**

Gravity or a component magnetostatic field H is a harmonic function in the upper half-space domain $B_e$. Both of them vanish at infinity with asymptotic behavior $H = O(r^{-n})$, $n \geq 2, r \rightarrow \infty$. As such, following (4.1.1), these fields can be reproduced in $B_e$ from respective boundary data as potentials due to simple layer boundary density $\sigma$ as

$$H(\mathbf{P}) = \int_S |\mathbf{q} - \mathbf{P}|^{-1} \sigma(\mathbf{q}) d\mathbf{q}, \mathbf{P} \in B_e.$$  (6.1.3)

It has been shown in section (4.1) that the $\sigma$ in (6.1.3) can be obtained as a unique solution of the boundary equation (4.1.2), i.e.

$$H(\mathbf{p}) = \int_S |\mathbf{q} - \mathbf{p}|^{-1} \sigma(\mathbf{q}) d\mathbf{q}, \mathbf{p} \in S.$$  (6.1.4)

Dividing the boundary S into piecewise flat subareas $\Delta S_j$ and assuming $\sigma$ is constant over a subarea, the formula (6.1.3) can be expressed in the form of (5.1.2) as

$$\tilde{H}(\mathbf{P}) = \sum_{j=1}^{n} \sigma_j \int_{\Delta S_j} |\mathbf{q} - \mathbf{P}|^{-1} d\mathbf{q},$$  (6.1.5)

47

where, $\tilde{H}(P)$ is the approximate value of H at P and the equation (6.1.4) can be written as

$$H(q_k) = \sum_{j=1}^{n} \sigma_j \int_{\Delta S_j} |q - q_K|^{-1} dq, \ k=1,2,3\ldots,n,$$

or, $b_k = \sum_{j=1}^{n} a_{kj}\sigma_j, k = 1,2,3\ldots\ldots,n,$ (6.1.6)

where,

$$a_{kj} = \int_{\Delta s_j} |q - q_k|^{-1} dq \tag{6.1.7}$$

and

$$b_k = H(q_K). \tag{6.1.8}$$

Depending on the position of $q_k$ two distinct cases arise in evalution of $a_{kj}$.

**Case-1:**

For $j \neq k$, the integral is regular and it can be evaluated either analytically or approximated by the centroid rule (Hess and Smith 1967) may suffice our purpose. According to centroid rule

$$a_{kj} \cong |q - q_K|^{-1} \int_{\Delta s_j} dq = |q_j - q_k|^{-1} \Delta S_j, \tag{6.1.9}$$

where, $q_j$ is the centroid (or nodal point) of the j-th subarea.

**Case-2:**

For $j = k$, the integral is singular and it is to be evaluated analytically. We know for a triangular area ABC with $q_k$ coinciding with the vertex A, following Jaswon and Symm (1977), or expression (5.2.5) the analytical value of the integral over ABC is

48

$$\int_{ABC} |\mathbf{q} - \mathbf{q_k}|^{-1} dq = \frac{2\Delta}{a} \ln \left( \frac{b+c+a}{b+c-a} \right),$$     (6.1.10)

a finite non-zero quantity, where a, b and c are the arm-lengths BC ,CA and AB respectively and $\Delta$ is the area of the triangle ABC. On evaluation of the coefficients $a_{kj}$, the equation (6.1.6) in $\sigma$ for $b_k$ given over S, can be solved by Gauss-Seidal iterative method since $a_{kk} \neq 0$ as seen in (6.1.10). On finding $\sigma_j$ over S, the field H in $B_e$ can be computed by (6.1.5).

In the present case, the gravity response $\Delta g$ and the topography S are both symmetrical about z-axis and the boundary (topography) is approximated by 30516 piecewise flat subareas. As such, $\sigma$ of equation (6.1.6) can be treated constant over the i-th ring and consequently, the n (=30516) equations of (6.1.6) reduce to N (=130) independent equations.

On computing the $\Delta g$ values at the centroids of the subareas by formula (6.1.1) with d=3, the approximate values of the coefficients $a_{kj}, k \neq j$, are computed by centroid rule (6.1.9) and the singular integrals $a_{kk}$ are evaluated analytically with help of (6.1.10). Subsequently, the equations (6.1.6) are solved by Gauss–Seidal iterative method with convergence condition $\epsilon = 0.00001$. It took 44 iterations to converge. The $\sigma_j$ at some representative rings are shown in column 5 of Table-6.1.2. The surface integral of $\sigma$ is found to be 0.017206. The $\sigma_j$ are negative in the outer part of S (Table-6.1.2) and as such, with increase in S, the integral is expected to attain the zero value as theoretically expected in (4.1.3). On finding the $\sigma_j$ over S, the up-continued $\Delta g$ values at level lines y = 0, z = 1.5; y = 0, z = 3, and y = 0, z = 5 are computed by formula (6.1.5) on evaluating the integrals by the centroid rule. The values so obtained are shown in column 4 of Table-6.1.3 along with the true values in column 3 for comparison. It is evident from Table-6.1.3 that the up-continued values of $\Delta g$ obtained by the discretised version of (6.1.3) agree with the true values to a good degree of accuracy.

49

Table-6.1.2 Simple and double layer boundary densities for Gravity field

| Ring No. | Nodal points of sub-area X | Y | Z | Boundary Density $\sigma$ | $\mu$ |
|---|---|---|---|---|---|
| 1 | 0.0800 | 0.0462 | 0.9989 | $0.449\times10^{-2}$ | $0.119\times10^{-1}$ |
| 2 | 0.2080 | 0.0557 | 0.9965 | $0.454\times10^{-2}$ | $0.119\times10^{-1}$ |
| 3 | 0.3272 | 0.0577 | 0.9921 | $0.436\times10^{-2}$ | $0.118\times10^{-1}$ |
| 17 | 2.1181 | 0.0679 | 0.6922 | $0.266\times10^{-2}$ | $0.921\times10^{-2}$ |
| 18 | 2.2489 | 0.0686 | 0.6522 | $0.251\times10^{-2}$ | $0.891\times10^{-2}$ |
| 19 | 2.3797 | 0.0692 | 0.6095 | $0.234\times10^{-2}$ | $0.860\times10^{-2}$ |
| 29 | 3.3804 | 0.0425 | 0.1057 | $0.157\times10^{-2}$ | $0.559\times10^{-2}$ |
| 30 | 3.4655 | 0.0436 | 0.0633 | $0.146\times10^{-2}$ | $0.567\times10^{-2}$ |
| 31 | 3.5525 | 0.0445 | 0.0313 | $0.130\times10^{-2}$ | $0.535\times10^{-2}$ |
| 62 | 7.2310 | 0.0832 | 0.0000 | $-0.156\times10^{-3}$ | $0.101\times10^{-2}$ |
| 63 | 7.3976 | 0.0832 | 0.0000 | $-0.153\times10^{-3}$ | $0.959\times10^{-3}$ |
| 64 | 7.5681 | 0.0871 | 0.0000 | $-0.149\times10^{-3}$ | $0.903\times10^{-3}$ |
| 123 | 29.0285 | 0.3341 | 0.0000 | $-0.800\times10^{-5}$ | $0.195\times10^{-4}$ |
| 124 | 29.6976 | 0.3418 | 0.0000 | $-0.785\times10^{-5}$ | $0.182\times10^{-4}$ |
| 125 | 30.3820 | 0.3496 | 0.0000 | $-0.779\times10^{-5}$ | $0.170\times10^{-4}$ |

($\sigma$ and $\mu$ stand for simple and double layer boundary densities over the boundary S)

Table-6.1.3: Continuation of gravity field in $B_e$

| Co-ordinates Along Y = 0 Z | X | True Gravity $\Delta g[t]$ | Field as potential of Simple layer $\Delta g[S]$ | Double layer $\Delta g[D]$ | Green's formula $\Delta g[G]$ |
|---|---|---|---|---|---|
| 1.5 | 0 | 0.04938 | 0.04952 | 0.04756 | 0.04870 |
| | 2 | 0.03768 | 0.03778 | 0.03720 | 0.03754 |
| | 4 | 0.02061 | 0.02065 | 0.02049 | 0.02058 |
| | 6 | 0.01066 | 0.01067 | 0.01061 | 0.01065 |
| | 8 | 0.00581 | 0.00582 | 0.00579 | 0.00580 |
| | 10 | 0.00341 | 0.00341 | 0.00339 | 0.00340 |
| 3.0 | 0 | 0.02777 | 0.02785 | 0.02732 | 0.02763 |
| | 2 | 0.02371 | 0.02378 | 0.02342 | 0.02363 |
| | 4 | 0.01600 | 0.01603 | 0.01587 | 0.01596 |
| | 6 | 0.00982 | 0.00984 | 0.00975 | 0.00980 |
| | 8 | 0.00600 | 0.00601 | 0.00596 | 0.00599 |
| | 10 | 0.00378 | 0.00379 | 0.00376 | 0.00378 |
| 5.0 | 0 | 0.01562 | 0.01567 | 0.01544 | 0.01557 |
| | 2 | 0.01426 | 0.01431 | 0.01411 | 0.01423 |
| | 4 | 0.01118 | 0.01121 | 0.01108 | 0.01116 |
| | 6 | 0.00800 | 0.00803 | 0.00793 | 0.00799 |
| | 8 | 0.00552 | 0.00555 | 0.00548 | 0.00552 |
| | 10 | 0.00380 | 0.00383 | 0.00378 | 0.00381 |

($\Delta g[t]$ & $\Delta g[S]$, $\Delta g[D]$, $\Delta g[G]$ are the true & reproduced gravity value by simple layer boundary density, double layer boundary density and Green's formula respectively)

In the next step, the vertical component magnetic data $T_z$ at the nodal points of S are computed by formula (6.1.2) with d = 3. It has been theoretically shown that this field also can be reproduced in the upper half-space domain from boundary data by simple layer formulation of the problem. Since this field is also symmetrical about z-axis, the procedure described for up-continuation of the gravity field $\Delta g$ is followed to find N (=130) and $\sigma_j$ s over S. In this case, the equations took 42 iterations to converge. The $\sigma_j$ values at some representative rings over S are shown in column 5 of Table-6.1.4. The surface integral of $\sigma$ in this case is found to be $-0.000529$, as theoretically expected, in (4.1.3). Subsequently, the $T_z$ values at level lines y = 0, z= 1.5; y = 0, z = 3 and y = 0, z = 5 are computed by formula (6.1.5) on approximating the integrals by centroid rule. The values so obtained are shown in column 4 of Table-6.1.5 along with the true values in column 3 for comparison. It is evident from Table-6.1.5 that the up-continued $T_z$ values agree with the true values to a good degree of accuracy.

Table-6.1.4 Simple and double layer boundary densities for magnetic field

| Ring No. | Nodal points of sub-area | | | Boundary density | |
|---|---|---|---|---|---|
| | x | y | z | $\sigma$ | $\mu$ |
| 1 | 0.0800 | 0.0462 | 0.9989 | $0.359\times10^{-2}$ | $0.587\times10^{-2}$ |
| 2 | 0.2080 | 0.0557 | 0.9965 | $0.360\times10^{-2}$ | $0.583\times10^{-2}$ |
| 3 | 0.3272 | 0.0577 | 0.9921 | $0.343\times10^{-2}$ | $0.579\times10^{-2}$ |
| 17 | 2.1181 | 0.0679 | 0.6922 | $0.127\times10^{-2}$ | $0.327\times10^{-2}$ |
| 18 | 2.2489 | 0.0686 | 0.6522 | $0.110\times10^{-2}$ | $0.303\times10^{-2}$ |
| 19 | 2.3797 | 0.0692 | 0.6095 | $0.932\times10^{-3}$ | $0.279\times10^{-2}$ |
| 29 | 3.3804 | 0.0425 | 0.1057 | $-0.159\times10^{-3}$ | $0.105\times10^{-2}$ |
| 30 | 3.4655 | 0.0436 | 0.0633 | $-0.276\times10^{-3}$ | $0.892\times10^{-3}$ |
| 31 | 3.5525 | 0.0445 | 0.0313 | $-0.377\times10^{-3}$ | $0.744\times10^{-3}$ |
| 62 | 7.2310 | 0.0832 | 0.0000 | $-0.953\times10^{-4}$ | $-0.168\times10^{-3}$ |
| 63 | 7.3976 | 0.0832 | 0.0000 | $-0.873\times10^{-4}$ | $-0.164\times10^{-3}$ |
| 64 | 7.5681 | 0.0871 | 0.0000 | $-0.799\times10^{-4}$ | $-0.160\times10^{-3}$ |
| 123 | 29.0285 | 0.3341 | 0.0000 | $0.750\times10^{-7}$ | $-0.596\times10^{-5}$ |
| 124 | 29.6976 | 0.3418 | 0.0000 | $0.867\times10^{-7}$ | $-0.558\times10^{-5}$ |
| 125 | 30.3820 | 0.3496 | 0.0000 | $0.987\times10^{-7}$ | $-0.522\times10^{-5}$ |

($\sigma$ and $\mu$ stand for simple and double layer boundary densities over the boundary S)

Table-6.1.5: Continuation of magnetic field in $B_e$

| Co-ordinates Along Y = 0 | | True comp. magn. field | Field as potential of | | |
|---|---|---|---|---|---|
| | | | Simple layer | Double layer | Green's formula |
| Z | X | $T_z[t]$ | $T_z[S]$ | $T_z[D]$ | $T_z[G]$ |
| 1.5 | 0 | 0.02194 | 0.02203 | 0.02108 | 0.02163 |
| | 2 | 0.01260 | 0.01265 | 0.01241 | 0.01255 |
| | 4 | 0.00309 | 0.00310 | 0.00305 | 0.00308 |
| | 6 | 0.00019 | 0.00018 | 0.00017 | 0.00018 |
| | 8 | -0.00036 | -0.00036 | -0.00036 | -0.00036 |
| | 10 | -0.00037 | -0.00037 | -0.00037 | -0.00037 |
| 3.0 | 0 | 0.00925 | 0.00929 | 0.00909 | 0.00919 |
| | 2 | 0.00672 | 0.00674 | 0.00660 | 0.00665 |
| | 4 | 0.00287 | 0.00287 | 0.00282 | 0.00285 |
| | 6 | 0.00081 | 0.00081 | 0.00080 | 0.00081 |
| | 8 | 0.00008 | 0.00007 | 0.00007 | 0.00007 |
| | 10 | -0.00013 | -0.00013 | -0.00013 | -0.00013 |
| 5.0 | 0 | 0.00390 | 0.00392 | 0.00383 | 0.00388 |
| | 2 | 0.00325 | 0.00326 | 0.00319 | 0.00323 |
| | 4 | 0.00195 | 0.00196 | 0.00192 | 0.00194 |
| | 6 | 0.00092 | 0.00092 | 0.00090 | 0.00091 |
| | 8 | 0.00034 | 0.00034 | 0.00033 | 0.00342 |
| | 10 | 0.00008 | 0.00008 | 0.00007 | 0.00007 |

($T_z[t]$ & $T_z [S]$, $T_z[D]$, $T_z[G]$ are the true & reproduced z-component of magnetostatic field value by simple layer boundary density, double layer boundary density and Green's formula respectively)

## ii) Up-continuation as Double Layer Potential

We know that gravity or a component magnetic field H due to a subsurface causative mass is a harmonic function in the upper half-space domain $B_e$ bounded below by the ground surface S. Both the fields vanish at infinity with asymptotic behaviour H= $O(r^{-n})$, $n \geq 2, r \to \infty$. As such, following (4.2.1), H can be reproduced in $B_e$ from the respective boundary data as potential of double layer boundary density as

$$H(P) = \int_{S_e} |q - P|^{-1} \mu(q) dq, P \in B_e.$$ (6.1.11)

For H specified over S, the $\mu$ over S can be obtained as a unique solution of the boundary integral equation (4.2.2), i.e.,

$$H(p) = 2\pi\mu(p) + \int_{S_e} |q - p|^{-1} \mu(q) dq, \ p \in S.$$ (6.1.12)

On discretisation, the formula (6.1.11) becomes

$$H(\mathbf{P}) = \sum_{j=1}^{n} \mu_j \int_{\Delta S_j} \hat{e} \, |\mathbf{q} - \mathbf{P}|^{-1} dq \qquad (6.1.13)$$

and the boundary equation ( 4.2.2) becomes

$$H(\mathbf{q_K}) = 2\pi\mu(\mathbf{q_k}) + \sum_{j=1}^{n} \mu_j \int_{\Delta S_j} \hat{e} \, |\mathbf{q} - \mathbf{q_k}|^{-1} dq$$

$$\text{or, } H_K = \sum_{j=1}^{n} (b_{kj} + 2\pi\delta_{kj})\mu_j, k = 1,2,3...n, \qquad (6.1.14)$$

$$\text{where } b_{kj} = \int_{\Delta S_j} \hat{e} \, |\mathbf{q} - \mathbf{q_k}|^{-1} dq = \int_{\Delta S_j} -|\mathbf{q} - \mathbf{q_k}|^{-2} (\mathbf{q} - \mathbf{q_k}).\hat{e} dq, \qquad (6.1.15)$$

$H_k = H(\mathbf{q_k}), \hat{e}$ is the normal towards $B_e$ at piecewise flat $\Delta S_j$ and $\delta_{kj}$ is the Kronecker delta defined as , $\delta_{kj} = 0$ for $j \neq k$ and $\delta_{kj} = 1$ for $j = k$.

Two distinct cases arise in evaluation of the coefficient $b_{kj}$.

## Case- 1:

For $j \neq k$, the integral is regular and it can be evaluated analytically or an approximation to it by centroid rule may suffice our purpose. Following the centroid rule of approximation

$$b_{kj} \cong -|\mathbf{q}_j - \mathbf{q}_k|^{-3} (\mathbf{q}_j - \mathbf{q}_k).\hat{e} \int_{\Delta S} dq = -|\mathbf{q}_j - \mathbf{q}_k|^{-3} (\mathbf{q}_j - \mathbf{q}_k).\hat{e}\Delta S_j.$$

## Case-2:

For $j = k$, $b_{kk}=0$, since $(\mathbf{q} - \mathbf{q}_k).\hat{e} = 0$, $\mathbf{q} \neq \mathbf{q}_k$, $\mathbf{q}, \mathbf{q}_k \in \Delta S_k$, $\Delta S_k$ being flat and the integral having a singularity at an isolated point $\mathbf{q}_k$, a set of measure zero.

On computing the gravity values at the nodal points of the subareas over S by the formula (6.1.1) with d=3, the coefficient $b_{kj}, j \neq k$ are computed by the centroid rule of approximation to integrals and the singular integral $b_{kk}$ is taken to be zero, as explained above. Because of the symmetry of S and H about z-axis, n (=30516) equations of (6.1.14) reduce to N (=130) independent equations. These equations are then solved for $\mu_j$ by Gauss–Seidal iterative method with convergence condition $\varepsilon = 0.00001$. The equations took to 5 iterations to converge and the surface integral of $\mu$ is found to be 0.9299 as theoretically expected in (4.2.4). The $\mu$-values so obtained are shown at some representative rings in column 6 of Table-6.1.2.

The gravity values along the level lines y = 0, z= 1.5; y = 0, z= 3 and y = 0, z= 5 are then computed as potential of double layer density $\mu$ by the formula (6.1.13) and these are exhibited in column 5 of Table-6.1.3 along with the true values in column 3 for comparison. It is evident from Table-6.1.3 that the gravity values, reproduced from the boundary data as potential of double layer boundary density, agree with the true values to a good degree of accuracy.

Subsequently, vertical component magnetic data, due to a unit vertically downward doublet, are computed as $H_k$ at the nodal points of S by the formula (6.1.2) with d = 3 and the equations (6.1.14) are solved for $\mu_j$ by Gauss–Seidal iterative method with convergence condition $\varepsilon = 0.00001$. The equations took 5 iterations to converge. The solution at some of the representative rings over S are shown in column 6 of Table-6.1.4. The solutions are positive over the central part of S and negative over the outer periphery. The surface integral of $\mu$ over S is found to be 0.03203 where its theoretically expected value by (4.2.5) is 0. Since the $\mu$ values are negative at periphery, the surface integral of the numerical $\mu$ over S is expected to be zero as S extends to infinity.

The vertical component magnetic values along the level lines y = 0, z= 1.5; y=0, z=3 and y=0, z=5 are then computed by (6.1.13) and these are shown in column 5 of Table-6.1.5 along with the true values in column 3 for comparison. It is evident from Table-6.1.5 that

the magnetic values obtained as double layer potential of boundary density agree with the true values to a good degree of accuracy.

### iii) Up-continuation by Green's Formula

For a harmonic function H, a gravity field $\Delta g$ or a magnetostatic component field $T_z$, with asymptotic behavior $H = O(r^{-n})$, $n \geq 2$, $r \to \infty$, defined in the upper half- space domain $B_e$ bounded below by a half-space boundary S, given H and $H_e'$ over S, H in $B_e$ can be reproduced by Green's formula (4.3.1) as

$$4\pi H(P) = \int_{S_e}' |q - P|^{-1} H(q)dq - \int_S |q - P|^{-1} H_e'(q)dq, \, P \in B_e,  \qquad (6.1.16)$$

as $P \to p \in S$, the boundary relation between H and $H_e'$ over S is given by (4.3.2) as

$$2\pi H(p) = \int_{S_e}' |q - p|^{-1} H(q)dq - \int_S |q - p|^{-1} H_e'(q)dq, \, p \in S  \qquad (6.1.17)$$

as discussed in article (4.3), given H over S, $H_e'$ over S can be obtained as a unique solution of the boundary integral equation

$$\int_S |q - p|^{-1} H_e'(q)dq = \int_{S_e}' |q - p|^{-1} H(q)dq - 2\pi H(p), \, p \in S.  \qquad (6.1.18)$$

The discretised versions of (6.1.16) and (6.1.18) are given below

$$4\pi H(P) = \sum_{j=1}^{n} H(q_j) \int_{\Delta S_j} {}_e' |q - P|^{-1} dq - \sum_{j=1}^{n} H_e'(q_j) \int_{\Delta S_j} |q - P|^{-1} dq, \, P \in B_e  \qquad (6.1.19)$$

and

$$\sum_{j=1}^{n} H_e'(q_j) \int_{\Delta S_j} |q - q_K|^{-1} dq = \sum_{j=1}^{n} H(q_j) \int_{\Delta S_j} {}_e' |q - q_K|^{-1} dq - 2\pi H(q_K), \, k = 1,2,3\ldots\ldots n,$$

$$(6.1.20)$$

55

where $H'_e(\mathbf{q}_j)$ and $H(\mathbf{q}_j)$ stand for the constant values of $H'_e(\mathbf{q})$ and $H(\mathbf{q})$ respectively over the j-th subarea $\Delta S_j$. Following the notations used for the coefficients in (6.1.6) and (6.1.14), the equation (6.1.20) can be expressed as

$$\sum_{j=1}^{n} a_{kj} H'_e(\mathbf{q}_j) = \sum_{j=1}^{n} b_{kj} H(\mathbf{q}_j) - 2\pi H(\mathbf{q}_k), \quad k = 1,2,...n$$

$$\text{or,} \sum_{j=1}^{n} a_{kj} H'_e(\mathbf{q}_j) = \sum_{j=1}^{n} \left[b_{kj} + \delta_{kj}(-2\pi)\right] H(\mathbf{q}_j) = D_K (\text{say}), k = 1,2,.....n, \quad (6.1.21)$$

where $\delta_{kj}$ is the Kronecker delta.

For H specified over the nodal points of the piecewise flat subareas $\Delta S_j$, the equation (6.1.21) can be solved for $H'_e$ by Gauss-Seidal iterative method on evaluation of the coefficients $a_{kj}$ and $b_{kj}$. On finding $H'_e$ over S, the field H in the upper half space domain $B_e$ can be computed by (6.1.19), the discretised version of (6.1.16).

On computing the gravity values $\Delta g_j [= H(\mathbf{q}_j)]$ at the nodal points of S by (6.1.1) with d=3, the $a_{kj}$ and $D_k$ values of (6.1.21) are computed following the procedures mentioned in subsections (6.1.3(i)) and (6.1.3(ii)) above. Since $\Delta g$ and S are both symmetrical about the z-axis, the n (=30516) equations of (6.1.21) reduce to N (=130) independent equations. These are then solved by Gauss–Seidal iterative method with convergence condition $\varepsilon = 0.00001$. The equations took 56 iterations to converge. The $H'_e$ values so obtained are shown as $\Delta g'_e$ in column 6 of Table-6.1.6 along with the true values for comparison. It is evident from Table-6.1.6 that the solution $H'_e$ reasonably agrees with the true values of $H'_e(\mathbf{q}_j)$.

On finding the $H'_e(q_j)$ values over S, the gravity values H are then computed at the level lines y = 0, z = 1.5; y=0, z=3 and y=0, z=5 by (6.1.19) and these are shown in Table-6.1.3 along with the true values for comparison. It is evident from Table-6.1.3 that the computed values agree with the true values to a good degree of accuracy.

Subsequently, the vertical component magnetic data $T_z$ are computed at the nodal points of the subareas over S by use of formula (6.1.2) with d = 3. In this case also the magnetic field is symmetrical about z-axis and consequently the n (=30516) equations in $H'_e$ of (6.1.21) reduce to N (=130) independent equations. On evaluation of coefficients $a_{kj}$ and $b_{kj}$ following the same procedure described earlier, the equations (6.1.21) are solved for $H'_e$ by Gauss-Seidal iterative method with $\varepsilon$ =0.00001. The equations took 51 iterations to

Table–6.1.6 Solution of Green's boundary equation for gravimetric and magnetostatic cases

| Ring No. | Nodal point of sub-area | | | True $\Delta g'_e(=\phi'_e)$ | Computed $\Delta g'_e(=\phi'_e)$ | True $T'_e(=\phi'_e)$ | Computed $T'_e(=\phi'_e)$ |
|---|---|---|---|---|---|---|---|
| | x | y | z | | | | |
| 1 | 0.0800 | 0.0462 | 0.9989 | $-0.312\times10^{-1}$ | $-0.343\times10^{-1}$ | $-0.234\times10^{-1}$ | $-0.254\times10^{-1}$ |
| 2 | 0.2080 | 0.0557 | 0.9965 | $-0.311\times10^{-1}$ | $-0.330\times10^{-1}$ | $-0.232\times10^{-1}$ | $-0.248\times10^{-1}$ |
| 3 | 0.3272 | 0.0577 | 0.9921 | $-0.309\times10^{-1}$ | $-0.318\times10^{-1}$ | $-0.229\times10^{-1}$ | $-0.237\times10^{-1}$ |
| 17 | 2.1181 | 0.0679 | 0.6922 | $-0.203\times10^{-1}$ | $-0.203\times10^{-1}$ | $-0.933\times10^{-2}$ | $-0.938\times10^{-2}$ |
| 18 | 2.2489 | 0.0686 | 0.6522 | $-0.192\times10^{-1}$ | $-0.192\times10^{-1}$ | $-0.816\times10^{-2}$ | $-0.819\times10^{-2}$ |
| 19 | 2.3797 | 0.0692 | 0.6095 | $-0.182\times10^{-1}$ | $-0.182\times10^{-1}$ | $-0.702\times10^{-2}$ | $-0.705\times10^{-2}$ |
| 29 | 3.3804 | 0.0425 | 0.1057 | $-0.110\times10^{-1}$ | $-0.126\times10^{-1}$ | $-0.355\times10^{-3}$ | $-0.552\times10^{-3}$ |
| 30 | 3.4655 | 0.0436 | 0.0633 | $-0.899\times10^{-2}$ | $-0.105\times10^{-1}$ | $0.837\times10^{-3}$ | $0.723\times10^{-3}$ |
| 31 | 3.5525 | 0.0445 | 0.0313 | $-0.677\times10^{-2}$ | $-0.849\times10^{-2}$ | $0.192\times10^{-2}$ | $0.185\times10^{-2}$ |
| 62 | 7.2310 | 0.0832 | 0.0000 | $0.116\times10^{-2}$ | $0.117\times10^{-2}$ | $0.693\times10^{-3}$ | $0.694\times10^{-3}$ |
| 63 | 7.3976 | 0.0832 | 0.0000 | $0.113\times10^{-2}$ | $0.114\times10^{-2}$ | $0.636\times10^{-3}$ | $0.638\times10^{-3}$ |
| 64 | 7.5681 | 0.0871 | 0.0000 | $0.109\times10^{-2}$ | $0.110\times10^{-2}$ | $0.584\times10^{-3}$ | $0.585\times10^{-3}$ |
| 123 | 29.0285 | 0.3341 | 0.0000 | $0.389\times10^{-4}$ | $0.537\times10^{-4}$ | $0.125\times10^{-5}$ | $0.136\times10^{-5}$ |
| 124 | 29.6976 | 0.3418 | 0.0000 | $0.364\times10^{-4}$ | $0.527\times10^{-4}$ | $0.112\times10^{-5}$ | $0.125\times10^{-5}$ |
| 125 | 30.3820 | 0.3496 | 0.0000 | $0.341\times10^{-4}$ | $0.523\times10^{-4}$ | $0.100\times10^{-5}$ | $0.116\times10^{-5}$ |

( $\Delta g'_e$ and $\Delta T'_e$ stands for the outward normal derivative of gravity and component magnetic fields)

converge. The $H_e'$ values at some representative rings over S are shown as $T_e'(=H_e')$ in column 7 of Table-6.1.6 for comparison with the true values of $T_e'$. It is evident from Table-6.1.6 that the computed $H_e'$ values agree with the true values to a reasonable accuracy.

Finally, with these $H_e'$ values known over S, the vertical component magnetic field H is computed along the level lines y = 0, z = 1.5; y= 0, z= 3 and y= 0, z= 5 by the formula (6.1.19) and these are exhibited in Table-6.1.5 along with true $T_z$ values for comparison. It is evident from Table-6.1.5 that the computed $T_z$ values agree with the true $T_z$ values to a good degree of accuracy.

## 6.2 Continuation from a General half-space Boundary

In earlier articles, upward continuation of a potential field, a gravity field or a component magnetic field, is carried out from a boundary symmetrical about z-axis when the fields are also symmetrical about the z-axis. It has been shown that upward continuation of gravity or a magnetic component field can be carried out either as a potential of a simple layer boundary density or as a potential of a double layer boundary density or by use of Green's formula without finding Green's function for the boundary. All the three formulations are theoretically sound and each of them reproduces the fields from the respective boundary data to a good degree of accuracy. However, it is found that reproduction of a field as a potential due to a double layer boundary density provides the simplest and the fastest numerical approach and it can be easily handled on a PC. Henceforth, upward continuation of gravity or a component field will be carried out as potential of double layer boundary density only.

### 6.2.1 Boundary Representing a Hilly Area

The topography of northwestern part of Vishakhapatnam–Srikakulam area, named as Lamaput-Araku area in this thesis, bounded by North latitudes 18.25 $^0$ and 18.5$^0$ and East longitudes 82.5$^0$ to 83$^0$, is considered as the boundary surface S for the model study. Survey of India topo-sheets in 1:50000 scale covering the area are divided into 2x2 sq. km grids and the topographic heights at the grid points are noted. These are then transferred to a cartesian reference frame with its origin at the crossing of 82.5$^0$E longitude and 18.25$^0$

north latitude, x-axis coinciding with 18.25°N latitude, y-axis coinciding with 82.5°E longitude and z-axis pointing upward. On conversion of distance into km, it is found that

Fig.6.2.1Topographic contour map of north west part of Vizag-Srikakulam Area
Contour interval = .05 km
(All co-ordinates are in km)



Origin of the frame refers to longitude 82.5° N and latitude 18.25° E respectively.
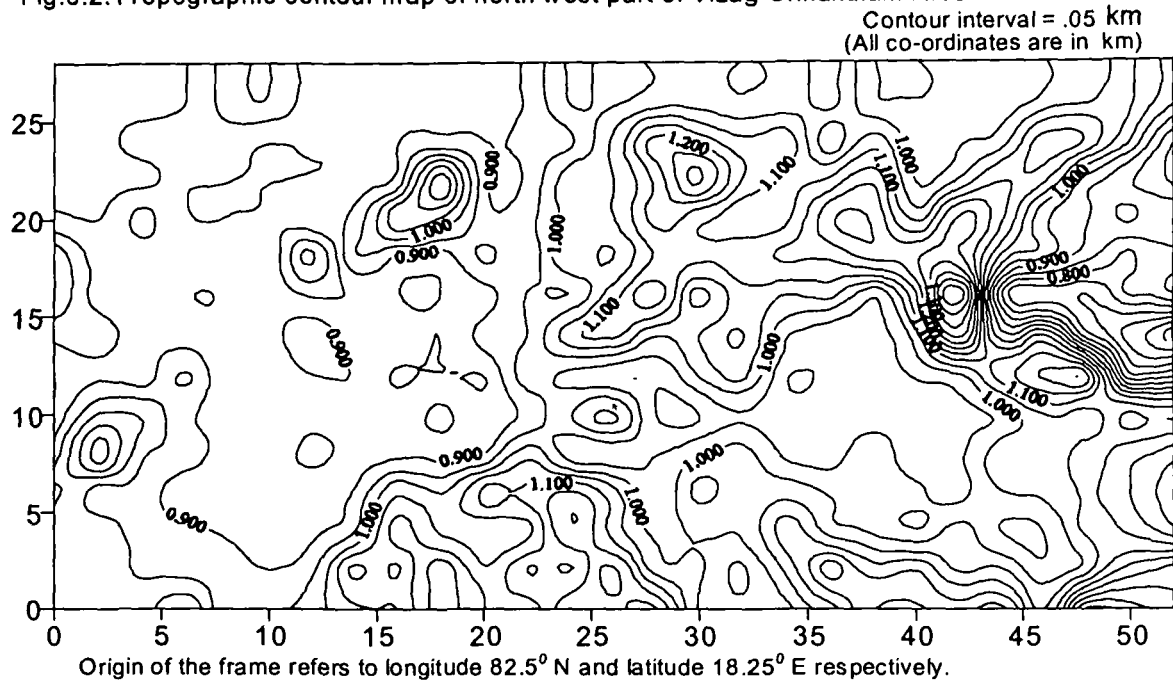
Table-6.2.1:Description of some triangular subareas over the topography of northwestern part of Vizag-Srikakulam area

| Vertices of ΔS | | | Area of ΔS | Aspect ratio | Direction cosine of outward normal to ΔS | | |
|---|---|---|---|---|---|---|---|
| x | y | z | ΔS | η | l | m | n |
| 24.00 | 0.00 | 1.2 | | | | | |
| 26.00 | 0.00 | 1.18 | 2.005 | 0.707 | 0.01 | 0.07 | 0.998 |
| 24.00 | 2.00 | 1.06 | | | | | |
| 30.00 | 4.00 | 1.01 | | | | | |
| 30.00 | 6.00 | 1.09 | 2.007 | 0.707 | -0.075 | -0.04 | 0.996 |
| 28.00 | 6.00 | 1.2 | | | | | |
| 28.00 | 14.00 | 0.98 | | | | | |
| 30.00 | 14.00 | 1.06 | 2.017 | 0.706 | -0.037 | -0.124 | 0.992 |
| 28.00 | 16.00 | 1.23 | | | | | |
| 26.00 | 24.00 | 1.06 | | | | | |
| 28.00 | 24.00 | 1.26 | 2.012 | 0.704 | -0.099 | 0.04 | 0.994 |
| 26.00 | 26.00 | 0.98 | | | | | |
| 30.00 | 26.00 | 1.02 | | | | | |
| 30.00 | 28.00 | 1.02 | 2.000 | 0.707 | -0.005 | 0 | 1.000 |
| 28.00 | 28.00 | 1.01 | | | | | |

59

the projection of the surface S on (x,y)-plane occupies an area bounded by x = 0 and x = 52 km and y = 0 and y = 28km. The topography with height varying from 0.45 to 1.615 km consists of 364 subareas each standing on 2x2 sq. km area on the (x,y)-plane. Each subarea is then sub-divided into two piecewise flat triangular subareas. This yields a total of 728 piecewise flat triangular subareas. Approximation of the surface by triangular subareas presents a surface without a gap between the subareas. The areas of the subareas approximating the surface varies from 2 to 2.12 sq. km and the aspect ratio $\eta$, defined as ratio of the smallest and the largest arm-length of a subarea, varies from 0.69 to 0.73. This indicates that no thin triangular subareas are involved in approximating the undulated surface by flat triangular subareas. The topographic heights as noted at the grid points are used to prepare a contour map of the topography of the area by Surfer-32 package and it is exhibited in Fig.6.2.1. Description of some of the subareas are shown in Table-6.2.1 in which (x,y,z) define the co-ordinates of the nodal point of a subarea, (l,m,n) define the direction cosines of the outward normal drawn on it.

## 6.2.2 Model Response

A thin rectangular plate with corners at (16,11.5), (36,11.5), (36,16.5) and (16,16.5) is placed a depth d = 3 units below the (x,y)-plane defined by z = 0 . The plate is then polarized by vertically downward doublets of strength $\mu$ = 1 per unit area.

Assuming the density $\rho$ of the plate to be 1, and the universal gravitational constant G =1, the gravity field at a point P(X,Y,Z) in a cartesian reference frame with z-axis upward, is given by, following Laskar (1994), as

$$\Delta g(X,Y,Z) = \int_{x=x_1}^{x=x_2} \int_{y=y_1}^{y=y_2} \frac{(Z-z)dxdy}{[(x-X)^2 + (y-Y)^2 + (z-Z)^2]^{3/2}}$$

$$= \tan^{-1} \frac{(x-X)(y-Y)}{Z[(x-X)^2 + (y-Y)^2 + (Z)^2]^{1/2}} \Bigg]_{x=x_1}^{x_2} \Bigg]_{y=y_1}^{y_2} , \qquad (6.2.1)$$

for the plate lying at (x,y)-plane at which z = 0 and its corner points are defined by $(x_1,y_1,0)$, $(x_2,y_1,0)$, $(x_2,y_2,0)$ and $(x_1,y_2,0)$. The vertical component magnetostatic field at

P(X,Y,Z) due to the polarised plate lying at the plane z = 0 in the same reference frame can be expressed as

$$T_z(X,Y,Z) = \frac{-(x-X)(y-Y)[(x-X)^2 + (y-Y)^2 + 2Z^2]}{Z^2[\{(x-X)^2 + (y-Y)^2 + Z^2\}^{3/2} + (x-X)^2(y-Y)^2\{(x-X) + (y-Y)^2 + 2Z^2\}^{1/2}]}$$

(6.2.2)

under the limits x varying from $x_1$ to $x_2$ and y varying from $y_1$ to $y_2$, as shown in (6.2.1)

### 6.2.3 Upward Continuation of Gravity Data

For the rectangular gravitating plate lying at depth d units below the plane z=0, its gravity responses at the nodal points of the subareas are computed with help of (6.2.1) on replacing Z by Z+d and fixing the values $x_1$ =16, $x_2$ =36, $y_1$ =11.5, $y_2$ = 16.5 and d=3. These are then denoted by $H_k$, k=1,2,...,n, and the n equations of (6.1.14) are formed. Subsequently, the coefficients $b_{kj}$ are evaluated by centroid rule and also by analytical means as discussed in article 5.2 and the n equations in n unknown $\mu_j$ are solved by Gauss-Seidal iterative method with $\varepsilon$ = 0.00001.

Table-6.2.2: Upward continuation of gravity field from an irregular boundary to a level z = 1.615

| Co-ordinate | True field | Analytical integration technique | | Approximate integration technique | |
|---|---|---|---|---|---|
| y | $\Delta_g$ | $\Delta_g$ | % err. | $\Delta_g$ | % err. |
| 1.8667 | 0.1752 | 0.1768 | -0.9333 | 0.1044 | 40.4045 |
| 3.7333 | 0.2557 | 0.2611 | -2.1194 | 0.1932 | 24.4439 |
| 5.6 | 0.3866 | 0.3905 | -1.0228 | 0.2979 | 22.94673 |
| 7.4667 | 0.6027 | 0.6094 | -1.1333 | 0.5361 | 11.0464 |
| 9.3333 | 0.9448 | 0.9228 | 2.3226 | 0.7663 | 18.8886 |
| 11.2 | 1.3907 | 1.4011 | -0.7551 | 1.2717 | 8.5558 |
| 13.0667 | 1.738 | 1.7188 | 1.0978 | 1.5043 | 13.4447 |
| 14.9333 | 1.738 | 1.7154 | 1.2911 | 1.3827 | 20.4415 |
| 16.8 | 1.3907 | 1.3551 | 2.5557 | 1.2193 | 12.3248 |
| 18.6667 | 0.9448 | 0.9302 | 1.549 | 0.8365 | 11.4616 |
| 20.5333 | 0.6027 | 0.591 | 1.932 | 0.5006 | 16.9407 |
| 22.4 | 0.3865 | 0.379 | 1.9568 | 0.3092 | 20.0186 |
| 24.2667 | 0.2557 | 0.2493 | 2.4845 | 0.1958 | 23.4366 |
| 26.1333 | 0.1752 | 0.1671 | 4.6382 | 0.1346 | 23.155 |

(The field is presented along the line x = 26 at the level z = 1.615, z = 0 defining the datum plane. The causative mass is a gravitating mass extending from x = 16 to 36 and y = 11.5 to 16.5, placed at d = 3 units below the plane z = 0. Topographic height varies from z = 0.45 to 1.615)

The equations took 5 iterations to converge when the coefficients $b_{kj}$ are evaluated analytically. The equations took the same number of iterations for the approximate values of $b_{kj}$ computed by the centroid rule. Finally, the up-continued values of the field at level z =1.615 are computed by (6.1.13) with H(P) representing $\Delta g$ in this case. The up-continued $\Delta g$ values so obtained along the North-south line defined by x = 26, z = 1.615, are shown in Table-6.2.2 along with the true values for comparison. The field values also computed by the same $\mu$ values by (6.1.13) along the line x = 26, z= 2.615 are exhibited in Table-6.2.3.

It is evident from Table-6.2.2 and Table-6.2.3 that the centroid method of approximation does not work when the field point is near the boundary. The result gradually improves at the central part of the continuation level $\overline{S}$ as its height increases. However, the results at the periphery of $\overline{S}$ detoriates in comparison to those at the central part, at the increase of height of $\overline{S}$. In the case of analytical values of the coefficients, the errors in the computed field values at $\overline{S}$, even when it grazes the boundary, are well within a tolerable error and these values can be used for further analysis of the problem.

Table-6.2.3: Upward continuation of gravity field from an irregular boundary to a level z = 2.615

| Co-ordinate | True field | Analytical integration technique | | Approximate integration technique | |
|---|---|---|---|---|---|
| y | $\Delta_g$ | $\Delta_g$ | % err. | $\Delta_g$ | % err. |
| 1.8667 | 0.1961 | 0.1903 | 2.9231 | 0.1788 | 8.7902 |
| 3.7333 | 0.2791 | 0.2820 | -1.0724 | 0.2706 | 3.0394 |
| 5.6 | 0.4066 | 0.4141 | -1.8414 | 0.3973 | 2.2971 |
| 7.4667 | 0.6004 | 0.6091 | -1.4445 | 0.6008 | -0.0693 |
| 9.3333 | 0.8744 | 0.878 | -0.4103 | 0.859 | 1.7568 |
| 11.2 | 1.1902 | 1.1941 | -0.3233 | 1.19149 | -0.3935 |
| 13.0667 | 1.4175 | 1.4058 | 0.8298 | 1.3988 | 1.3199 |
| 14.9333 | 1.4175 | 1.4008 | 1.1812 | 1.3828 | 2.446 |
| 16.8 | 1.1902 | 1.1763 | 1.1725 | 1.186 | 0.3554 |
| 18.6667 | 0.8744 | 0.87 | 0.498 | 0.8746 | -0.0274 |
| 20.5333 | 0.6004 | 0.5985 | 0.323 | 0.5942 | 1.0298 |
| 22.4 | 0.4066 | 0.4031 | 0.8615 | 0.4001 | 1.589 |
| 24.2667 | 0.2791 | 0.2722 | 2.4621 | 0.2714 | 2.7315 |
| 26.1333 | 0.1961 | 0.1815 | 7.4131 | 0.1837 | 6.3086 |

(The field is presented along the line x = 26 at the level z = 2.615, z = 0.0 defining the datum plane. The causative mass is a gravitating mass extending from x = 16 to 36 and y = 11.5 to 16.5, placed at d = 3 units below the plane z = 0. Topographic height varies from z = 0.45 to 1.615.)

Fig. 6.2.2 Contour map of upward continued gravity anomaly at level z = 1.615 using analytical integration over the subareas
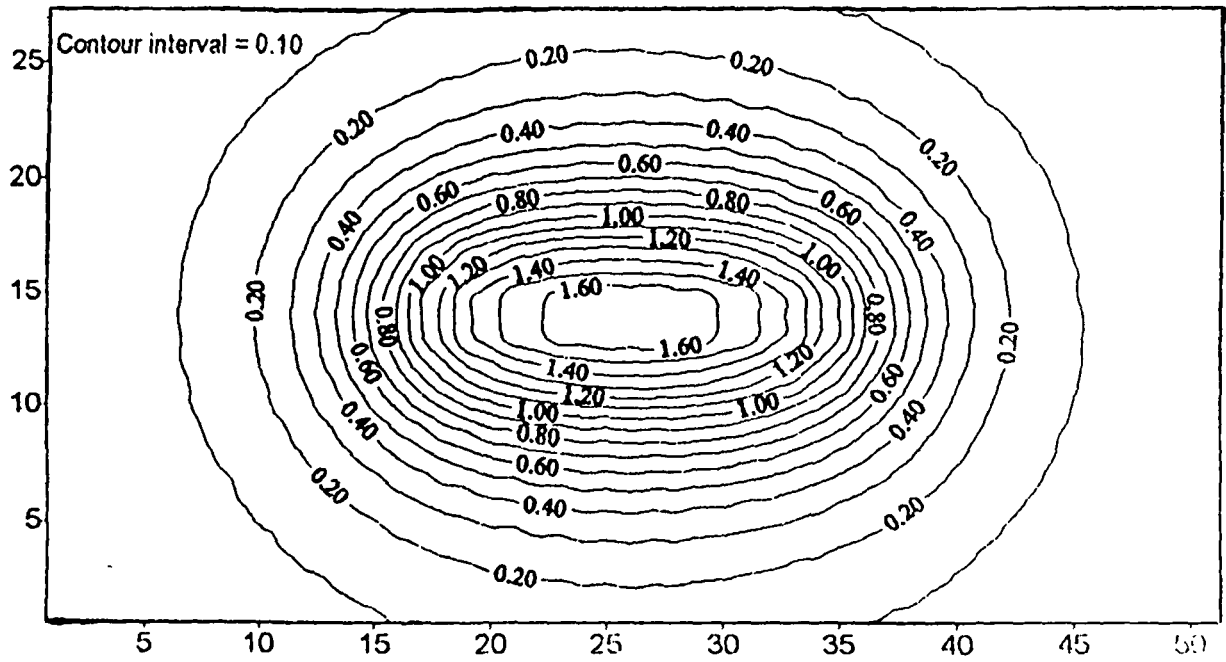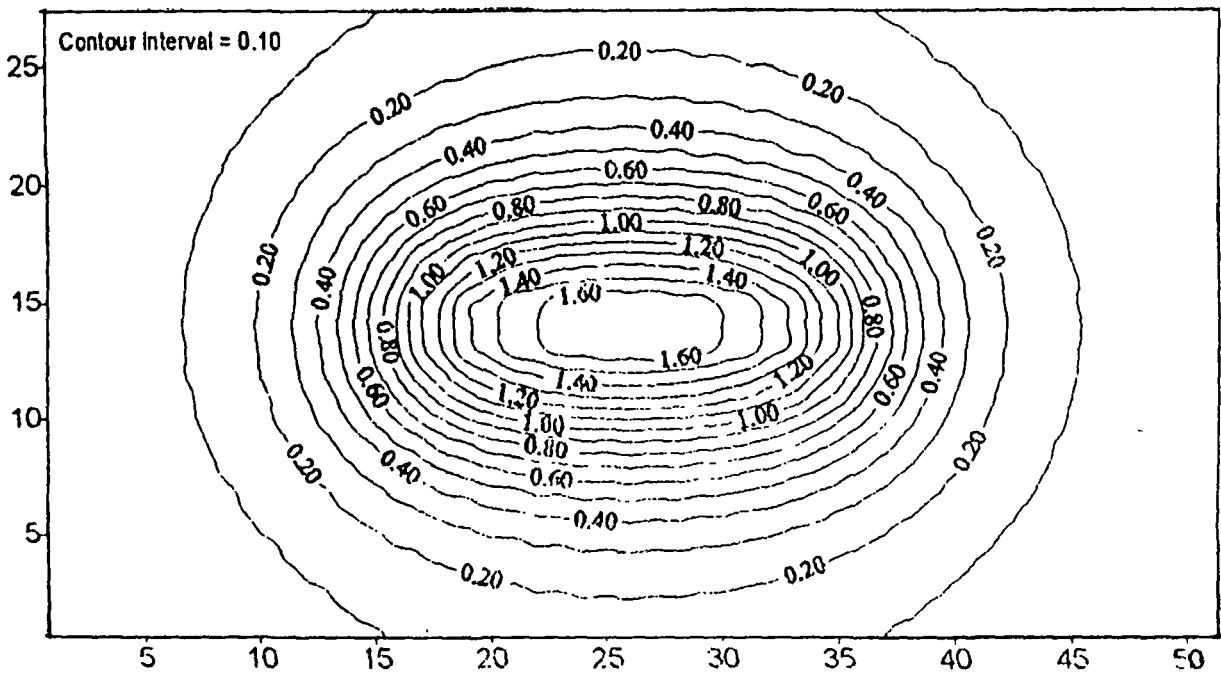


Fig. 6.2.3 Contour map of true gravity anomaly at level z = 1.615

The contour map of the gravity values obtained at level z = 1.615 by use of analytical values of the integrals is shown in Fig.6.2.2 and that obtained from the true values is shown in Fig.6.2.3. It is evident from these maps that the contour map of gravity values, obtained by use of analytical values of the integrals, is very much similar to that drawn from the true values of the gravity field at the same level.

## 6.2.4 Upward Continuation of Magnetic Data

For the rectangular polarised plate lying at a depth d units below the plane z=0, its vertical component magnetic field is computed at the nodal points (x,y,z) of the subareas by the formula(6.2.2)on replacing Z by (Z+d) and assigning $x_1$ =16, $x_2$ =36, $y_1$ =11.5, $y_2$ =16.5 and d = 3. These are then dented by $H_k$, k=1,2,3,....,n and the n (=728) equations of (6.1.14) are formed. Subsequently, the coefficients $b_{kj}$ are evaluated by centroid rule and also by analytical means. The n equations are then solved by Gauss–Seidal iterative method with ε = 0.00001. The equations converge in 5 iterations in both the cases. In the next step, two sets of the vertical component magnetic field $T_z$ at level z = 1.615 are computed by (6.1.13). Once using the $\mu_j$ values obtained from the $b_{kj}$ evaluated analytically and also using those obtained from the approximated $b_{kj}$. The entire procedure

Table-6.2.4: Upward continuation of vertical component magnetic field from an irregular boundary to a level z = 1.615

| Co-ordinate | True field | Analytical integration technique | | Approximate integration technique | |
|---|---|---|---|---|---|
| y | $T_z$ | $T_z$ | % err. | $T_z$ | % err. |
| 3.4667 | 0.00951 | 0.00894 | 6.03355 | 0.00807 | 15.18841 |
| 6.9333 | 0.01459 | 0.01418 | 2.82722 | 0.01349 | 7.58785 |
| 10.4000 | 0.01667 | 0.01529 | 8.25731 | 0.01340 | 19.61296 |
| 13.8667 | -0.04494 | -0.04906 | -9.14751 | -0.03903 | 13.14802 |
| 17.3333 | -0.28578 | -0.27809 | 2.68956 | -0.25323 | 11.38880 |
| 20.8000 | -0.38888 | -0.37762 | 2.89614 | -0.34518 | 11.23850 |
| 24.2667 | -0.39471 | -0.37214 | 5.71770 | -0.25694 | 34.90245 |
| 27.7333 | -0.39471 | -0.37765 | 4.32147 | -0.28781 | 27.08134 |
| 31.2000 | -0.38888 | -0.37108 | 4.57674 | -0.30903 | 20.53419 |
| 34.6667 | -0.28578 | -0.27631 | 3.31224 | -0.24618 | 13.85516 |
| 38.1333 | -0.04494 | -0.04932 | -9.73235 | -0.03774 | 16.02971 |
| 41.6000 | 0.01667 | 0.01178 | 29.32914 | 0.00538 | 67.72171 |
| 45.0667 | 0.01459 | 0.01415 | 3.07438 | 0.01310 | 10.22968 |
| 48.5333 | 0.00951 | 0.00933 | 1.96036 | 0.00854 | 10.20152 |

(The field is presented along the line y = 14 at the level z = 1.615, z = 0 defining the datum plane. The causative mass is a vertically polarised horizontal plate extending from x = 16 to 36 and y = 11.5 to 16.5, placed at d = 3 units below z = 0. Topographic height varies from z = 0.45 to 1.615.)

of computation of $T_z$ at the continuation level $\bar{S}$ is either carried out by analytical means or by centroid of approximation to an integral. The field values obtained along line y=14 at height z=1.615 are shown in Table-6.2.4 along with the true values of $T_z$ for comparison. It is evident from Table-6.2.4 that the field values computed at a level $\bar{S}$ near the boundary can be obtained with reasonable accuracy if the integrals involved in the expression (6.1.13) and (6.1.14) are computed analytically.

Again, it is evident from Table-6.2.4 that the computed field at (41.6,14,1.615) is with unacceptable error. It is to be noted here that this field point lies above a sharp cliff of the boundary. As such, the error in the computed field at the point is abnormally high. This error will be minimized if the subareas are made smaller in size around the cliff of the boundary. The contour maps of the true field values at level z=1.615 and those made at the same level from the field values obtained by analytical and approximate means of computation are shown in Fig.6.2.4, Fig.6.2.5 and Fig.6.2.6 respectively. It is evident from Fig.6.2.4 and Fig.6.2.5 that at a level near the boundary, the field values obtained on analytical means of computation produce a contour map that preserves nearly all the characters of the field near the boundary.

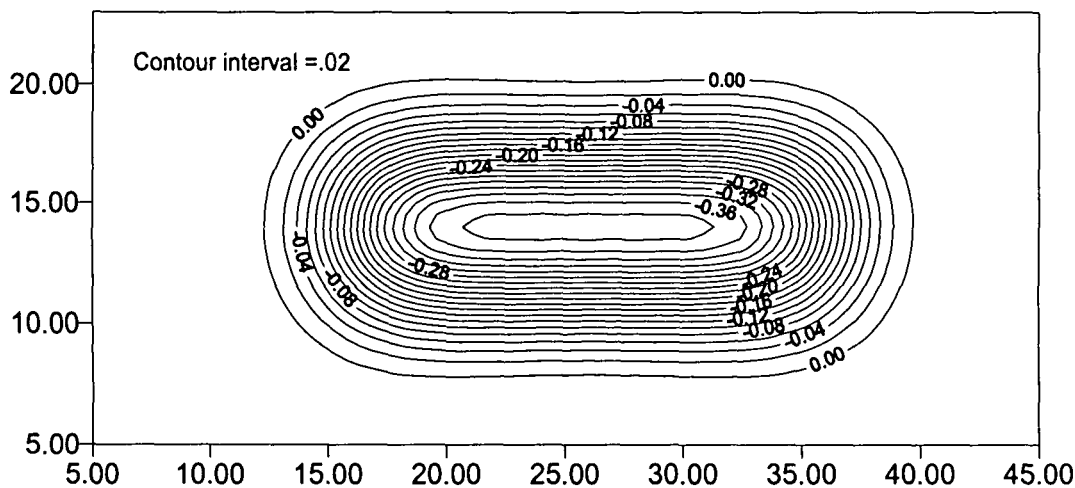Fig.6.2.4 Contour map of vertical component magnetic at anomaly at level z = 1.615

Fig.6.2.5  Contour map of vertical component magnetic anomaly at level z = 1.615 using analytical integration over the subareas
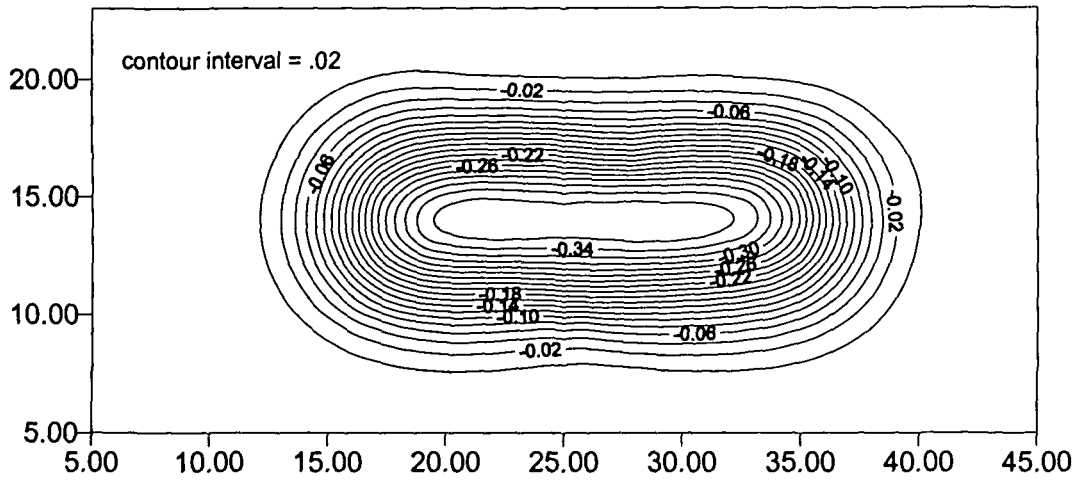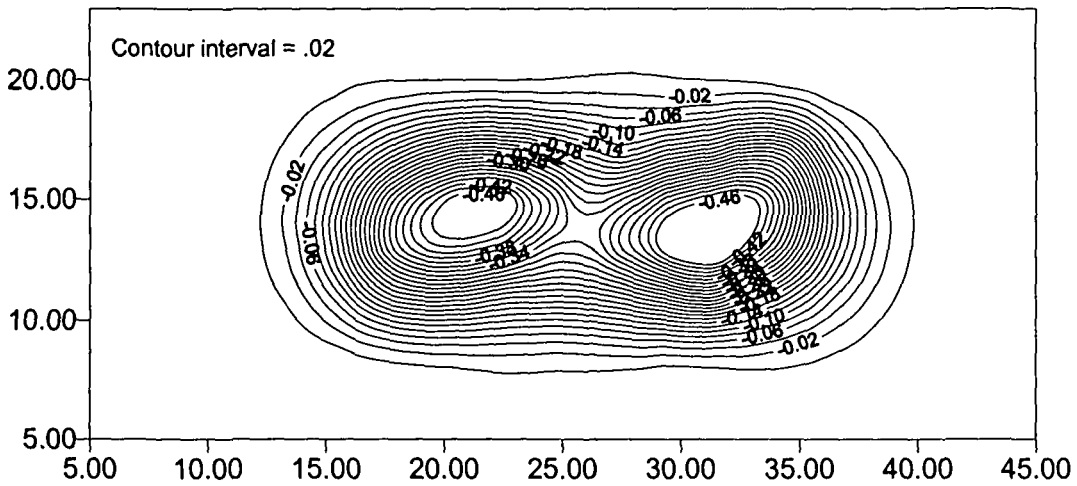


Fig.6.2.6  Contour map of vertical component magnetic anomaly at level z = 1.615 using centroid approximation of integration over the subareas



On the contrary, the contour map of the field values obtained by use of approximation of the integrals over the subareas presents a distorted picture of the field which can not be used for any practical purpose.

# Chapter-7

# Application to Geophysics

## Processing and Interpretation of Ground Magnetic Data of Vishakhapatnam-Srikakulam Area

## Introduction

Vishakhapatnam-Srikakulam area of Andhra Pradesh lies in the northeastern part of Eastern Ghats, a pre-Cambrian belt of peninsular India (Fig.7.1.1). Its coastal part is relatively flat in comparison to the rugged Lamaput-Araku area at the northwest. The topographic height varies from 20 to 300 m in the coastal area and from 450 to 1600 m in

Fig. 7.1.1 Andhra Pradesh and the study area



67
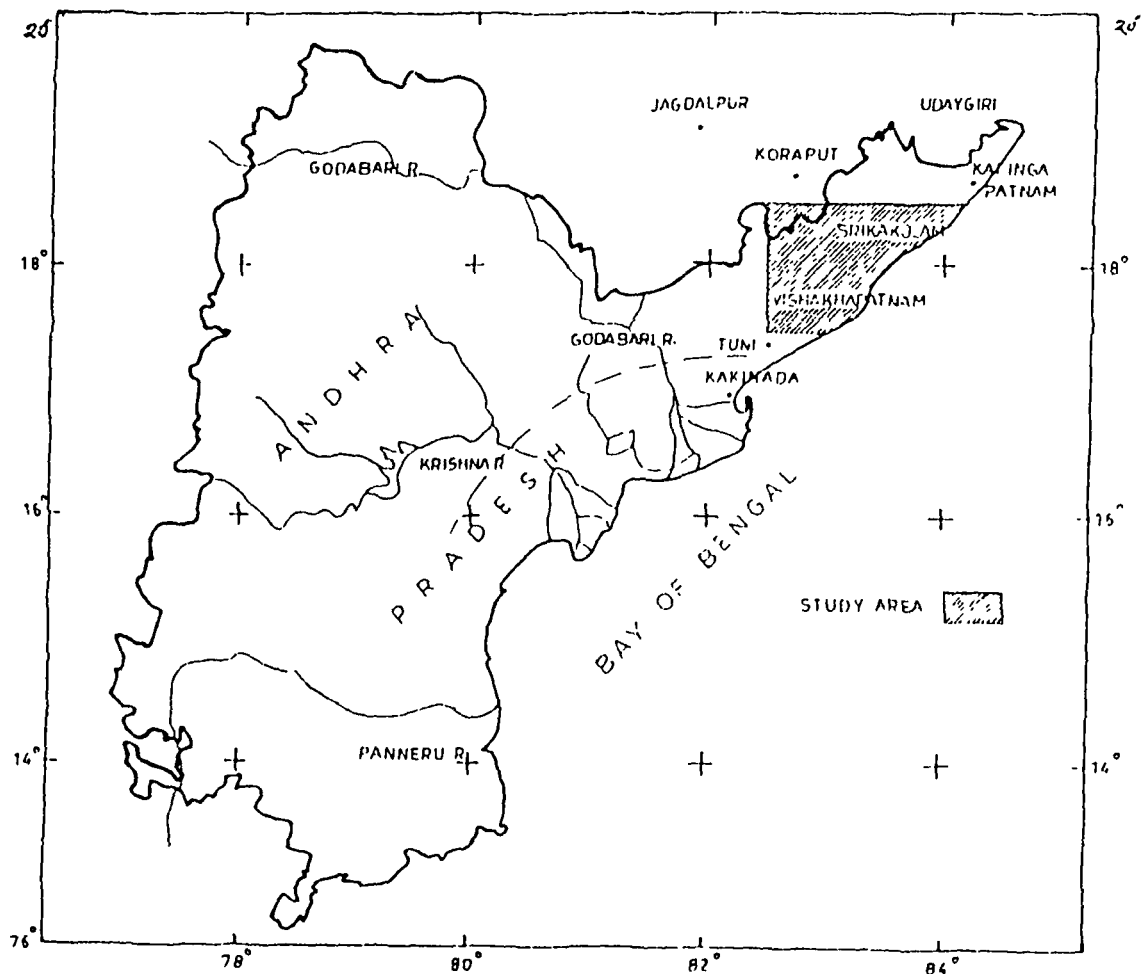
Araku area. The Eastern Ghats constitutes the most metamorphosed sector of the pre-Cambrian rocks in the Indian shield. Geology of the area is complex. Nature of the basement, origin of the constituent rocks and their structure are yet to be clearly
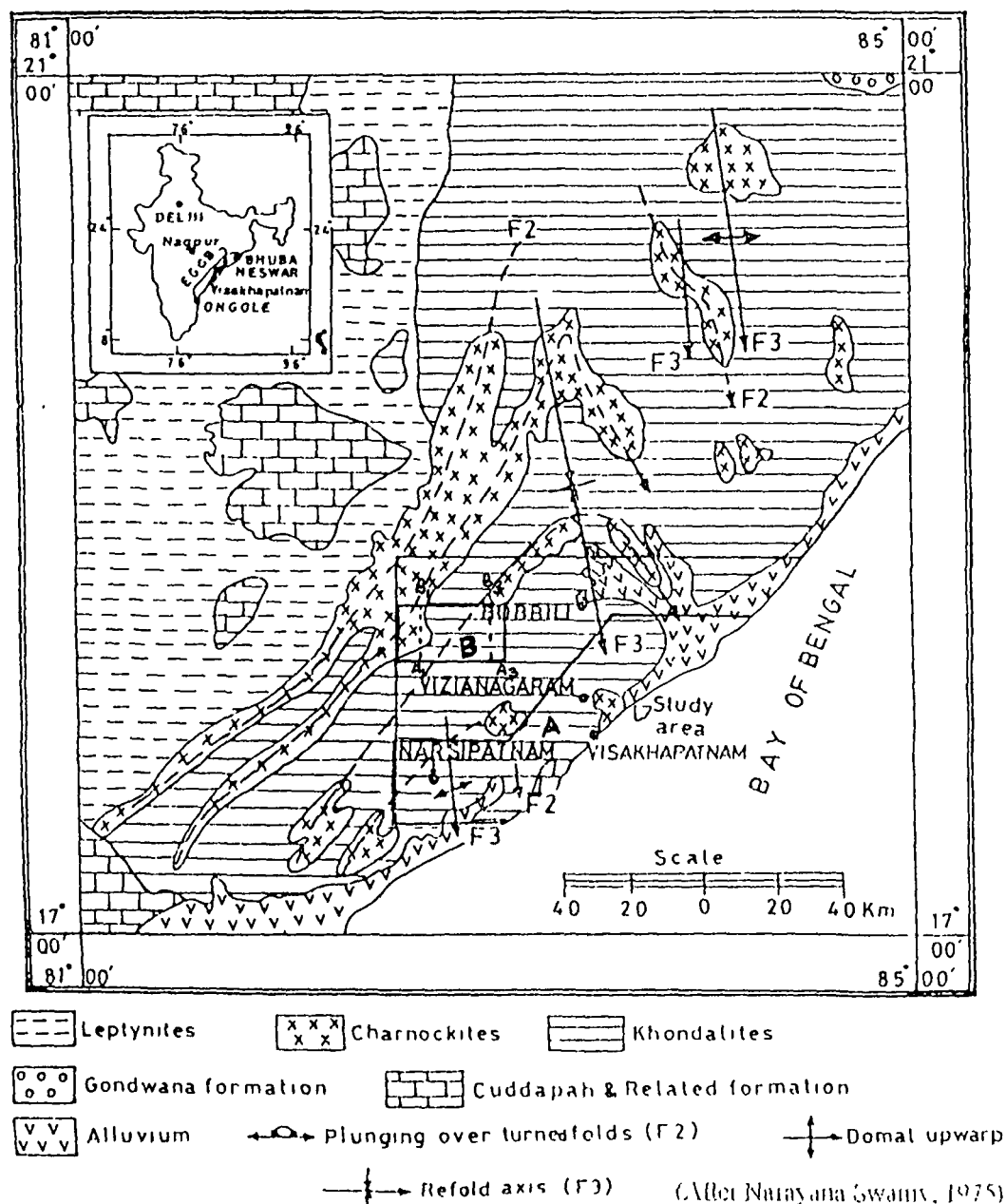
Fig. 7.1.2.Geological map of Vishakhapatnam-Srikakulam area and the study area A and B



understood. Geological investigations were extensively carried out in the Eastern Ghat region by many workers focussing on mineral, petrology, geo-chemical and other aspects. The geological map of the area, showing the structures and tectonics of eastern Ghats, suggested by Swamy (1975) is reproduced in Fig.7.1.2. Subrahmanyam (1978, 1983),

Subrahmanyam and Verma (1986) studied the gravity map published by National Geophysical Research Institute (NGRI) for broader details such as major faults and crustal thickness. Regional magnetic surveys on a local scale were conducted in parts of Vizianagaram district of Andhra Pradesh by Rao et al (1990), Murthy et al (1991). The surveys inferred a shallow magnetic interface of Charnokites, which has been repeatedly faulted and folded due to successive stages of deformation in the Eastern Ghats.

Charnokites, the popular rock type in this belt, is magnetic in nature. To infer the structure, depth and dimensions of the Charnokite rocks in the northeastern coastal districts of Vishakhapatanam, Vizianagaram and Srikakulam covering an area of about 15000 sq. km of Andhra Pradesh, magnetic survey with proton-precision magnetometer was carried out by Andhra University (Murthy and Rao 2001) over the area.

The magnetic anomalies are noisy and these are poorly correlated with the surface geology (Murthy and Rao 2001). On upward continuation of the observed field using harmonic analysis of profile magnetic data, they derived distinct anomaly trends running NE-SW at the southern part and EW trend at the northern part of the area. Based on termination of anomaly closures and displacement of anomaly trends, they have predicted existence of five faults striking in almost NS direction. On modeling of smooth magnetic profiles they have concluded that the Charnokite form the magnetic basement in the area.

# 7.1 THE COASTAL PART OF VISHAKHAPATNAM-SRIKA -KULUM AREA

## 7.1.1 Topography and Geology of the Area

The area under study covers the relatively flat coastal areas consisting of Vizianagaram, Vishakhapatnam and a part of Srikakulam districts of Andhra Pradesh. This is a part of the area bounded by $17.5^0$ and $18.5^0$N latitudes and $82.5^0$ and $84.5^0$E longitudes. The topographic height varies from 20 to 300 mts. in general in the area and as such, for all practical purpose, the data acquired over the area can be assumed as if these were acquired over a flat terrain.

The area is mostly covered by alternate patches of Khondalites and Leptynites in general with a few isolated patches of Charnokites lying exposed towards the northwestern part and alluvium covering a narrow coastal part of the area. (Fig.7.1.2, Swami 1975). The Khondalites are non-magnetic in nature, the Leptynites are weakly magnetized and the Charanokites are strongly magnetised with susceptibility varying from $12 \times 10^{-4}$ to $24 \times 10^{-4}$ cgs units (Murthy and Rao 2001).

## 7.1.2 Magnetic Data

The magnetic survey was conducted by use of proton-precision magnetometer on a regional scale by Andhra University. A total of 3117 stations were occupied covering the entire Vishakhapatnam-Srikakulam area, putting an average density of 1 station per 3 to 4 sq. km. On carrying out all normal corrections such as diurnal and International Geomagnetic Reference Field (IGRF), a copy of the data was given to Tezpur University.

Fig. 7.1.3. Total field magnetic anomaly map of a part of Vishakhapatnam-Srikakulam area (Contours are plotted in an assumed datum plane)



(The axes are in km. scale and (0,0) of the reference frame is defined by Long. 82 5°N and Lat. 17.5°E)

70
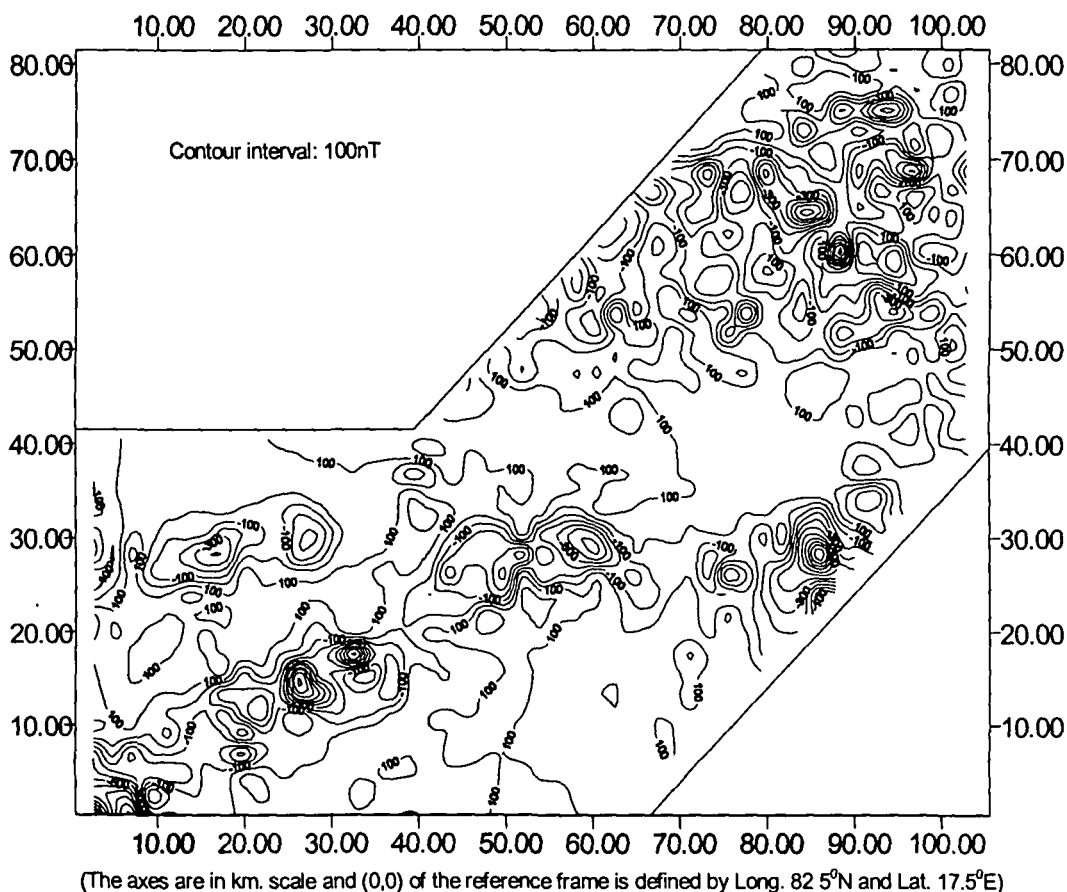
The accuracy of the magnetometer reading is 1 nT and that of the reduced anomaly is believed to be within ± 5 nT (Murthy and Rao 2001).

A contour map of the magnetic anomaly, drawn by use of Surfer-32 package is presented in Fig.7.1.3. It is evident from Fig.7.1.3. the coastal area is adequately covered by magnetic stations. It is also evident in Fig.7.1.3 that the magnetic response of the basement is heavily masked by the response of shallow or nearly exposed unconsolidated magnetic sediments. Further, a careful examination reveals that a basement high platform exists in the Kalingpatnam-Udayagiri area at the northeastern corner of the area.

## 7.1.3 Upward Continuation of Magnetic Field over a Flat Terrain

The coastal area approximately bounded by lines joining $(82.5^0E, 17.5^0N)$, $(83.125^0E, 17.5^0N)$, $(83.5^0E, 17.875^0N)$, $(83.5^0E, 18.25^0N)$, $(83.25^0E, 18.25^0N)$, $(82.875^0E, 17.875^0N)$ and $(82.5^0 E, 17.875^0N)$ covering 5532 sq. km area is divided into 5532 equal sq. subareas and the coordinates of their nodal points are noted in a cartesian reference frame with x-axis coinciding with $17.5^0N$ latitudes, y-axis coinciding with $82.5^0E$ longitudes and z-axis pointing upward. The total field magnetic data with station coordinates in km are considered for computing vertical component magnetic data at each station by use of the formula $T_z = Tsin\theta$, where $T_z$ is the vertical component of the total field T and $\theta$ is the angle of inclination of earth's magnetic field at the station. A contour map of the vertical component magnetic field is prepared with help of Surfer-32 contouring package. Subsequently, the vertical component magnetic data at the nodal points are interpolated by inverse distance weighted interpolation formula (Watson and Philip 1985). Finally, following (5.1.13), the field is continued upward at a level z = 1 km, z = 0 defining the assumed datum plane. The contour map of the vertical component magnetic field is shown in Fig.7.1.4.

It is evident from Fig.7.1.4 that the high frequency magnetic response that masks the trend of the magnetic field of the basement, as seen in Fig.7.1.3, is removed when the field is obtained at the level 1 km above the assumed datum level z =0. The anomaly map clearly shows a series of magnetic lows aligned in the form of an arc that continues up to the sea extending from southwest corner of the area. This is followed by another E-W

Fig. 7.1.4 Vertical component of magnetic anomaly map
(Contours are plotted at a height of 1km from the assumed datum plane)
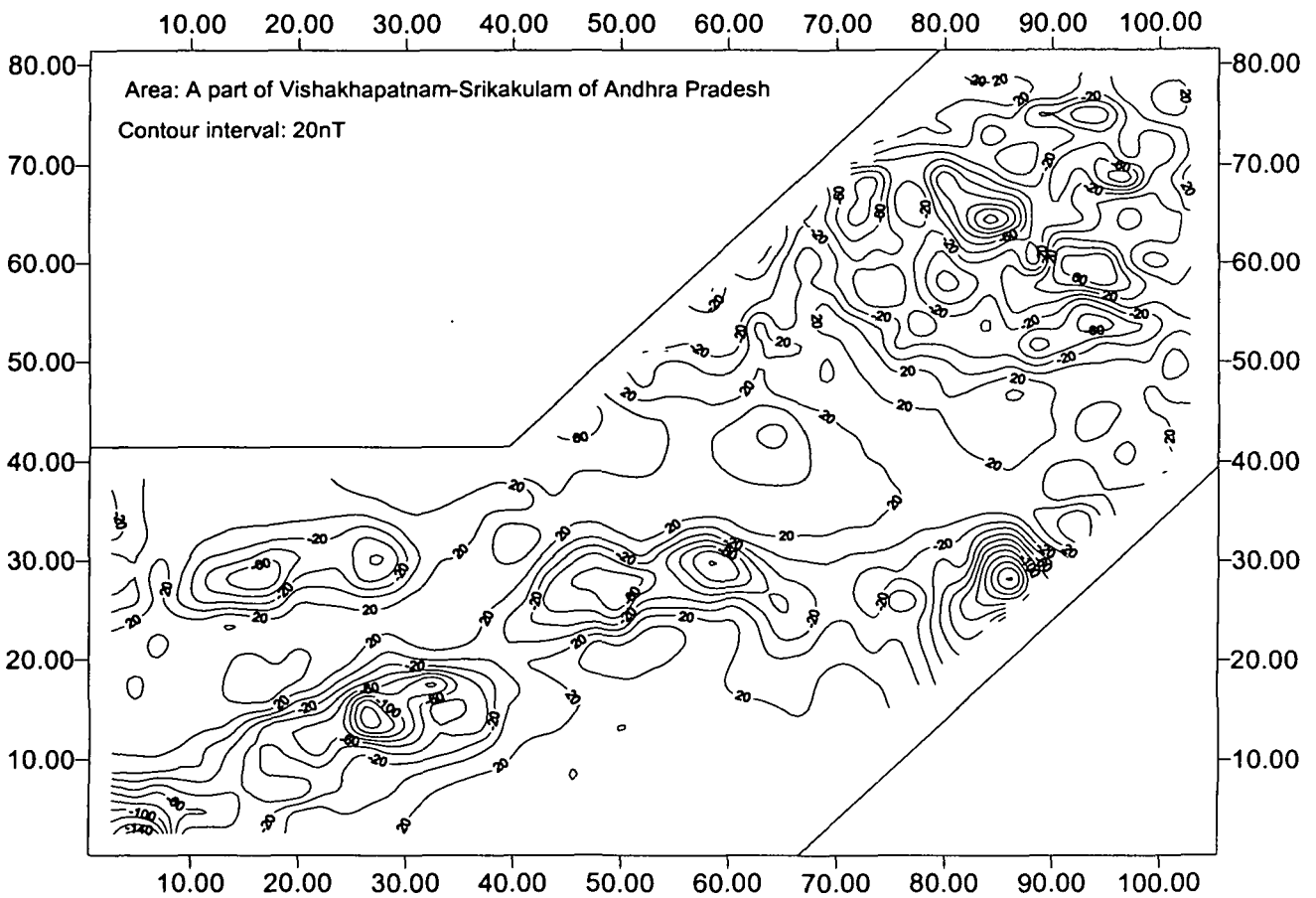


trending magnetic low at its north separated by a NW-SE trending elongated magnetic
high that continues upto the magnetic high platform at northeast.

## 7.1.4 Determination of Depth to the Subsurface Magnetic Causatives

To compute the study of the data, we considered 28 two-dimensional profiles on the
datum plane and DEPTHDNC software developed at KDMIPE and modified at Tezpur
University is used to determine point-to-point depth along the profiles. It is evident from
the magnetic anomaly maps exhibited in Fig.7.1.3 and Fig.7.1.4 that the magnetic
response at the ground surface is a combination of responses of shallow and deeper
magnetic causatives. To determine the depth to the causatives, 28 two-dimensional total
field magnetic profiles along the lines $L_1, L_2, \ldots., L_{22}$ are considered. Latitude, longitude
and magnetic inclination of end points of each line are shown in Table-7.1.1.

The total field magnetic data along each of the 28 lines are read from a large anomaly map prepared in 1: 250,000 scale as we move from south to north. The data read along the line $L_{12}$ are shown in Table-7.1.2. Subsequently, the vertical component field $T_z$ along each line is obtained from total field data T as described earlier.

Finally, the depth computed along the line $L_{12}$ is shown Fig.7.1.5 and Table-7.1.3 for shallow and deeper magnetic causatives. Following the same procedure for all 28 lines,

Fig. 7.1.5  Top of the shallow magnetic sediment and basement along line L12



Distance (km)
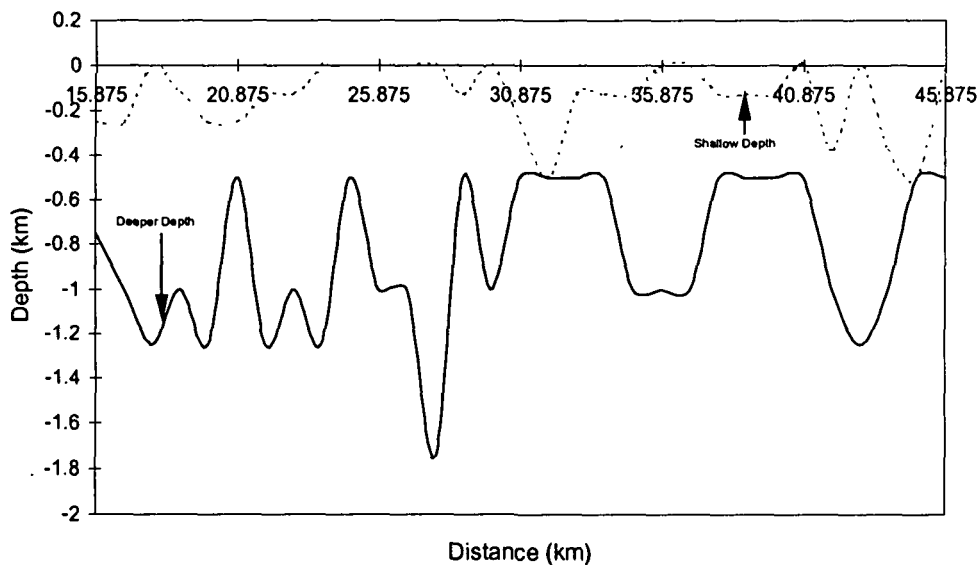
contour maps for depth to the shallow magnetic causative masses and deeper magnetic causative masses are presented in Fig.7.1.6 and Fig.7.1.7 respectively.

It is evident from Fig.7.1.6 that the area is mostly covered by exposed or nearly exposed unconsolidated magnetic sediments with patches of non-magnetic sediments at places. Fig. 7.1.7 reveals that a NE-SW trending central high axis extends from southwest to the northeast corner of the area where it merges with the basement high platform of Kalingapatnam-Udayagiri area. Two nearly semi-circular basement highs one at north of (82.97 $^0$E, 17.56 $^0$N) and the other at northwest of (83.47$^0$E, 17.8$^0$N) lie at the south of the central high axis with their axes aligned in north and northwest directions respectively. The structural highs revealed in Fig.7.1.7, the semicircular features in particular, are in agreement with concept of Swami (1975) about the basement in the area.

73

Table-7.1.1 Description of the 2-D lines used for computation of depth to shallow and deeper magnetic causatives

| | Initial points | | | End points | | |
|---|---|---|---|---|---|---|
| Line | Longitude | Latitude | Inclination | Longitude | Latitude | Inclination |
| L1 | $84.0540^0$ | $18.2500^0$ | $21.5172^0$ | $83.6208^0$ | $18.5000^0$ | $22.0930^0$ |
| L2 | $83.9673^0$ | $18.1250^0$ | $21.2468^0$ | $83.6208^0$ | $18.5000^0$ | $22.1151^0$ |
| L3 | $83.8932^0$ | $18.1250^0$ | $21.2536^0$ | $83.5000^0$ | $18.5000^0$ | $22.1261^0$ |
| L4 | $83.7335^0$ | $18.0000^0$ | $20.9905^0$ | $83.4577^0$ | $18.5000^0$ | $22.1300^0$ |
| L4A | $83.6967^0$ | $18.0676^0$ | $21.1461^0$ | $83.5687^0$ | $18.5000^0$ | $22.1198^0$ |
| L4B | $83.8033^0$ | $18.0000^0$ | $20.9836^0$ | $83.6315^0$ | $18.3750^0$ | $21.8357^0$ |
| L5 | $83.6022^0$ | $18.0000^0$ | $21.0034^0$ | $83.4120^0$ | $18.5000^0$ | $22.1342^0$ |
| L5A | $83.6220^0$ | $17.8750^0$ | $20.7236^0$ | $83.3543^0$ | $18.5000^0$ | $22.1394^0$ |
| L6 | $83.5880^0$ | $17.8750^0$ | $20.7264^0$ | $83.3122^0$ | $18.5000^0$ | $22.1433^0$ |
| L6A | $83.5880^0$ | $17.8750^0$ | $20.7264^0$ | $83.3128^0$ | $18.5000^0$ | $22.1432^0$ |
| L7 | $83.5728^0$ | $17.8750^0$ | $20.7280^0$ | $83.1767^0$ | $18.3750^0$ | $21.8781^0$ |
| L8 | $83.5433^0$ | $17.8750^0$ | $20.7309^0$ | $82.9155^0$ | $18.5000^0$ | $22.1796^0$ |
| L9 | $83.5610^0$ | $17.7500^0$ | $20.4508^0$ | $82.7817^0$ | $18.5000^0$ | $22.1919^0$ |
| L10 | $83.4332^0$ | $17.7500^0$ | $20.4638^0$ | $82.6197^0$ | $18.5000^0$ | $22.2067^0$ |
| L11 | $83.4602^0$ | $17.6250^0$ | $20.1830^0$ | $82.6197^0$ | $18.2750^0$ | $21.9230^0$ |
| L12 | $83.3380^0$ | $17.6250^0$ | $20.1956^0$ | $82.5517^0$ | $18.3750^0$ | $21.9363^0$ |
| L13 | $83.2500^0$ | $17.6250^0$ | $20.2047^0$ | $82.8380^0$ | $18.0000^0$ | $21.0784^0$ |
| L14 | $83.1888^0$ | $17.6250^0$ | $20.2110^0$ | $82.6597^0$ | $18.0000^0$ | $21.0959^0$ |
| L15 | $83.2358^0$ | $17.5000^0$ | $19.9284^0$ | $82.6408^0$ | $18.0000^0$ | $21.0978^0$ |
| L16 | $83.0153^0$ | $17.6250^0$ | $20.2289^0$ | $82.5775^0$ | $18.0000^0$ | $21.1040^0$ |
| L17 | $83.0868^0$ | $17.5000^0$ | $19.9440^0$ | $82.6408^0$ | $17.8750^0$ | $20.8210^0$ |
| L18 | $82.9953^0$ | $17.5000^0$ | $19.9536^0$ | $82.5962^0$ | $17.8750^0$ | $20.8255^0$ |
| L19 | $82.8897^0$ | $17.5000^0$ | $19.9647^0$ | $82.5563^0$ | $17.8750^0$ | $20.8295^0$ |
| L20 | $82.7970^0$ | $17.5000^0$ | $19.9744^0$ | $82.4788^0$ | $17.8750^0$ | $20.8372^0$ |
| L20A | $82.7970^0$ | $175000^0$ | $19.9744^0$ | $82.5000^0$ | $17.7500^0$ | $20.5586^0$ |
| L21 | $82.7593^0$ | $17.5000^0$ | $19.9784^0$ | $82.4765^0$ | $17.7500^0$ | $20.5610^0$ |
| L22 | $82.6232^0$ | $17.5000^0$ | $19.9927^0$ | $82.5000^0$ | $17.6250^0$ | $20.2820^0$ |
| L22A | $82.6991^0$ | $17.5000^0$ | $19.9847^0$ | $82.5000^0$ | $17.6858^0$ | $20.4167^0$ |

74

Table7.12 Total Field Magnetic Data Along Line L12

| Distance (km.) | Field (nT) | Distance (km.) | Field (nT) |
|---|---|---|---|
| 6.875 | 375 | 20.625 | -50 |
| 7.000 | 350 | 21.250 | -50 |
| 7.500 | 300 | 22.250 | -40 |
| 8.000 | 250 | 23.125 | -30 |
| 8.375 | 200 | 25.000 | 0 |
| 8.750 | 150 | 26.375 | 50 |
| 9.250 | 100 | 27.500 | 75 |
| 9.750 | 50 | 28.750 | 100 |
| 10.250 | 0 | 31.000 | 120 |
| 10.875 | -50 | 33.375 | 125 |
| 12.000 | -100 | 35.625 | 150 |
| 13.000 | -100 | 38.500 | 175 |
| 15.250 | 0 | 40.750 | 150 |
| 15.750 | 50 | 42.000 | 125 |
| 16.250 | 100 | 43.625 | 100 |
| 16.750 | 150 | 44.250 | 50 |
| 17.125 | 200 | 45.625 | 50 |
| 17.625 | 250 | 47.250 | 50 |
| 18.125 | 250 | 50.000 | 5 |
| 18.750 | 150 | 52.000 | 0 |
| 19.000 | 100 | 52.750 | -50 |
| 19.250 | 50 | 54.250 | -100 |
| 19.500 | 0 | 56.250 | -100 |
| 19.750 | -50 | 57.875 | -100 |

Table 7.1.3. Depth to shallow and deeper magnetic causatives along line L12

| Distance in km | Shallow depth in km | Deeper depth in km | Distance in km | Shallow depth in km | Deeper depth in km |
|---|---|---|---|---|---|
| 15.875 | -0.25 | -0.75 | 31.875 | -0.5 | -0.5 |
| 16.875 | -0.25 | -1 | 32.875 | -0.125 | -0.5 |
| 17.875 | 0 | -1.25 | 33.875 | -0.125 | -0.5 |
| 18.875 | -0.125 | -1 | 34.875 | -0.125 | -1 |
| 19.875 | -0.25 | -1.25 | 35.875 | 0 | -1 |
| 20.875 | -0.25 | -0.5 | 36.875 | 0 | -1 |
| 21.875 | -0.125 | -1.25 | 37.875 | -0.125 | -0.5 |
| 22.875 | -0.125 | -1 | 38.875 | -0.125 | -0.5 |
| 23.875 | 0 | -1.25 | 39.875 | -0.125 | -0.5 |
| 24.875 | | -0.5 | 40.875 | 0 | -0.5 |
| 25.875 | | -1 | 41.875 | -0.375 | -1 |
| 26.875 | 0 | -1 | 42.875 | 0 | -1.25 |
| 27.875 | 0 | -1.75 | 43.875 | -0.375 | -1 |
| 28.875 | -0.125 | -0.5 | 44.875 | -0.5 | -0.5 |
| 29.875 | 0 | -1 | 45.875 | 0 | -0.5 |
| 30.875 | -0.25 | -0.5 | | | |

Fig. 7.1.6 Depth contour map of shallow magnetic elements

AREA: VISHAKHAPATNAM-SRIKAKULAM

CONTOUR INTERVAL= 100m
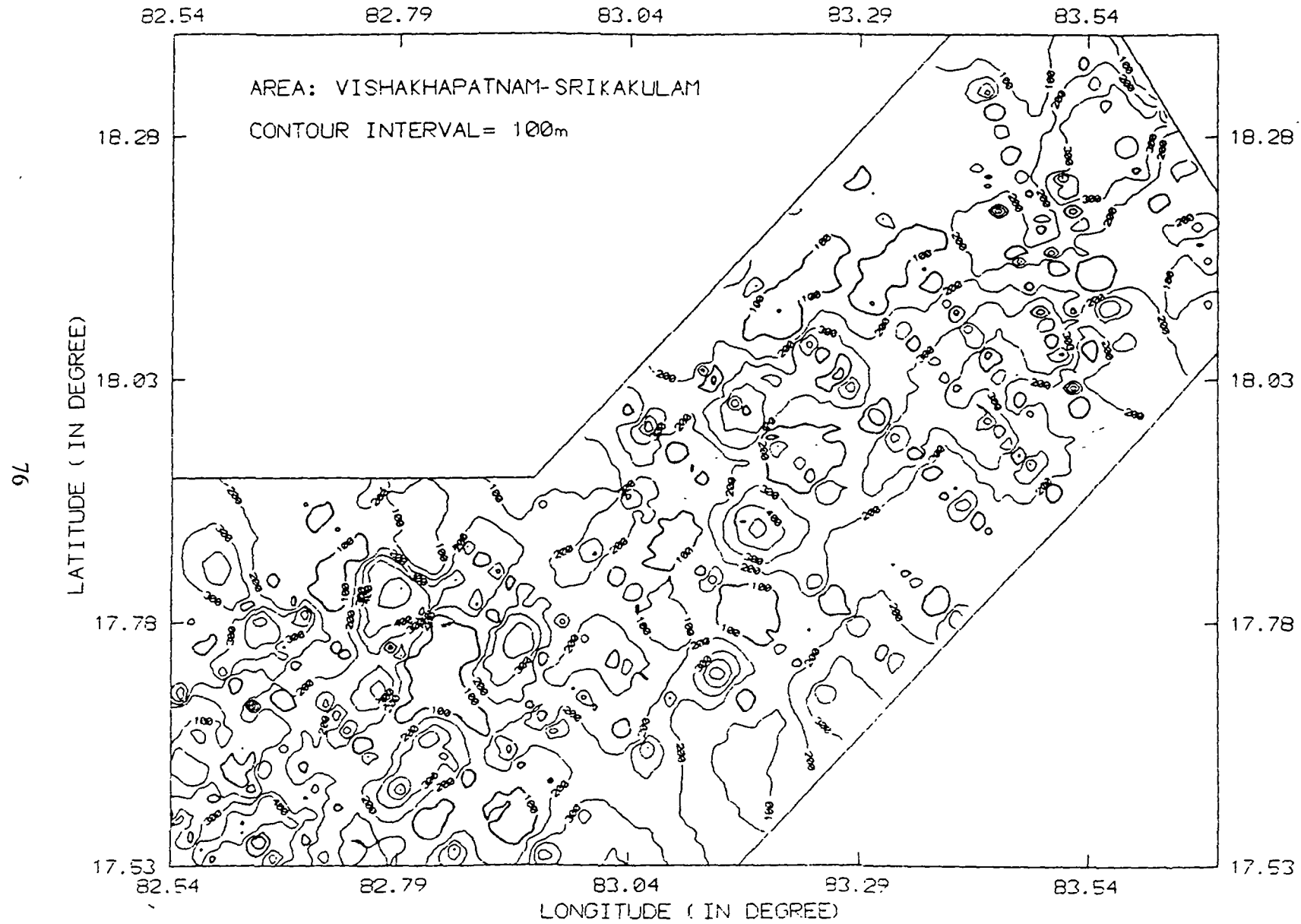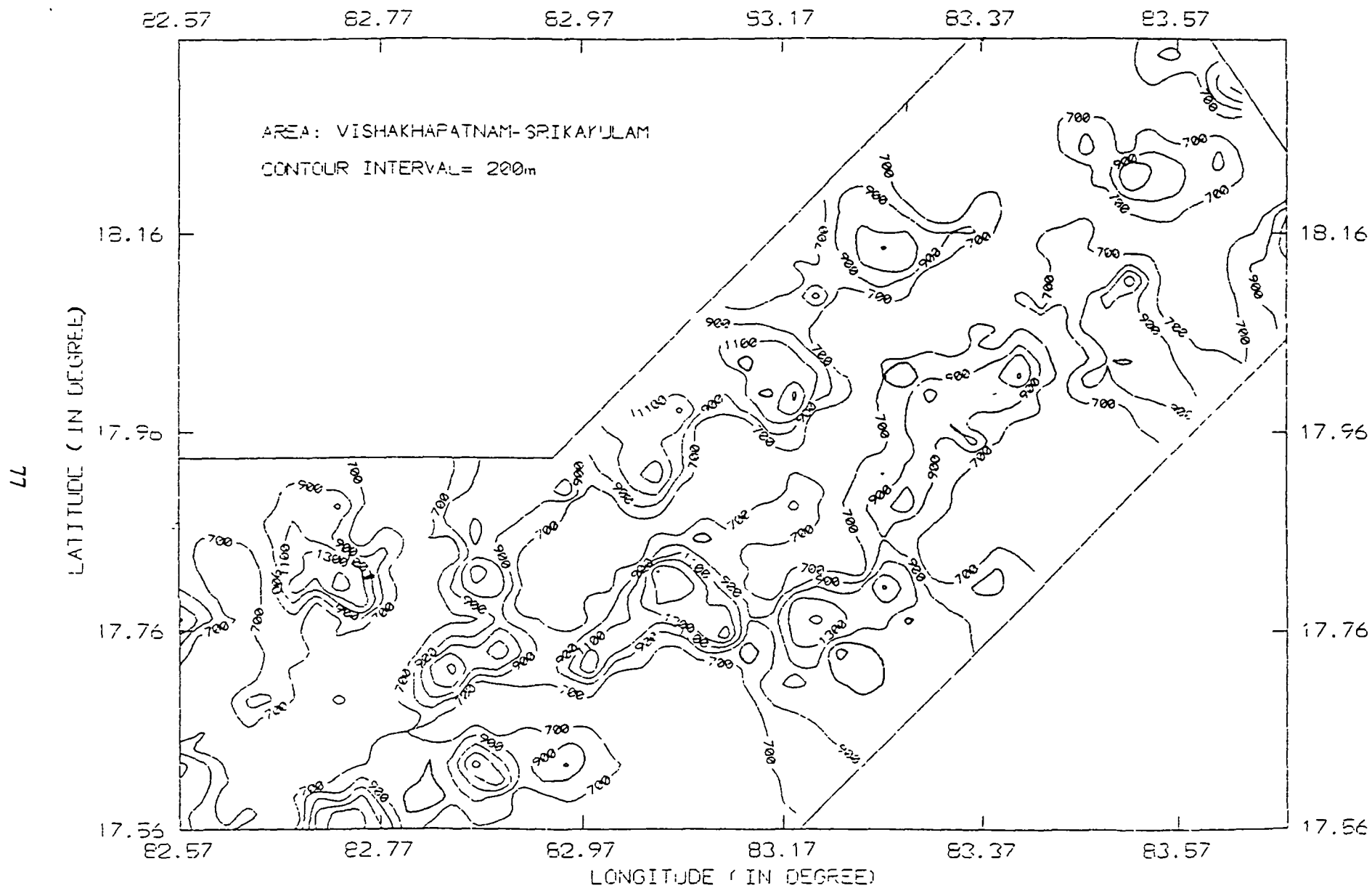
LATITUDE ( IN DEGREE)

LONGITUDE ( IN DEGREE)

Fig. 7.1.7 Depth contour map of deeper magnetic elements

The area under discussion, with topographic height-variation 20-300mt, contains exposed or nearly exposed unconsolidated magnetic sediments. The depth to the basement in the area varies from 0.5 to 1.5 km in general. Under the above geological set up, processing of ground magnetic data, assuming as if these were acquired over a horizontal plane, is bound to lead to inaccurate depth not only to the shallow magnetic sediments but also to the basement. For a reliable result, the topography must be taken into account in processing of ground magnetic data in the area. However, the analysis carried out assuming the data were acquired over a horizontal plane, is expected to provide a lead to further work in the area, in addition to revealing a general information about the geometry of the basement.
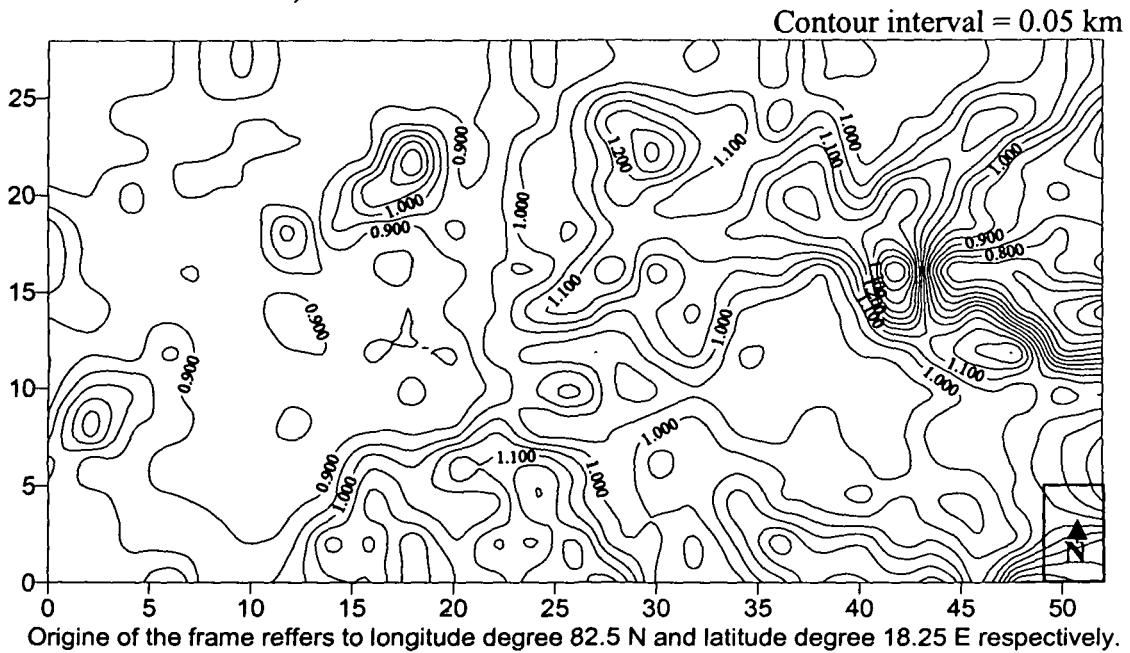
For interpretation of the magnetic data, a generalized geological map of the area in A4 size paper, presented by Swami (1975), was consulted. For a reliable interpretation of the magnetic data, a good geological map in 1:50,000 scale is required. Since the area falls in a restricted zone, the said map remained inaccessible in the present work. As such, the locations of the exposed or nearly exposed magnetic sediments, identified from the magnetic data, are to be verified on a detailed geological map of the area.

## 7.2 Hilly Area of Lamaput-Araku Region

### 7.2.1 Topography and Geology of the Area

Lamaput-Araku area bounded by north latitudes $18.25^0$ and $18.5^0$ and east longitudes $82.5^0$ and $83^0$ marked as area B in Fig.7.1.1 is a hilly terrain of northwestern part of Vishakapatnam-Srikakulam area. The topography of the area is shown in Fig.7.2.1. It is evident from Fig.7.2.1 that the topographic height varies from 450 to 1600 mts in the area. The western part of the area is mostly covered by exposed Charnokites and the rest by Khondalites. As already stated, the Khondalites are non-magnetic and the Charnokites are strongly magnetic in nature with susceptibility varying from $12 \times 10^{-4}$ to $24 \times 10^{-4}$ cgs units. (Murthy and Rao 2001).

Fig. 7.2.1. Topographic contour map of north west part of Srikakulam (Lamaput - Araku area) of Andhra Pradesh

Contour interval = 0.05 km



Origine of the frame reffers to longitude degree 82.5 N and latitude degree 18.25 E respectively.

## 7.2.2 Magnetic Anomaly and its Qualitative Interpretation

The area is covered by 163 magnetic stations with an average of about 1 station per 9 sq. km. The total field magnetic data are assumed acquired over a flat terrain and a contour map of the magnetic anomaly is prepared with help of Surfer–32 package. The map so

Fig. 7.2.2. Total field magnetic anomaly map of Lamaput -Araku area of Andhra Pradesh (Assuming data are acquired over a horizontal plane)

Contour interval = 50nT
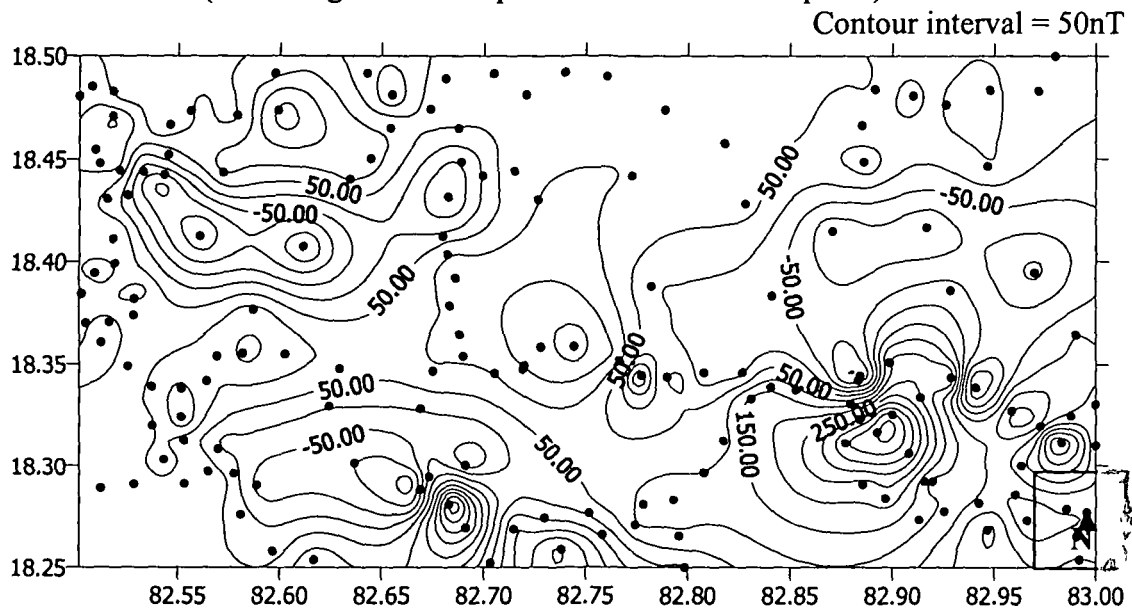


(Both the axes are in degree latitude and longitude)

79

prepared is shown in Fig.7.2.2. It is evident from Fig.7.2.2 that a magnetic high runs in NW–SE direction flanked by magnetic lows on both sides. The total field magnetic data are then used to find the vertical component field on finding the angle inclination of earth's magnetic field at each station.

## 7.2.3 Quantitative Analysis of the Magnetic Data

The topography is now approximated by 728 piecewise flat triangular subareas as described in article (5.2.2). The area of each subarea, coordinates of its vertices and nodal point (centroid) and the direction cosines of the outward drawn normal to it are noted. Subsequently, the vertical component field at the centroid of each subarea is interpolated from the boundary data by use of inverse distance weighted interpolation formula (Watson and Philip 1985). On setting the boundary data at the nodal points, the n (= 728) equations (5.1.13) are formed and these are solved for the double layer boundary density $\mu_j$ by Gauss-Seidal iterative method on evaluation of the coefficient $b_{kj}$ by analytical means as described earlier. The equations took 5 iterations to converge with convergence condition of $\epsilon = 0.00001$. Finally, the field values are computed at levels $z = 1.615$ and 2.115 km aMSL on analytical evaluation of the integrals involved in (5.1.12). The up-continued field values so obtained are shown in contour maps in Fig.7.2.3 and Fig.7.2.4 respectively.

Fig. 7.2.3 Vertical component magnetic field of Lamaput –Araku area
(Using analytical means of integration over subareas)
Height of the plane = 1.615 km (aMSL)
Contour interval = 20nT
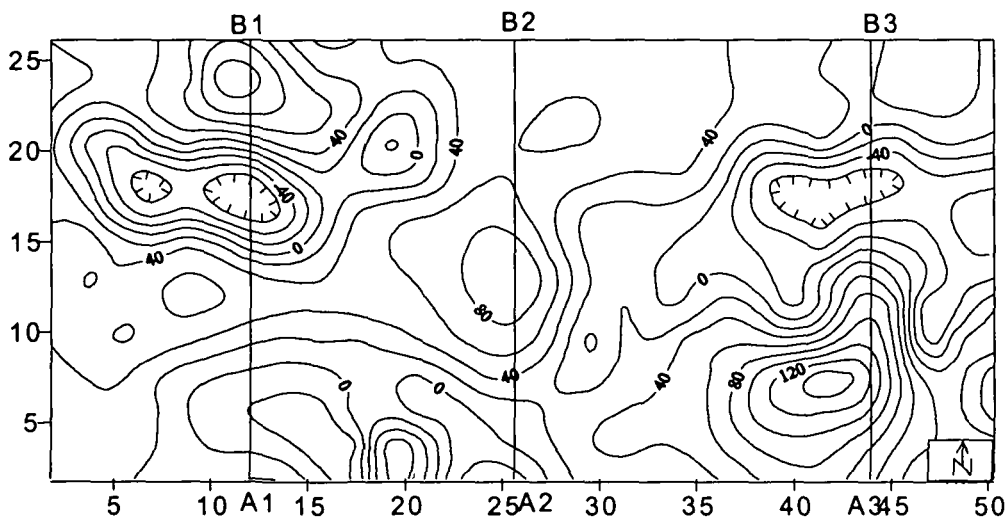


(Distances are in km and (0,0) refers to longitude 82.5° E and latitude 18.25° N.)

Fig. 7.2.4 Vertical component magnetic field of Lamaput –Araku area
(Using analytical means of integration over subareas)

Height of the plane = 2.115 km (aMSL)
Contour interval = 10nT



(Distances are in km and (0,0) refers to longitude 82.5° E and latitude 18.25° N.)
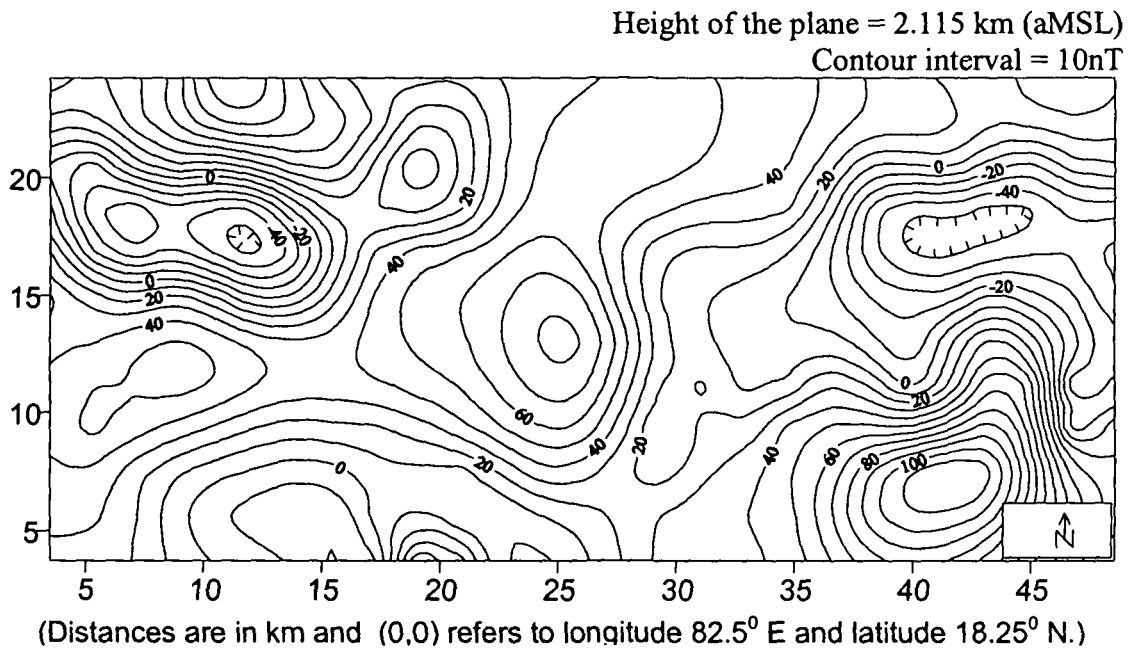
It is evident from Fig.7.2.3 and Fig.7.2.4 that a magnetic high is aligned in NW-SE direction in the area. This partially supports the general alignment of the structural elements in the area arrived earlier from the total field magnetic data that in the western part, the structural elements are aligned in NE-SW direction near Tuni at south and their orientation becomes NW-SE as we move towards Koraput at north.

## 7.2.4 Determination of Depth to the Subsurface Magnetic Causatives

To determine the depth to the subsurface magnetic causatives, two lines A1-B1 and A3-B3 are chosen in the area along which the anomaly contours at level z = 1.615 km aMSL provide an approximate two-dimensional character of the field (Fig.7.2.3). In a local cartesian reference frame with its origin at the crossing of 82.5°E longitude and 18.25°N latitude, x-axis coinciding with latitude 18.25°N, y-axis coinciding with 82.5° E longitude and z-axis pointing upward, the line A1-B1 with end points at (82.61°E, 18.25°N) and (82.61°E, 18.5°N) and A3-B3 with end points (82.91°E, 18.25°N) and (82.91°E, 18.5°N) are defined by x = 12 and 43 km respectively.

81

In the next step, the field values along the lines are read from the contour–map of the vertical component magnetic field exhibited in Fig.7.2.3. Subsequently, using the DEPTHDNC software, depth to the shallow and deeper magnetic causatives are determined at a regular interval of 1 km along the lines A1-B1 and A3-B3 and exhibited in Fig. 7.2.5 and Fig.7.2.6 respectively. As the A2-B2 line crosses very few numbers of contour lines so this line is not taken into consideration for depth determination.

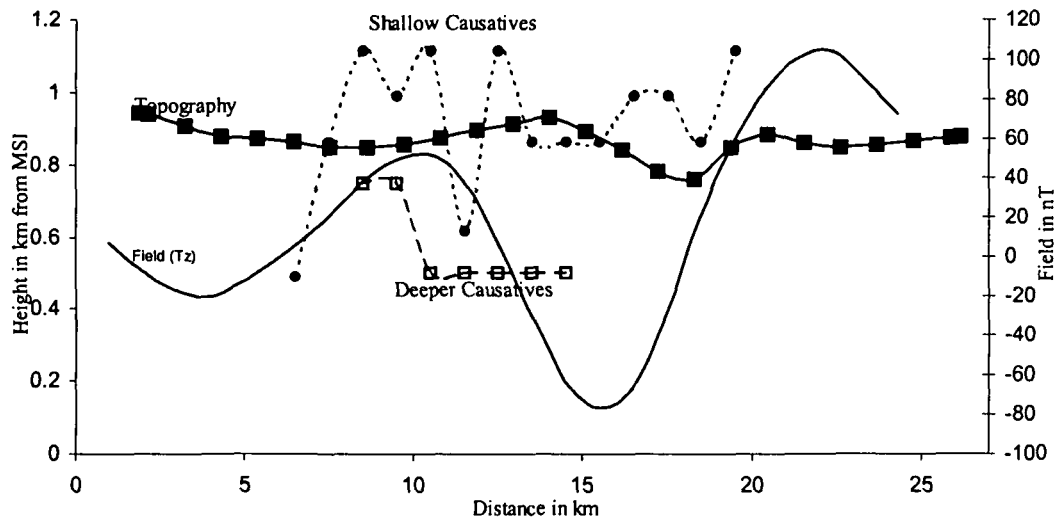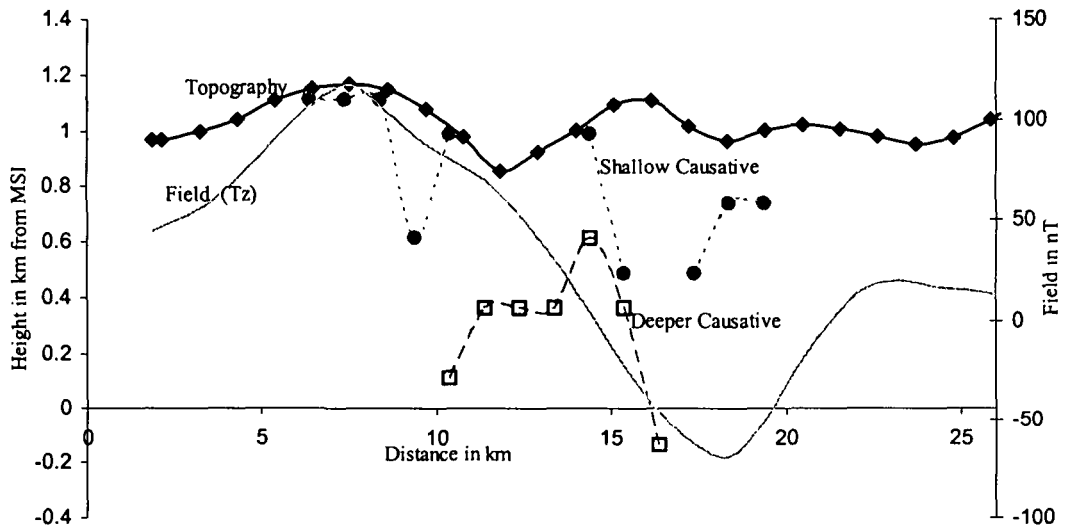Fig. 7.2.5 Topography, depth to causatives and field profile along line
A1B1



Fig.7.2.6 Topography, depth to causatives and field profile along line
A3B3

It is evident from Fig.7.2.5 that the basement, (stable Charnokites (Swami 1975)) along A1-B1 shows existence of a E-W trending fault across the line at a distance 10 km north of 18.25 $^0$ N latitude with its up thrown side towards south at a height of 0.8 km aMSL and the down thrown side towards north at depth of about 0.55 km aMSL. The existence of the fault is clearly reflected in the magnetic profile at the same location. Further, the topographic high above it is pushed by a couple of km towards the down thrown side indicating the direction of thrust at the location. The upthrust features do not corroborate the sub-thrust features in the area.

A strange phenomenon is observed in the computed depth to the shallow magnetic sediments along the lineA1-B1. The results indicate presence of magnetic sediments in the free-space above the ground surface. This happens when the data are with large random error. The source of error might be in the up-continued field or in the basic data, which are possibly acquired over exposed magnetic materials. The topography along A1-B1 is nearly flat as evident in the topographic profile exhibited in Fig.7.2.5. As such, the high fluctuating random error in the up-continued data cannot come from up-continuation of the field from boundary data. It is likely to come from the acquired data. On projecting the line on the geological map of the area presented in Fig.7.1.1, we find the entire line A1-B1 lies on the exposed Charnokites, which is strongly magnetic in nature.

The results obtained on analysis of A3-B3 profile is exhibited in Fig.7.2.6. It is evident from Fig.7.2.6 that the topographic height along the line varies from 850 to 1170 mt with the lowest depression at around 12 km north of 18.25$^0$N latitude. The basement along the line appears with three successive E-W trending faults having their reflections on the magnetic profile. In this case also the topographic high has a shift towards north from the location of the basement high along the line.

In this case, the computed depth to the shallow magnetic sediments (unconsolidated Charnokites) as seen in the Fig.7.2.6, lie below the topographic surface along the line except probably at around x = 12 km, where the topographic low might be having some exposed magnetic sediments. The line A3-B3 entirely lies over the non-magnetic Khondalites in the area (Fig.7.1.1).

The basement high at a distance of around 15 km from the end A3 of the line A3-B3 is probably the continuation of the NW-SE trending basement high predicted from the anomaly map over the area. Its continuation across A1-B1 remains unidentified, as the data-length is insufficient to compute the depth to the northern portion of A1-B1.

Approximation of the topography by triangular sub areas provides the best possible approximation to it. This produces a surface having no gap between the sub areas. In contrast, approximation of topography by square or rectangular subareas provides a surface having gaps between the sub areas in general.

The triangular subareas used in the present study are each of about 2 sq. km in area. This is a bit larger in size than the one in which we can reasonably assume that a function is constant over it. Further, approximation of a boundary by use of such large subareas may not be a good approximation of the true surface. This is evident in Fig.7.2.7 where we find the true geometry of the topography along the line A3-B3 is a bit crude representation of the topography.

The topography along a line in a shallow geological basin generally follows a geometry of the basement along the line and as such the topographic high corroborates the basement high in a basin. In the present case, the topographic highs along the lines A1-B1 and A3-B3 are shifted towards north from up-thrown to down-thrown sides of E-W trending basement faults across the line. This indicates a northward thrust was the cause of the present set-up of the landmass at the locality. A similar study all over the area is expected to throw some light in the genesis of formation of the landmass in the area.

# Chapter-8

# CONCLUSION

Gravity or a component magnetic field can be reproduced in the upper half-space domain from a general boundary as potential of simple as well as double layer boundary density. The fields also can be continued upward from the boundary by Green's formula without finding Green's function for the boundary. Of all the above formulations of the problem, double layer formulation is numerically superior to others and it also can be easily handled on a computer.

For the field point lying near the boundary, approximation of integrals fails to reproduce the field correctly in a field problem in particular, and where the subareas are large in size in general; whereas the analytical means of computation produce results acceptable for any practical purpose.

The technique so developed when applied to the magnetic data of Vishakhapatnam-Srikakulam area, the up-continued field clearly revealed the basement trend in the coastal area on continuation to a level $z=1$km where the basement trend remained masked in the field at the assumed datum level $z=0$. When applied to the magnetic data of Lamaput-Araku area, the rugged northwestern hilly region, up-continuation of the field to a common level nearly grazing the highest mountain peak in the area clearly reveals the alignment of the basement features. And further analysis of the up-continued field not only identifies the exposed charnokites but also reveals the direction of the thrust that deformed the landmass in the area.

# REFERENCES

Bhattacharyya, B.K. and Chan, K.C., 1977, *Reduction of magnetic and gravity data on an arbitrary surface acquired in a region of high topographic relief,* Geophys., 42, 1411 – 1430.

Courtillot, V.E., Ducruix, J. and Le Muel, J.L., 1973, *Le Prolongement d'un champ de potential dun contour quelconque sur un contour horizontal : Une application de la methode de Backus et Gilbert, Ann.* Geophys., 29, 361 – 366.

Ducruix, J., Mouel, J.L. and Courtillot, V.E. 1974, *Continuation of three-dimensional potential fields measured on an uneven surface,* Geophys. J.R. astro. Soc. 38, 299 – 314.

Hammer, S., 1939, *Terrain correction for gravimeter stations,* Geophysics, 4, 184 – 195.

Hess, J. L. and Smith, A.M.O., (1967), *Calculation of potential flow about arbitrary bodies in "Progress in Aeronautical Sciences",* v. 8 ( D.Kuchemann ed.), Pargamon Press, London.

Jaswon, M.A. and Symm, G.T., 1977, *Integral equation methods in potential theory and elastostatics,* Academic Press, London.

Kellogg, O.D., 1929, *Foundations of potential theory,* Fredrick Ungar Publishing Company, New York.

Kumar, R, Barman, M.M. and Laskar,S.K., 1992, *Processing and interpretation of ground gravity-magnetic data acquired in Hardwar-Rishikesh area, UP,* ONGC report ,KDMIPE, Dehradun, India.

Kress, R. 1989, *Linear integral equations, Applied mathematical sciences*, v.82, Springer-Verlog

Laskar, S.K., 1971, *Solutions of certain Integral Equations in Potential Theory*, The City University, London.

Laskar, S. K., (1977), *An approximation to surface integrals in solution of boundary value problems of potential theory*, Proc. The first National Convection on Applied Numerical Analysis, Banglore, 253-264.

Laskar, S.K. 1984, *Upward continuation of two-dimensional gravity-magnetic data from an irregular terrain* , Bulletin of ONGC, 21, 75-82.

Laskar, S.K. 1994, *Gravity magnetic data interpretation: Theory and Practice*, KDMIPE, ONGC, Dehradun, India

Murthy, I.V.R, Polinaidu, B. and Rao, A.T., 1991, *Magnetic anomalies and basement structure around Vizianagaram, Andhra Pradesh*, J. Goel.Soc.India, 37, 272 - 286.

Murthy, I.V.R , and Rao, P.R., 2001 , *Magnetic unomalies and basement structure around Viziannagaram , Vishakhapatnam and Srikakulam districts of Andhra Pradesh , India*, International Association for Gondwana Research , Japan, 4 (3), 443-454 .

Rao, V. Venkateswara, Murthy, I. V. R. and Rao, A.T., 1990, *Magnetic anomalies and tectnonics of Gostani river basin in Eastern Ghats of India*, j. Geol. Soc. India, 35, 287-295.

Smirnov, V. I., 1964, *Integral equations and partial differential equations: a course of higher mathematics*, v.-iv, Pergamon, London

Subrahmanyam, C., 1978, *On the reduction of gravity anomalies to the Geotectonics of the Pre-Cambrian terrains of the South Indian Sheild,* J. Geol. Soc. India, 19, 251-263

Subrahmanyam, C. (1983), *An overview of gravity anomalies of Precambrian metamorphic terrains and their boundary relationship in the southern Indian shield In: Naqui, S.M. and Roger, J.J.W. (Eds.), Precambrian of South India.* Geol. Soc. India, Mem. No. 4, 553-556

Subrahmanyam, C. and Verma, R.K. (1986) *Gravity Field, Structure and Tectonics of the Eastern Ghats.* Tectnophysics, v.126, 195-212.

Swami, S.N., 1975, *Proposal for charnokite - khondalite system in the Archaean Sheild of Peninsular India,* Geol., Soc. India. , Misc. Publ. No. 23 , 1-16.

Waston, D.F., Philip, G.M., 1985, *A refinement of inverse ·distense weighted (IDW) interpolation,* Geoprospecting 2 (4), 315-327.